USZ Universitäts Spital Zürich

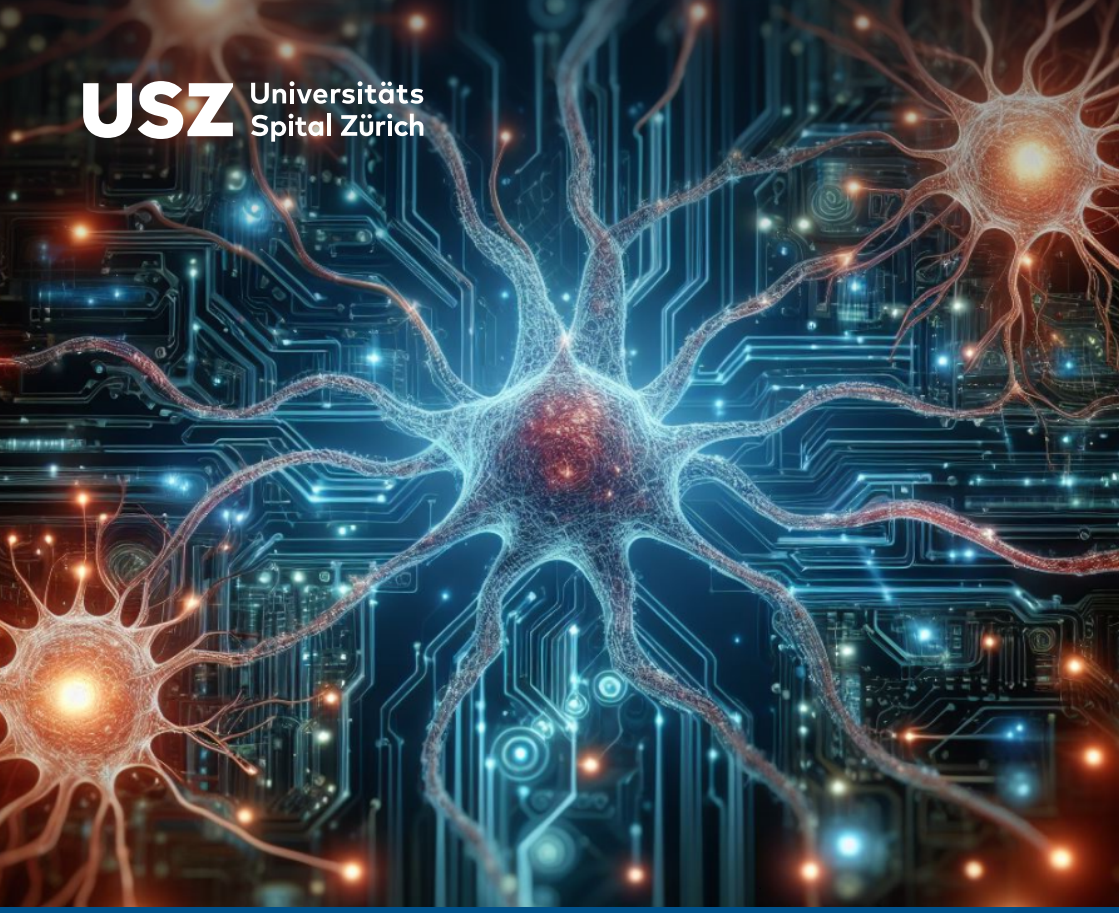

23rd Day of Clinical Research

Artificial Intelligence am USZ Research & Vision

Donnerstag, 16. Mai 2024, 8.30 – 17.00 Uhr
Grosser Hörsaal OST, Universitätsspital Zürich

Verleihung Day of Clinical Research Preis 2024
Georg-Friedrich-Götz-Preisverleihung 2024

Wir wissen weiter.

Committee Day of Clinical Research

Cinelli Paolo, PD Dr.
Distler Oliver, Prof. Dr.
Moch Holger, Prof. Dr.
Schneider Robin, MBA
Senti Gabriela, Prof. Dr.
Speck Roberto, Prof. Dr
Van den Broek Maries, Prof. Dr.
von Eckardstein Arnold, Prof. Dr.
Wegener Susanne, Prof. Dr.
Weller Michael, Prof. Dr.
Witzel Isabell, Prof. Dr.
Zinkernagel Annelies, Prof. Dr.

Table of contents

Cover:

Image created by Microsoft Copilot, powered by DALL-E

Programm

Donnerstag, 16. Mai 2024

Grosser Hörsaal Ost

Götz-Preisverleihung

08.30 Uhr **Begrüssung der Gäste**
durch Beatrice Beck Schimmer, Prof. Dr. med.
Direktorin Universitäre Medizin Zürich, Universität Zürich

08.35 Uhr **Einführung und Würdigung der Preisträgerin**
Barbara Stähli, Prof. Dr. med., EMBA, MPH, FESC
durch Frank J. Rühli, Prof. Dr. Dr., Dekan Medizinische Fakultät, Universität Zürich

08.40 Uhr **Kurzreferat von Prof. Dr. med. Barbara Stähli EMBA, MPH, FESC**
«Timing of Complete Revascularization with Multivessel PCI for Myocardial Infarction»
Klinik für Kardiologie, Universitätsspital Zürich

08.55 Uhr **Preisverleihung durch Prof. Dr. med. Beatrice Beck Schimmer**
Direktorin Universitäre Medizin Zürich, Universität Zürich

09.05 Uhr **Einführung und Würdigung des Preisträgers**
Tobias Weiss, Dr. med. Dr. sc. nat.
durch Frank J. Rühli, Prof. Dr. Dr., Dekan Medizinische Fakultät, Universität Zürich

09.10 Uhr **Kurzreferat von Dr. med. Dr. sc. nat. Tobias Weiss**
«Antikörper-Zytokin-Konjugate – ein neuer vielversprechender immuntherapeutischer Ansatz beim Glioblastom»
Klinik für Neurologie, Universitätsspital Zürich

09.25 Uhr **Preisverleihung durch Prof. Dr. med. Beatrice Beck Schimmer**
Direktorin Universitäre Medizin Zürich, Universität Zürich

09.30 Uhr **Coffee Break**

Day of Clinical Research - Preisverleihung

10.00 Uhr **Einführung - Day of Clinical Research**
Gabriela Senti, Prof. Dr. med., Direktorin Forschung und Lehre, Universitätsspital Zürich

10.10 Uhr **Session 1: Cardiovascular/Metabolism/Endocrinology**
The COPI coatomer regulates lipoprotein metabolism
Grigorios Panteloglou, Dr. sc. nat., Institut für Klinische Chemie, Universitätsspital Zürich

10.20 Uhr **Session 2: Hematology/Oncology**
Acquisition of an Immunesuppressive Microenvironment after CD19 CAR T Cell treatment in B Cell Precursor Acute Lymphoblastic Leukemia
Marianna Ponzo, Dr., Klinik für Medizinische Onkologie und Hämatologie, Universitätsspital Zürich

10.30 Uhr **Peptide-Guided Adaptor-CAR T-Cell Therapy for the Treatment of SSTR2-expressing Neuroendocrine Tumors**
Christian Pellegrino, Dr. sc. ETH, Klinik für Medizinische Onkologie und Hämatologie, Universitätsspital Zürich

10.40 Uhr **Session 3: Head Region/Neuroscience**
Targeting the IDH1R132H mutation in gliomas by CRISPR/Cas precision base editing
Flavio Vasella, Dr. sc. nat., Klinik für Neurochirurgie, Universitätsspital Zürich

10.50 Uhr **Session 4: Infection/Immunity/Inflammation/Systemic Diseases**
Single-cell Staphylococcus aureus agr quorum-sensing dynamics during signal pulses and community interactions
Julian Bär, Dr. sc., Klinik für Infektionskrankheiten und Spitalhygiene, Universitätsspital Zürich

11.00 Uhr **Session 5: Mixed Topics**
Safety assessment of the SGLT2 inhibitors empagliflozin, dapagliflozin and canagliflozin during pregnancy: An ex vivo human placenta perfusion and in vitro study
Sabrina Kuoni, M. Sc., Klinik für Geburtshilfe, Universitätsspital Zürich

11.15 Uhr **Lunch / Poster viewing**

Veranstaltungsthema – Artificial Intelligence am USZ

13.00 Uhr **Einführung und Moderation durch**
Gabriela Senti, Prof. Dr. med. und Chairman Björn Menze. Prof. Dr. med.

13.10 Uhr **Imaging Artificial Intelligence AI and diagnostic information:**
Biomedical Image Analysis and Machine Learning at USZ
Björn Menze, Prof. Dr. med, Abteilung für Quantitative Biomedizin, DFL, Universitätsspital Zürich, Institut für Quantitative Biomedizin, Universität Zürich

Diagnostik

13.40 Uhr **AI in Radiology – Research and Application at USZ**
Jonas Kluckert, Institut für diagnostische und interventionelle Radiologie, Universitätsspital Zürich

14.00 Uhr **Deep learning for improved outcome predictions in ischemic stroke**
Lisa Herzog, Dr., Klinik für Neuroradiologie, Universitätsspital Zürich

Therapie

14.20 Uhr **Synthetic medical image generation in radiation oncology and beyond**
Stephanie Tanadini-Lang, PD Dr. sc. nat., Klinik für Radio-Onkologie, Universitätsspital Zürich

14.40 Uhr **Clinical nuances of Mixed Reality application in Neurosurgery**
Elisa Colombo, Dr. med., Klinik für Neurochirurgie, Universitätsspital Zürich

15.00 Uhr **Coffee Break**

15.15 Uhr **Outlook Clinical Artificial Intelligence AI beyond image:**
Workflow Enhancement and MRI-free Neuronavigation
Ender Konukoglu, Prof. Dr., Biomedizinische Bildverarbeitung, ETH Zürich

Plattformen / Projekte

15.45 Uhr **Computational Pathology meets Spatial Transcriptomics**
Viktor Kölzer, Prof. Dr. med., Institut für Medizinische Genetik und Pathologie, Universitätsspital Basel und Universitätsspital Zürich / Universität Zürich

16.05 Uhr **Diagnostics and prediction with digital pathology and imaging mass cytometry**
Andreas Wicki, Prof. Dr. med. Dr. phil., Klinik für Medizinische Onkologie und Hämatologie, Universitätsspital Zürich / Universität Zürich

16.25 Uhr **Ende der Veranstaltung**

Cardiovascular / Metabolism / Endocrinology

Basic Research

610
F. Guan, C. Brunckhorst, F. Duru, F. Ouyang, AM. Saguner
Epicardial Catheter Ablation of Ventricular Tachycardia in Patients of Arrhythmogenic Cardiomyopathy - from a university hospital report in Switzerland

611
F. Guan, C. Brunckhorst, T. Wolber, A. Breitenstein, N. Molitor, G. Suna, F. Duru, AM. Saguner
High-density Mapping-Guided Ventricular Tachycardia Ablation in Patients with Ischemic Cardiomyopathy: Outcomes from a Tertiary Center Cohort in Switzerland

613
S. Guerra, D. Birrer, P. Clavien, B. Humar
Metabolic needs define the physiological limits of the liver's regenerative capacity

620
E. Gorica, S. Costantino, A. Elkhal, O. Dzemali, F. Paneni, H. Rodriguez Cetina Biefer
NAD+ Supplementation as a Potential Therapeutic Approach in Cardiotoxicity

621
K. Krebs, A. Rossi, S. Jurisic, M. Gajic, T. Albertini, P. Heiniger, A. Galafton, A. Pazhenkottil, P. Kaufmann, R. Buechel, D. Benz, A. Giannopoulos
Effect of Image Reconstruction Algorithms in Pericoronary Adipose Tissue Attenuation obtained with Coronary CT Angiography

627
Z. Steffek, D. Benz, T. Albertini, M. Gajic, S. Jurisic, A. Pazhenkottil, P. Kaufmann, R. Büchel, A. Giannopoulos
Non-invasive Longitudinal Hemodynamic Phenotypes of Coronary Arteries with Atherosclerosis and Association with Myocardial Perfusion

628
S. Makieva, M. Saenz-de-Juano, C. Almiñana, S. Bauersachs, S. Bernal-Ulloa, M. Xie, A. Velasco, N. Cervantes, M. Sachs, T. Cavazza, S. Ulbrich, B. Leeners
The in vitro maturation rate of human oocytes is enhanced following uptake of extracellular vesicles originating from mature follicles.

646
A. Mongelli, S. Mohammed, E. Gorica, A. Mengozzi, M. Telesca, C. Matter, F. Paneni, F. Ruschitzka, S. Costantino
Long non-coding RNA PANDA drives diabetic vascular dysfunction by promoting endothelial senescence and oxidative damage

654
FG. Beltrami, KGP. Boyle, C. Brunckhorst, F. Duru, CM. Spengler, AM. Saguner
Ventricular arrhythmia burden during different physical activities in patients with Arrhythmogenic Right Ventricular Cardiomyopathy: Preliminary Analysis

656
K.D. Raghvendra, GA. Azzarito, MR. Rosselli, BL. Leeners
Transcriptomic Profiling of SARS-CoV-2 Spike Protein S1 Subunit Mediated Changes in Human Vascular Endothelial cells, -Pericytes, -Smooth Muscle Cells and Lymphatic Endothelial cells: Evidence for Differential Gene Regulation

664
L. Ilcheva, V. Ntinopoulos, N. Papadopoulos, A. Häussler, H. Rodríguez Cetina Biefer, O. Dzemali
Five years of single-center experience in performing transapical transcatheter aortic valve implantation

670
I.S. Martinez Lopez, B. Battilana, M. Haberecker, D. Kračun, M. Kirschner, I. Opitz
Understanding the contribution of different cell types in the development of chronic thromboembolic pulmonary hypertension (CTEPH)

687
A. Joachimbauer, N. Cadosch, C. Gil-Cruz, C. Perez-Shibayama, K. Frischmann, F. Tanner, F. Ruschitzka, B. Ludewig, D. Schmidt
Echocardiographic strain predicts the progression of acute autoimmune myocarditis to inflammatory cardiomyopathy

690
E. Payne, A. Joachimbauer, N. Cadosch, C. Gil-Cruz, C. Perez-Shibayama, K. Frischmann, F. Tanner, F. Ruschitzka, B. Ludewig, D. Schmidt
Acute and chronic myocardial inflammatory disease - the explorative prospective ImmpathCarditis study

709
C. Almiñana, S. Makieva, M. Saenz-de-Juano, S. Bauersachs, S. Bernal-Ulloa, M. Xie, A. Velasco, N. Cervantes, M. Sachs, T. Cavazza, S. Ulbrich, B. Leeners
Treatment of oocytes with follicular fluid-derived extracellular vesicles during in vitro maturation induces changes in the proteomic profile and organelle distribution

711
I. Martinez Lopez, T. Papasotiropoulos, F. Schläpfer, S. Ulrich, I. Opitz, M. Kirschner
MicroRNA Expression Correlates with Clinical Presentation of Chronic Thromboembolic Pulmonary Hypertension

716
G. Panteloglou, A. Othman, P. Zanoni, E. Schlumpf, M. Yalcinkaya, S. Kakava, S. Radosavljevic, R. Meier, M. Futema, S. Humphries, R. Geha, A. Shum, W. März, B. van de Sluis, J. Kuivenhoven, J. Robert, L. Rohrer, a. von Eckardstein
The COPI coatomer regulates lipoprotein metabolism

Clinical Trials

624
L. Sazgary, E. Theano Samara, A. Stüssi, M. Guckenberger, F. Ruschitzka, T. Wolber, N. Molitor, G. Fu, G. Suna, D. Hofer, A. Breitenstein, CB. Brunckhorst, F. Duru, AM. Saguner
The Impact of Clinical Audits on Patient Radiation Exposure for Device Procedures

635
E. Rho, C. Martinetti, B. George, T. Schachtner, F. Ruschitzka, M. Frank
Patient characteristics and outcomes of an inter- and multidisciplinary nephrology and cardiology clinic

659
L. Rings, A. Häussler, L. Mavrova-Risteska, V. Ntinopoulos, P. Fleckenstein, M. Tanadini, H. Rodriguez Cetina Biefer, O. Dzemali
Lactate dehydrogenase is not a reliable postoperative marker for hemolysis in paravalvular leakage for sutureless valves

662
L. Ilcheva, V. Ntinopoulos, A. Häussler, I. Tudorache, P. Risteski, H. Rodriguez Cetina Biefer, O. Dzemali
Early and long-term outcomes of mitral valve surgery after transcatheter edge-to-edge repair: two center experience over 5 years

671
M. Van Hemelrijck, J. Sromicki, P. Risteski, I. Tudorache, A. Häussler, M. Frank, B. Hasse, H. Rodriguez Cetina Biefer, O. Dzemali
Aortic graft infection after surgery for acute aortic syndrome

685
A. Majcher, P. Bjorklund, A. Holfeld, A. Othman, G. Lauria, J. Hardfeldt, B. Angelin, T. Hornemann
The increased Alanine to Serine ratio in T2D relates to diabetic neuropathy by driving the formation of neurotoxic 1-deoxysphingolipids in skin

720
R. Erlebach, A. Buhlmann, R. Andermatt, B. Seeliger, K. Stahl, C. Bode, R. Schüpbach, P. Wendel-Garcia, S. David
Carboxyhemoglobin Predicts Oxygenator Performance and Imminent Oxygenator Change in Extracorporeal Membrane Oxygenation

Hematology / Oncology

Basic Research

638
M. Kirschner, F. Schläpfer, M. Meerang, I. Opitz
Dysregulated microRNAs contribute to chemotherapy-resistance of pleural mesothelioma

639
M. Kirschner, V. Orlowski, F. Schläpfer, M. Meerang, I. Opitz
Novel microRNAs are associated with presence of pleural mesothelioma and response to chemotherapy

641
J. Mengers, M. Haberecker, M. Kirschner, N. Bosbach, O. Lauk, i. Opitz, m. Meerang
Low Ki-67 Positive Index is a Prognostic Factor for Better Survival Outcomes of Patients Treated with Intracavitary Cisplatin-Fibrin

643
J. Trepl, C. Pasin, D. Schneidawind, N. Mueller, M. Manz, A. Bankova, I. Abela
Evaluating Tixagevimab/Cilgavimab Prophylaxis in Allogeneic Hematopoietic Cell Transplantation Recipients for COVID-19 Prevention

648
LV. Heeb, A. Gupta, L. Huynh-Russo, E. Breuer, P. Clavien
Assessing the therapeutic potential of immunotherapies to control colorectal cancer metastasis in the regenerating liver

650
Y. Chen, S. Steiner, C. Hagedorn, S. Kollar, A. Pliego-Mendieta, M. Haberecker, J. Plock, C. Britschgi, L. Planas-Paz, C. Pauli
Acquired NF2 mutation confers resistance to TRK inhibition in an ex vivo LMNA::NTRK1 rearranged soft tissue sarcoma cell model

657
C. Pellegrino, N. Favalli, L. Volta, R. Benz, S. Puglioli, G. Bassi, K. Zitzmann, CJ. Auernhammer, S. Nölting, C. Magnani, D. Neri, F. Beuschlein, MG. Manz
Peptide-Guided Adaptor-CAR T-Cell Therapy for the Treatment of SSTR2-expressing Neuroendocrine Tumors

658
A. Kraft, M. Meerang, MB. Kirschner, V. Boeva, I. Opitz
A Comparative Analysis of Secreted miRNAs Reveals Candidate Biomarkers for Pleural Mesothelioma Detection

667
D. Basu, H. Bolck, J. Theurillat, H. Moch
Development of a Mechanistic Understanding and Therapeutic Strategy for TFE3-Rearranged Renal Cell Carcinoma

672
J. Jang, R. Werner, M. Kirschner, M. Honegger, E. Casanova Zimmermann, S. Märsmann, P. Cinelli, W. Jungraithmayr, I. Opitz
A novel 3D culture of lung adenocarcinoma cells with mesenchymal stromal cells

674
L. Volta, R. Myburgh, C. Pellegrino, C. Koch, M. Maurer, F. Manfredi, M. Hofstetter, A. Kaiser, F. Schneiter, J. Müller, M. Buehler, R. De Luca, N. Favalli, C. Magnani, T. Schroeder, D. Neri, M. Manz
Efficient Combinatorial Adaptor-Mediated Targeting of Acute Myeloid Leukemia with CAR T-Cells

676
S. Traxel, C. Beerli, F. Schmidt, V. Dinh-Van, RF. Speck, S. Bredl
Turning the tumor hot: Genetically engineered macrophages to disrupt the cold tumor microenvironment

688
M. Roncador, F. Bayer, J. Kuipers, M. Manz, N. Beerenwinkel, S. Böttcher, S. Balabanov
Dissecting the complexity of the MDS-AML continuum in 7480 patients with Bayesian covariate-aware clustering.

693
M. Meerang, M. Kirschner, F. Schläpfer, M. Ronner, E. Felley-Bosco, I. Opitz
Molecular Characterization and Validation of Live Cell Biobank for Pleural Mesothelioma

694
S. Changkhong, F. Schläpfer, M. Ronner, E. Felley-Bosco, M. Kirschner, I. Opitz, M. Meerang
Characterization of cancer associated fibroblast cell cultures from the mesothelioma cell bank

696
R. Werner, M. Eisenberg, S. Ries, T. Papasotiropoulos, N. Steinmann, M. Antonoff, I. Opitz
Perioperative outcomes following lung resection in metastatic non-small cell-lung cancer: Results of a large multicenter database

698
M. Ponzo, L. Drufuca, C. Buracchi, S. Nucera, C. Bugarin, G. Rossetti, R. Bonnal, B. Rambaldi, A. Biondi, G. Gaipa, M. Pagani, C.F. Magnani
Acquisition of an Immunesuppressive Microenvironment after CD19 CAR T Cell treatment in B-Cell Precursor Acute Lymphoblastic Leukemia

699
R. Werner, K. Chiffi, D. Schneiter, S. Hillinger, O. Lauk, I. Opitz
Surgical complexity of anatomical lung resections after induction immunotherapy for locally advanced or metastatic non-small cell lung cancer

710
A. Paunoiu, R. Dal Bello, P. Wallimann, M. Guckenberger, S. Tanadini-Lang
Longitudinal radiomics for liver cancer patients treated with magnetic resonance-guided radiotherapy

Clinical Trials

615
C. Litchfield, R. Nienhold, M. Adamczyk, U. Wagner, M. Schmid, D. Seidl, D. Aguilera, V. Kölzer, M. Zoche, J. Rüschoff, H. Moch, A. Sobottka-Brillout
Diagnostic Whole Genome Sequencing: Hydra of hopes and hurdles

677
R. Dal Bello, J. von der Grün, S. Tanadini-Lang, N. Andratschke, P. Balermpas, M. Guckenberger
Technical preparation for a Phase I Clinical Study of e-FLASH Radiotherapy for Palliative Treatment of Superficial Skin Lesions of Malignant Melanomas

Head Region / Neuroscience

Basic Research

632
F. Vasella, R. Weber, A. Klimko, M. Silginer, M. Lamfers, M. Neidert, L. Regli, G. Schwank, M. Weller
Targeting the IDH1R132H mutation in gliomas by CRISPR/Cas precision base editing

681
E. Voloviceva, S. Kakava, S. Sandra, A. von Eckardstein, J. Robert
Role of apolipoprotein E in the cerebrovasculature

697
F. Costa, G. Indiveri, J. Sarnthein
Real-time HFO analysis for intraoperative ECoG

714
V. Dimakopoulos, J. Sarnthein
Multicenter comparison of interictal high frequency oscillations as a predictor of seizure freedom

Clinical Trials

660
A. Hülsmeier
The atypical sphingolipid C18SOΔ14Z is a biomarker for DEGS1 related hypomyelinating leukodystrophy

Infection / Immunity / Inflammation / Systemic Diseases

Basic Research

617
E. Parietti, D. Bivona, A. Tarnutzer, D. Bongiorno, N. Musso, S. Stefani, SM. Shambat, AS. Zinkernagel
Assessment of Staphylococcus aureus phenotypic heterogeneity mediated by small colony variant formation

618
E. Parietti, A. Gómez Mejia, CC. Chang, J. Bär, S. Shambat, AS. Zinkernagel
Rifampicin impairs intracellular eradication of Staphylococcus aureus by human macrophages

619
J. Bär, SGV. Charlton, A. Tarnutzer, GS. Ugolini, E. Secchi, AS. Zinkernagel
Single-cell Staphylococcus aureus agr quorum-sensing dynamics during signal pulses and community interactions

629
K. Michalek, S. Bhattacharjee, T. Loosli, K J. Metzner
Elucidating the role of cellular factors in the formation of defective HIV-1 proviruses

630
CC. Chang, A. Gomez Mejia, E. Cauwenberghs, S. Shambat, S. Brugger
Adjuvant microbiota-transplantation to cure chronic and recurrent bacterial infections

634
J. Tschumi, L. Jörimann, M. Zeeb, K. Neumann, M. Stöckle, E. Bernasconi, S. Yerly, M. Cavassini, A. Rauch, P. Schmid, R D. Kouyos, H F. Günthard, K J. Metzner
Similar Changes in Proviral Landscapes Over 10 Years in People With Diverging HIV Reservoir Dynamics

636
A. Movasati, C. Leemann, K. Neumann, R. Chen, R. Regös, K. Metzner
Comprehensive Characterization of HIV-1 Evolution in A Long-Term Experimental Evolution Study

637
AGM. Gomez-Mejia, SMS. Mairpady Shambat, ES. Sosa, MH. Huemer, ASZ. Zinkernagel
Staphylococcus aureus adaptation to antibiotic stress modulates tolerance and survival

640
S. Hertegonne, A. Tarnutzer, S. Mairpady Shambat, A. Zinkernagel
Staphylococcus aureus induces differential functional responses in neutrophils during acute infection

647
L. Ihm, R. Speck, N. Kadzioch
The pathogenic significance of USP18 in HIV pathogenesis

649
M. Determann, L. Luise, M. Schwarzfischer, A. Niechcial, M. Wilmink, M. Walker, D. Pöhlmann, MR. Spaliner, Y. Morsy, F. Sella, M. Levesque, VH. Koelzer, AL. Frei, S. Buch, J. Hampe, C. Datz, C. Schafmayer, M. Heikenwälder, M. Scharl, S. Blümel
Hepatic cytotoxic T cells in metabolic dysfunction-associated steatohepatitis are regulated by protein tyrosine phosphatase non-receptor type 2

665
M. Labarile, J. Fellay, CW. Thorball, K. Kusejko, A. Calmy, M. Stöckle, A. Rauch, B. Surial, M. Cavassini, E. Bernasconi, J. Notter, HF. Günthard, J. Nemeth, PE. Tarr, C. Pasin, RD. Kouyos
Genetic and non-genetic risk factors affect the risk of Type 2 Diabetes in the Swiss HIV Cohort Study

666
T. Loosli, A. Hauser, J. Josi, N. Han, S. Ingle, A. van Sighem, L. Wittkop, J. Vehreschild, F. Ceccherini-Silberstein, G. Maartens, M. Gill, C. Sabin, L. Johnson, R. Lessells, H. Günthard, M. Egger, R. Kouyos
Predicting Dolutegravir resistance in South Africa: A modelling study

669
K. Arnke
Diversity of bone derifed skeletal stem-cells – New targets for clinical applications

673
J. Baum, C. Boggon, R. Nora, L. Isa, SD. Brugger
Microbiota engineering for the eradication of S. aureus

686
J. Bergada Pijuan, J. Baum, C. Chang, A. Gómez-Mejia, S. Mairpady Shambat, T. Fuhrer, M. Zampieri, R. Kouyos, A. Zinkernagel, S. Brugger
Commensal Bacteria as Probiotic Candidates: Unraveling the Molecular Interplay between Nasal Commensals

689
MM. Müller, NJ. Wegmann, DM. Heuberger, G. Kadler, B. Seeliger, RA. Schüpbach, S. David
Low plasma levels of the endothelial soluble Tie-2 receptor predict mortality in patients with sepsis and ARDS

701
E. Sarti, R. Wolfensberger, C. Dolle, S. Sander, R. Speck, J. Nemeth
M. tuberculosis promotes intracellular survival manipulating the c-MYC pathway to redirect macrophages maturation

719
L. Linzmeier, E. Goljat, V. Matus, M. Determann, M. Wilmink, M. Schwarzfischer, R. Sanchez Alvarez, D. Pöhlmann, N. Joller, M. Scharl, M. Spalinger
The macrophage specific effect of PTPN23 KO in colonic inflammation and alveolar infection

Clinical Trials

652
J. Duran Ramirez, K. Kusejko, K. Metzner, M. Huber, Y. Martin, Stöckle, A. Calmy, L. Decosterd, M. Cavassini, E. Bernasconi, P. Schmid, H. Günthard, D. Braun, S. SHCS
Uptake and Discontinuation of the Long-Acting Duo in The Swiss HIV Cohort Study: Preliminary Analysis on Cabotegravir Plus Rilpivirine

655
D. Wimmersberger, K. Kusejko, S. Brugger, D. Haerry, M. Stöckle, J. Notter, A. Calmy, M. Cavassini, E. Bernasconi, E. Colin-Benoit, H. Günthard, D. Braun
Acceptance of doxycycline post-exposure prophylaxis and four-component meningococcal B vaccine for the prevention of bacterial sexually transmitted diseases in men who have sex with men and transgender women living with HIV in Switzerland

675
T. Obenhuber, T. Scheier, T. Stutz, M. Hug, D. Fontein, A. Kaiser, S. Schoene, P. Steiger, S. Brugger, W. Zingg, P. Schreiber
An outbreak with multidrug-resistant Acinetobacter baumannii on a burn ICU and its control with multifaceted containment measures

680
TA. Schweizer, J. Würmli, J. Prinz, M. Wölfle, R. Marti, H. Koliwer-Brandl, R. Zbinden, A. Egli, H. Walt, L. Imhof, P. Bosshard, Y. Achermann
Photodynamic therapy with protoporphyrin IX precursors using artificial daylight improves skin antisepsis for orthopaedic surgeries

683
PW. Schreiber, LD. Hoessly, K. Boggian, D. Neofytos, C. van Delden, A. Egli, M. Dickenmann, C. Hirzel, O. Manuel, M. Koller, S. Rossi, V. Banz, B. Schmied, L. Guerke, M. Matter, O. de Rougemont, M. Bonani, D. Golshayan, A. Schnyder, D. Sidler, F. Haidar, S. Kuster, S. Stampf, N. Müller, S. Swiss Transplant Cohort Study
Surgical site infections after kidney transplantation are independently associated with graft loss

Mixed Topics

Basic Research

609
P. Wolint, S. Hofmann, J. von Atzigen, R. Böni, I. Miescher, M. Calcagni, MY. Emmert, J. Buschmann
Angiogenic foot print of human stem cell-based secretome - assessment of vascular network complexity with relevance to regenerative medicine

612
I. Miescher, N. Schaffner, J. Rieber, G. Meier Buergisser, E. Ongini, A. Milionis, Y. Yao, V. Vogel, J.G. Snedeker, P. Giovanoli, M. Calcagni, J. Buschmann
Reducing peri-tendinous adhesion to zero: commodity materials hyaluronic acid/PEO are highly efficacious when applied as electrospun tubes around repaired tendons

614
N. Ziak, A. Abidi Ostorero, M. Generali, T. Hornemann, M. Lone
Understanding the selective neurotoxicity of Serine-palmitoyltransferase mutations towards motor and sensory neurons

616
S. Salemi, L. Breitenmoser, V. Baumgartner, D. Planta, M. Horst, D. Eberli
Comparative Analysis of Mitochondrial Function in Human Neuropathic and Normal Bladder Detrusor Smooth Muscle Cells

622
I. Miescher, J. Rieber, T. Schweizer, M. Orlietti, A. Tarnuter, F. Andreoni, G. Meier Buergisser, P. Giovanoli, M. Calcagni, J. Snedeker, A. Zinkernagel, J. Buschmann
In vitro assessment of Bacterial Adhesion and Biofilm Formation on Novel Bioactive, Biodegradable Electrospun Fiber Meshes Intended to Support Tendon Rupture Repair

623
V. Ntinopoulos, H. Rodriguez Cetina Biefer, I. Tudorache, N. Papadopoulos, D. Odavic, P. Risteski, A. Haeussler, O. Dzemali
Data extraction from unstructured medical records with the GPT-4 chatbot

631
M. Rechsteiner, M. Kirschner, R. Werner, H. Moch, B. Sobottka-Brillout, J. Rüschoff, A. Curioni-Fontecedro, I. Opitz
Optimization by site and time of liquid biopsy for CGP in early cancer detection: a technical evaluation

633
L. Weidmann, C. Laux, K. Castrezana Lopez, D. Harmacek, B. George, S. von Moos, T. Schachtner
Immunosuppression and transplantation-related characteristics affect the difference between eGFR equations based on creatinine compared with creatinine and cystatin C in kidney transplant recipients

642
A. Astourian, L. Fabbella, M. Hartmann, V. Vongrad, D. Rodriguez Gutierrez, B. Leeners
Human Endometrial Assembloids: A Tool for Studying Cellular Interplay in Endometriosis

651
N. Han, T. Loosli, A. Hauser, J. Josi, L. Johnson, R. Lessells, H. Günthard, M. Egger, R. Kouyos
The impact of long-acting cabotegravir and rilpivirine on the HIV epidemic and resistance dynamics in South Africa – a modelling study

653
L. Jones, H. Rodriguez, R. Katzschmann, O. Dzemali
Using Metamaterials and Cardiac Tissue Engineering to engineer Robust and Contractile Cardiac Tissue Patches

661
M. Gort, S. Arni, J. Schumacher, T. Aigner, K. van Tilburg, S. David, G. Lang, M. Kirschner, M. Meboldt, I. Schmitt-Opitz
Silicone Additive Manufacturing of Artificial Lungs

668
S. Kuoni, R. Steiner, L. Saleh, R. Lehmann, N. Ochsenbein-Kölble, AP. Simões-Wüst
Safety assessment of the SGLT2 inhibitors empagliflozin, dapagliflozin and canagliflozin during pregnancy: An ex vivo human placenta perfusion and in vitro study

679
M. Rechsteiner, U. Wagner, A. Wethmar, S. Voglis, R. Reimann
Fast-track CNV calling by Nanopore technology for meningioma classification

682
C. Haslinger, R. Brun, N. Ochsenbein-Kölble, W. Korte
Prospective, repeated observation of peripartum coagulation components in 1309 parturient women identifies coagulation factor XIII as a promising therapy approach in postpartum hemorrhage

684
P. Wallimann, B. Pouymayou, M. Mayinger, S. Nowakowska, A. Boss, M. Guckenberger, S. Tanadini-Lang, N. Andratschke
A new method to quantify signal intensity changes in glioblastoma during radiotherapy on an MR-Linac

691
L. Zurfluh, S. Santos, M. Mennet, O. Potterat, U. von Mandach, M. Hamburger, N. Ochsenbein-Kölble, AP. Simões-Wüst
Bryophyllum pinnatum Attenuates Oxytocin-Induced Pro-inflammatory Signalling Pathways in Human Myometrial Cells

702
Y. Kalbas, F. Klingebiel, S. Halvachizadeh, M. Teuben, A. Hülsmeier, T. Hornemann, R. Pfeifer, P. Cinelli, HC. Pape
Systemic lipidomic profile changes align with injury severity and predict outcomes in polytraumatized patients.

703
Y. Kalbas, F. Klingebiel, S. Halvachizadeh, M. Teuben, M. Weisskopf, A. Hülsmeier, T. Hornemann, R. Pfeifer, P. Cinelli, HC. Pape
Lipidomic analysis reveals relevant lipid profile changes in a porcine model with hemorrhagic shock and multiple injuries.

704
E. Ranieri, R. Brun, N. Ochsenbein-Kölble, W. Korte, C. Haslinger
D-dimer levels during pregnancy and postpartum: non-applicability of regularly used cut-offs for diagnosis of suspected pulmonary embolism

706
F. Bourquin, P. Verloo, T. Hornemann
Newly identified Mutation in Serine Palmitoyl-Transferase is linked to neuropathy and crystalline retinopathy

707
C. Dorfer, M. Kubli, S. Balabanov
Towards Automated Interpretations of Blood Laboratory Results

708
S. Kakava, E. Schlumpf, A. von Eckardstein, J. Robert
The low-density lipoprotein receptor defines the trafficking of high-density lipoprotein by brain endothelial cells

712
M. Mastall, G. Dunkel, D. Villars, M. Silginer, N. Okada, C. Rössig, T. Weiss, B. Weigelin, M. Weller, P. Roth
VEGFR2-specific CAR T cells with anti-glioma and anti-angiogenic activity against glioblastoma

713
R. Odabasi, K. Gegenschatz-Schmid, L. Moser, L. Krattiger, P. Briquez, N. Ochsenbein-Kölble, M. Ehrbar
Bioengineering Smart Regenerative Biomaterials for the Healing of Fetal Membrane Defects

715
K. Arnke
Fibroblast produced ECM for improved osteogenesis

718
K. Arnke
Influence of Dextran Derivatives on trilineage Differentiation

Clinical Trials

644
N. Jucker, D. Alceste, M. Serra, HAJ. Meijer, A. Thalheimer, RE. Steinert, AC. Spector, D. Gero, M. Bueter
Effect of Roux-en-Y Gastric Bypass on Microstructural Parameters of Ingestive Behavior in Adult Females with Obesity during a Four-Bottle Preference Test.

645
M. Serra, D. Alceste, H. Hauser, N. Jucker, PJM. Hulshof, HAJ. Meijer, A. Thalheimer, RE. Steinert, PA. Gerber, AC. Spector, D. Gero, M. Bueter
Validity Assessment of the SNAQ App for Estimation of Daily Energy Intake in Adult Females with Normal Weight and Obesity.

700
S M. Pickering, G. Pontarollo, A E. Kremer
Seladelpar treatment reduces Interleukin-31 and Pruritus in patients with Primary Biliary Cholangitis

705
D. Kundert
Reduction in surgical site infections thanks to microbial reduction of the nasal cavity with antimicrobial photodynamic therapy

717
I. Iskender, S. Hillinger, D. Schneiter, O. Lauk, G. Lang, I. Opitz, C. Caviezel
Is it Safe to Remove Chest Drains Without a Priori Chest X-ray Following Anatomical Lung Resections in Patients With Non-Small Cell Lung Cancer

609

P. Wolint[2], S. Hofmann[2], J. von Atzigen[2], R. Böni[3], I. Miescher[2], M. Calcagni[2], MY. Emmert[1], J. Buschmann[2]

Angiogenic foot print of human stem cell-based secretome - assessment of vascular network complexity with relevance to regenerative medicine

Institute for Regenerative Medicine (IREM), University of Zurich[1], Plastic Surgery and Hand Surgery, University Hospital Zurich[2], White House Center for Liposuction, Zurich[3]

Introduction:
Angiogenesis, the formation of new blood vessels, plays a crucial role in tissue regeneration. However, standardizing angiogenesis assessments remains challenging. In this study, these issues were addressed by comparing different matrices as well as mesenchymal stem cell (MSC)-derived secretomes of different cell formats and by introducing a modified angiogenic activity index (AAI) combined with a novel angiogenic profile.

Methods:
Collagen I, egg white, Jellagel, Matrigel were evaluated and the angiogenic potential of human MSC-derived secretomes harvested from spheroids with a size of 250 or 8000 cells and single cell cultures were assessed, both by performing the chicken aortic ring assay. Aortas were isolated from chicken embryos after 14 days of fertilization and cut in small rings of approximately 1 mm thickness. After secretome treatment was performed, microscopic images were taken on days 1, 4 and 7 and analyzed using software ImageJ. Based on the parameters, the AAI was calculated and the angiogenic profile was established.

Results:
Matrigel outperformed other matrices in promoting angiogenesis. Egg white and collagen matrix showed no outgrowth after 7 days. According to the AAI, the spheroid small secretome group had decreased angiogenesis compared to the control group, while both the single cells and spheroid large secretome groups exhibited pro-angiogenic values. The large group of spheroids showed the most comprehensive proangiogenic profile compared to all groups studied.

Conclusion:
MSC-derived secretomes, with particular attention to large spheroids, are influential in angiogenesis. The aortic ring assay is a powerful tool for assessing angiogenic potential. Standardization through the AAI could enhance the validity and reproducibility of results, with potential applications in regenerative medicine.

610

F. Guan[1], C. Brunckhorst[1], F. Duru[1], F. Ouyang[1], AM. Saguner[1]

Epicardial Catheter Ablation of Ventricular Tachycardia in Patients of Arrhythmogenic Cardiomyopathy - from a university hospital report in Switzerland

Univerisity Hospital Zurich[1]

Introduction:
Arrhythmogenic left ventricular cardiomyopathy (ALVC) as a subtype of arrhythmogenic cardiomyopathy (ACM) is increasingly being recognized. Cardiac magnetic resonance (CMR) has emerged as the primary imaging modality for the diagnosis of ACM. In patients with right-dominant ACM (ARVC) and recurrent sustained ventricular tachycardia (VT), endocardial +/-epicardial ablation yields good clinical outcomes in the long-term. However, studies on VT ablation in ACM with LV involvement are scarce. We sought to investigate clinical outcomes of VT ablation in ACM patients with LV involvement.

Methods:
The study included patients from the Zurich ACM Registry who met 2020 “Padua Criteria” for ACM and underwent VT ablation between January 2018 and July 2023. Epicardial ablation was performed in patients with recurrent sustained VT despite endocardial ablation, those lacking and endocardial substrate or if the ECG of the VT / substrate on CMR was suggestive of an epicardial origin. Catheter ablation was guided by activation/entrainment mapping for mappable VT, and pace mapping/voltage mapping during sinus rhythm for unmappable VT. Consecutive follow-up of all patients was performed according to our protocol.

Results:
Twenty-one ACM patients underwent n=24 VT ablation procedures. Of those 20 patients, 6 patients (30%) had LV involvement on CMR. Eight (33%) patients underwent epicardial +/- endocardial ablation. Among patients receiving epicardial ablation, 3 patients (38%) had LV involvement. These three underwent a single ablation procedure, which was epicardial only. Total follow-up was 30 months (range 4-43). Three-month sustained VT/VF recurrence rates were 12% in the ACM group with LV involvement vs 25% in ACM without LV involvement. All patients with sustained VT/VF recurrence underwent repeat ablation via an epicardial approach within 3 months and were free of sustained VT/VF thereafter during a median follow-up of 12 months. One-year recurrence rate did not differ between ACM patients with LV involvement vs. without LV involvement (7.7% vs 8.3%, $P=0.117$). Seven out of eight epicardial ablations achieved freedom from VT/VF after one-year follow-up. One ARVC patient with previous endocardial ablation had recurrent VT one month after epicardial ablation, which was free of VT after Flecainide combined with beta-blocker. No significant differences were found in the use of beta-blockers and antiarrhythmic drugs between both groups (ACM with LV involvement vs. without LV involvement) at baseline and during one-year follow-up.

Conclusion:
Single or adjuvant epicardial substrate ablation of VT in arrhythmogenic cardiomyopathy is promising in terms of postprocedural VT free survival, especially in patients with left ventricular involvement demonstrated by CMR.

611

F. Guan[1], C. Brunckhorst[1], T. Wolber[1], A. Breitenstein[1], N. Molitor[1], G. Suna[1], F. Duru[1], AM. Saguner[1]

High-density Mapping-Guided Ventricular Tachycardia Ablation in Patients with Ischemic Cardiomyopathy: Outcomes from a Tertiary Center Cohort in Switzerland

Univerisity Hospital Zurich[1]

Introduction:
Substrate-based ablation has emerged as a successful technique for VT ablation, especially in patients with ischemic cardiomyopathy with markedly reduced left ventricular function. High-density mapping catheters provide high-resolution electroanatomical maps and better discrimination of abnormal substrates and local activation in the heart chambers, making them a valuable and safe resource in the electrophysiology laboratory. The purpose of this study was to investigate differences in procedural characteristics and clinical outcomes of VT ablation with ischemic cardiomyopathy. VT ablations were guided by two mapping strategies: high-density mapping using a high-density mapping catheter and conventional mapping using an ablation catheter.

Methods:
Patients with ischemic cardiomyopathy receiving VT ablation at the Heart Center of the University Hospital Zurich between January 2018 and June 2023 were retrospectively included. Procedural characteristics and clinical outcomes were compared between patients receiving high-density mapping with a multielectrode-mapping catheter vs conventional mapping with a single-tip irrigated ablation catheter.

Results:
Eighty-four patients with ischemic cardiomyopathy who underwent VT ablation were consecutively included (mean age 67 ± 12 years, mean LVEF 32 ± 11 %, 79 (94%) males). Fifty-seven (68 %) procedures were performed using high-density mapping, and 27 (32 %) conventional mapping. In the high-density mapping and conventional mapping group, the total procedure time was 256 ± 77 min vs. 232 ± 61 min ($P < 0.05$) and the total fluoroscopic dose was 1643 ± 204 µGy.m^2 vs. 948 ± 105 µGy.m^2 ($P < 0.05$), respectively,. However, there was no difference between the two groups in terms of acute success (84% vs 80%, $P > 0.05$) or major complications (5% vs 4%, $P > 0.05$). The mean duration of follow-up was 2.6 years (4 - 51 months). The 1-year mortality rates were 4% vs 7% in the high-density mapping and conventional mapping groups, respectively ($P < 0.05$). The 3-month and 1-year single-procedural sustained VT/VF-free rates were 77% vs 59% and 74% vs 63%, respectively ($P < 0.05$). The 1-year incidence of sustained VT/VF recurrence was 7.0 per 100 person-years in high-density mapping group, compared with 7.4 per 100 person-years in the conventional group.

Conclusion:
VT ablation in patients with ischemic cardiomyopathy using high-density mapping appears to be superior to conventional mapping in terms of reducing postprocedural VT/VF recurrence and a subsequent reduction of overall mortality.

612

I. Miescher[3], N. Schaffner[3], J. Rieber[3], G. Meier Buergisser[3], E. Ongini[1], A. Milionis[2], Y. Yao[2], V. Vogel[2], J.G. Snedeker[1], P. Giovanoli[3], M. Calcagni[3], J. Buschmann[3]

Reducing peri-tendinous adhesion to zero: commodity materials hyaluronic acid/PEO are highly efficacious when applied as electrospun tubes around repaired tendons

Balgrist University Hospital Zurich[1], ETH Zurich[2], Plastic Surgery and Hand Surgery, University Hospital Zurich[3]

Introduction:
Tendon injuries go ahead with a long healing time because of the poor regenerative tissue capacity. Re-rupture, adhesion to the surrounding tissue, scarring and joint stiffness are common clinical problems after surgery. Despite progress in the treatment options, tendon repair remains difficult and methods to improve tendon healing are of big interest.

We produced an electrospun DegraPol® (DP) tube containing a layer of hyaluronic acid and polyethylene oxide (HA/PEO), with the aim to use HA as biolubricant and improve the anti-adhesive effect of the DegraPol® tube used in earlier studies applied in a rabbit full laceration Achilles tendon model. In order to investigate attachment of tenocytes on the scaffolds and extracellular matrix (ECM) production, tenocyte seeded scaffolds were analyzed with scanning electron microscopy (SEM) and light microscopy after immunocytostaining. Properties of the new electrospun material were examined with SEM and by mechanical tests.

Methods:
Implants were produced using an in-house assembled electrospinning device. For the in vivo experiment, three New Zealand White rabbits received the HA/PEO/DP tube implanted for three weeks before rabbits were sacrificed. Tendons were extracted and histologically analyzed with Picrosirius Red. Cell seeded scaffolds were stained for Collagen I and cell attachment was examined on SEM images. Surface morphology of the different scaffolds was investigated using SEM images and mechanical properties were determined using a uniaxial load test machine.

Results:
Application of HA/PEO containing DP tube reduced adhesion of sutured tendons significantly by about 50 % compared to sutured tendons treated with pure DP implants and reached adhesion levels as in native tendons. Scanning electron microscope images show that tenocytes are able to attach to the fibers and Collagen I labeling proofs that tenocytes are capable to produce ECM. Scanning electron microscopy images show a network of random fibers with a diameter of about 6 µm in average in every material. Pore sizes of HA/PEO containing scaffolds were larger than in pure DP scaffolds but overall diameters are similar with sizes from from 8 to 15 µm in average. Mechanical tests showed better mechanical properties of HA/PEO containing tubes with higher axial values than transversal values demonstrating the anisotropy of the material.

Conclusion:
Our electrospun DP implant with a layer of HA/PEO reduced adhesion formation in a rabbit full laceration Achilles tendon model significantly compared to a pure DP implant, reaching a level comparable to healthy tendons. In vitro studies have shown that rabbit tenocytes are able to attach on every scaffold material and to produce ECM. Surface morphology of the different materials was similar showing a network of random fibers. The mechanical properties of HA/PEO/DP tubes were increased compared to pure DP tubes facilitating the handling of the implants during surgery. Our results demonstrate that an additional HA/PEO layer on an electrospun DP scaffold shows promising potential in reducing adhesion formation after tendon surgery and has great prospect for a clinical application in the future.

613

S. Guerra[1], D. Birrer[1], P. Clavien[2], B. Humar[1]

Metabolic needs define the physiological limits of the liver's regenerative capacity

Laboratory of the Swiss Hepato-Pancreato-Biliary and Transplantation Center, Department of Surgery, University Hospital Zurich[1], Privatklinik Bethanien, Toblerstrasse 51, 8044 Zürich[2]

Introduction:
The capacity of the liver to regenerate is outstanding but limited. The need to perform metabolic tasks also after tissue loss may restrain the proliferative ability of hepatocytes. To provide evidence for the latter, we took advantage of ALPPS surgery, where portally ligated lobes remain *in situ.* At the same time, the non-ligated future liver remnant (FLR) regenerates at unprecedented speed. We pursued the hypothesis that ligated lobes function like an auxiliary liver to unleash the regenerative potential of the FLR.

Methods:
Mice were divided into groups undergoing either sham or ALPPS surgery. Tissue from the sham liver, the FLR, and the adjacent ligated right median lobe (RML) was separately analysed by omics (metabolomics/lipidomics alongside transcriptomics). To address the role of ligated lobes (LLs), functional surgery was designed to create ALPPS variants with gain or loss of ligated volume.

Results:
Principal Component Analysis (PCA) was applied to significantly distinct metabolites derived from sham and ALPPS liver lobes. It unveiled a marked metabolic divergence between the FLR and RML, specifically during the major growth phase post-ALPPS. While the FLR and RML exhibited heightened energy demands driven by active lipid oxidation, activities related to cell cycle and proliferation were specifically upregulated in the FLR. Vice versa, the RML was enriched with classic metabolic liver tasks (gluconeogenesis, glycogen synthesis, bile acid metabolism, bilirubin clearance, xenobiotic detoxification, and synthetic function) as corroborated by immunohistochemistry. Functional surgery revealed a strict dependence of the FLR regenerative speed on the presence of LLs.

Conclusion:
Our observations propose that the ligated lobes function as an auxiliary liver during the process of ALPPS regeneration. This auxiliary role allows the future liver remnant (FLR) to dedicate itself entirely to proliferation, thereby accelerating the regenerative process. Our findings provide the first functional evidence for metabolic pressure as a critical determinant defining the liver's regenerative capacity.

614

N. Ziak[2], A. Abidi Ostorero[1], M. Generali[1], T. Hornemann[2], M. Lone[2]

Understanding the selective neurotoxicity of Serine-palmitoyltransferase mutations towards motor and sensory neurons

Institute for Regenerative Medicine of University of Zurich[1], University Hospital Zurich[2]

Introduction:
Sphingolipids (SLs) are a diverse class of lipids that play crucial roles in various cellular functions, including cell structure and signaling. Dysregulation in their metabolism contributes to various neurological disorders such as Amyotrophic Lateral Sclerosis (ALS). Notably, ALS manifests as specific degradation of motor neurons while sparing sensory neurons. Certain mutations in the serine-palmitoyltransferase (SPT), the first and rate-limiting enzyme in the de novo SL synthesis, are linked to ALS. Interestingly, another group of mutations in the same enzyme leads to an opposing clinical phenotype, namely Hereditary Sensory and Autonomous Neuropathy type 1 (HSAN1). It manifests as sensory loss, including pain, pressure, temperature and vibration. HSAN1 mutations result in the pathological formation of atypical and neurotoxic 1-deoxysphingolipids (1-deoxySL) by altering the substrate specificity of the enzyme from serine to alanine. Whereas SPT-ALS mutations impair the homeostatic control of the enzyme, which results in an uncontrolled and overshooting formation of SL species. This PhD project aims to unravel the mechanisms causing selective neurotoxicity of the SPT-ALS and SPT-HSAN1 mutations toward sensory and motor neurons, by studying the differentiation of mutant cells into the respective neuron types.

Methods:
In vitro models for neuron differentiation: We will start with a simple in vitro model, in which neuronal differentiation is induced trough transcription factor overexpression. By a genetic engineering approach, the cells are transfected with a vector, carrying at least the master of neuronal differentiation transcription factor Neurogenin-2 (NGN2). After adding doxycycline, neuronal differentiation is induced. This model is called induced Neurons (iNeurons). We are interested in all models in the sphingolipid profiles of mature motor and sensory iNeurons looks and how it changes during the differentiation. Further, we are curious what happens when we perturb the sphingolipid metabolism. ALS can be mimicked by supplementing with ceramide, whereas HSAN1 is imitated by adding 1-deoxysphinganine and increasing the alanine to serine ratio. The effects of pharmacological inhibitors, which specifically block enzymes, e.g., Myriocin for SPT, could also be assessed. The more complex model is generating an isogenic iNeurons model by introducing patient specific mutations by CRISPR-Cas9. The mutations L39del and F40S41del for ALS, C133W for HSAN1 and S331 for the mixed phenotype will be used.As a more physiological model we will differentiate patient derived induced pluripotent stem cells (iPSCs) into motor and sensory neurons by a small-molecule approach. The patient derived iPSCs carry the same mutations as in the second iNeurons experiment. As control, cell lines serve DW8 and HMGU1. All cell lines are differentiated into both neuron types. The neuron differentiation will be monitored, including assessment of specific developmental markers through immunohistochemistry and quantitative PCR, e.g., Hb9 for motor/ BRN3A for sensory neurons. The sphingolipid profiles will be assessed by mass spectrometry. Searching for biomarkers in lipid profiles: sphingolipid profiles of patients having SPT mutations will be compared, including both previously published mutants and recently identified mutants.

Results:
Preliminary results indicate that there are differences in differentiation between the control cell lines (DW8, HMGU1) and the mutant cell lines.

Conclusion:
The in vitro models models allow us to study and manipulate pathomechanisms underlying selective neurotoxicity in sensory neurons and motor neurons, potentially revealing novel therapeutic targets. Additionally, the characterization of ALS-associated SPT variants will be carried out. Potential biomarkers, which we find in this analysis, could assist in the diagnosis, but might also play a role in idiopathic ALS cases.

615

C. Litchfield[1], R. Nienhold[1], M. Adamczyk[1], U. Wagner[1], M. Schmid[1], D. Seidl[1], D. Aguilera[1], V. Kölzer[1], M. Zoche[1], J. Rüschoff[1], H. Moch[1], A. Sobottka-Brillout[1]

Diagnostic Whole Genome Sequencing: Hydra of hopes and hurdles

University Hospital Zürich, Department of Pathology and Molecular Pathology, Zürich, Switzerland[1]

Introduction:
The continuous advancement of next generation sequencing (NGS) has made whole genome sequencing (WGS) cost-effective and practical for clinical diagnostics. Although classical targeted NGS panels cover key markers of the most prevalent tumors, studies evaluating WGS in a clinical setting suggest improved off-label treatment options for patients with rare cancers or end-stage diseases. Therefore, the Department of Pathology and Molecular Pathology at the University Hospital Zürich aims to establish WGS for diagnostic purposes.

Methods:
Total nucleic acids were extracted from the tumor and matched-control tissue. Next-generation sequencing was performed with an average coverage of 60x for tumor and 30x for normal. In-house bioinformatics pipelines have been established to analyze raw data and identified established and emerging biomarkers.

Results:
Our primary objective was to compare the outcomes of WGS against a well-established gold standard of targeted NGS panel in the metastatic melanoma Tumor Profiler cohort. The majority of SNVs reported by FoundationOne CDx were detected by WGS, and we observed a strong correlation of the variant allele fraction. Our results also showed a strong correlation for TMB and absolute CNVs. The validation of MSI, HRD and structural variants are planned following the sequencing of additional cancer entities, where these biomarkers are well represented. Furthermore, WGS enables detecting emerging biomarkers, which currently cannot be validated due to a lack of standards. We also propose possible solutions concerning regulations for germline testing, automated variant annotation and reimbursement by health insurance companies. Lastly, we created an automated reporting engine that condenses the obtained information to the level of a conventional NGS report.

Conclusion:
Based on this experience, we are planning a study employing WGS for cancer patients who have completed therapy. Here, we aim on (1) validating the clinical utility of WGS and (2) gaining additional knowledge with WGS in diagnostic routine.

616

S. Salemi[1], L. Breitenmoser[1], V. Baumgartner[1], D. Planta[1], M. Horst[1], D. Eberli[1]

Comparative Analysis of Mitochondrial Function in Human Neuropathic and Normal Bladder Detrusor Smooth Muscle Cells

Department of Urology, University Hospital Zürich[1]

Introduction:
Tissue engineering and cell-based therapies utilizing smooth muscle cells present potential alternative treatments for conditions such as end-stage lower urinary tract dysfunction (ESLUTD), urinary incontinence, and bladder dysfunction. While the use of autologous cells has been considered, concerns arise regarding the maintenance of a pathological phenotype in neuropathic detrusor smooth muscle cells during culture. Therefore, the aim of this project is to compare hSMCs derived from neuropathic and normal pediatric bladder detrusor biopsies, investigating various parameters related to mitochondrial function.

Methods:
Human bladder-derived smooth muscle cells (SMCs) were isolated and characterized using flow cytometry. Proliferation was assessed through the WST-1 assay. Mitochondrial metabolic changes were analyzed using mitoplate and Seahorse assays. The expression of mitochondrial-related genes and proteins was investigated through real-time PCR, immunoblotting, and immunofluorescent staining.

Results:
Neuropathic hSMCs exhibited reduced proliferation and decreased expression of contractile markers. Tissue analysis indicated a decreased muscle-to-collagen ratio with disrupted muscle bundles infiltrated by collagen. Metabolic analysis revealed normal but potentially impaired respiration, pyruvic acid, and α-ketobutyric acid metabolism, along with significantly decreased lactate production. In neuropathic cells, a reduction in the expression of mitochondrial genome regulator TFAM, complex IV subunit COX4I1, and regulator PGC-1α was observed. However, membrane potential, reactive oxygen species regulation, and fission-fusion dynamics remained normal.

Conclusion:
The results imply a partial reduction in mitochondrial function in neuropathic hSMCs, without complete loss. Addressing these mitochondrial aspects may offer a potential means to improve cell function and reverse their pathological characteristics. This study suggests that autologous hSMCs remain a viable option for developing tissue-engineered bladder grafts, providing a potential strategy to enhance treatment for neuropathic bladder patients.

617

E. Parietti[2], D. Bivona[1], A. Tarnutzer[2], D. Bongiorno[1], N. Musso[1], S. Stefani[1], SM. Shambat[2], A. Zinkernagel[2]

Assessment of Staphylococcus aureus phenotypic heterogeneity mediated by small colony variant formation

Department of Biomedical and Biotechnological Sciences (BIOMETEC), Section of Microbiology, University of Catania, Catania, Italy[1], Department of Infectious Diseases and Hospital Epidemiology, University Hospital Zurich, University of Zurich, Zurich, Switzerland[2]

Introduction:
S. aureus small colony variants (SCVs) represent a subpopulation of bacteria, which acquired mutations in genes involved in metabolism, leading to an extended generation time compared to their parental strain. SCVs are able to persist intracellularly in nonprofessional phagocytes and are often difficult to eradicate with antibiotics alone resulting in recurrent infections. The aim of this project was to investigate the capacity of *S. aureus* SCV to adapt to the stressful environment in the host and antibiotics. To this end, we compared two clinical *S. aureus* strains, the wild-type (WT) (IS1) and its naturally occurring counterpart SCV (IS2) strain, isolated from a patient with osteomyelitis.

Methods:
Both *S. aureus* strains were genotypically characterized by whole genome sequencing. For the phenotypical characterization, growth was analyzed in liquid culture and kinetic of colony growth on blood agar plate was quantified with ColTapp. To characterize the stress response, survival of bacteria and antibiotic tolerance capacity was measured after 3 days of pH5.5 stress or after extended nutrient deprivation (1, 3, 6 days).

Results:
The two strains were identified as MSSA-ST1. A point mutation with deletion in a gene encoding for a cysteine hydrolase was found in SCV-IS2 strain. A comparable growth rate of the two strains were observed, but an extended lag-phase for SCV-IS2 compared to WT-IS1 was identified. After 3 days of pH-stress, the survival rate of the two strains was comparable, but a higher formation of persisters in SCV-IS2 was measured as compared to WT-IS1. A higher persister formation in IS2 was observed also after extended nutrient deprivation.

Conclusion:
The SCV-IS2, due to the genetic mutation, showed a higher capacity to adapt to the host stress environment, such as acid pH and nutrient deprivation, and survive high concentrations of antibiotic, leading to an increased antibiotic tolerance. The genetic mutation in the cysteine hydrolase resulting in a truncated protein could be responsible for the observed phenotype. Nevertheless, further studies are needed to better assess the role of this mutation in SCV formation and persistence.

618

E. Parietti[1], A. Gómez Mejia[1], CC. Chang[1], J. Bär[1], S. Shambat[1], A. Zinkernagel[1]

Rifampicin impairs intracellular eradication of Staphylococcus aureus by human macrophages

Department of Infectious Diseases and Hospital Epidemiology, University Hospital Zurich, University of Zurich, Zurich, Switzerland[1]

Introduction:
Staphylococcus aureus is one of the major causes of both community and hospital associated infections, ranging from superficial skin lesions to life-threatening infections such as bacteremia and pneumonia to chronic/recurrent infections, including endocarditis and osteomyelitis. Infections with *S. aureus* are very difficult to treat, not only due to the development of antibiotic resistance, but also because of the formation of so-called persister cells. Persisters are a subpopulation of bacteria in a dormant phase that can survive high concentrations of antibiotics. It has been observed that the intracellular milieu of the host cells can trigger the formation of *S. aureus* non-stable small colonies (nsSCs) which have been associated to an increase in persistence. In this context, macrophages represent a privileged niche for *S. aureus* persistence. Therefore, the failure to completely eradicate persisters can result in relapse of infections when persisters resume growth upon removal of antibiotic treatment. Rifampicin in an antibiotic that can penetrate the host cells and target intracellular bacteria. It is also known to have immunomodulatory properties, and interact with host immune cells altering mitochondrial function, bioenergetics and immune cell function. In this project, we study the effect of rifampicin during *S. aureus* infection of macrophages, investigating the effect of the drug on macrophage activation and effector response and the effectiveness of rifampicin in eradicating intracellular *S. aureus* persisters.

Methods:
Human monocyte-derived macrophages (hMDMs) were infected with *S. aureus* and different combinations of antibiotics (flucloxacillin and rifampicin, alone or in combination) were used to treat macrophages after the infection along with rifampicin pre-treatment. First, we determined *S. aureus* uptake by macrophages and the kinetic of intracellular survival, making a comparison among different antibiotic treatments. In addition, we assessed *S. aureus* persister formation inside macrophages by measuring colony size heterogeneity using automated plates imaging and the ColTapp software. In a second step, we performed a multi-parametric flow cytometry analysis to measure the intracellular reactive oxygen spices (ROS) and reactive nitrogen spices (RNS), antimicrobial molecules used by macrophages, which were recently found to play a role in the generation of intracellular persisters.

Results:
We found that pre-treatment of macrophages with rifampicin increased the phagocytosis of *S. aureus* by macrophages and reduced the intracellular killing capacity against *S. aureus*. At the same time, the pre-treatment of macrophages with rifampicin reduced intracellular *S. aureus* nsSCs, which were associated with an increase in persistence. Our flow cytometry data showed that pre-treatment of macrophages with rifampicin dampened intracellular RNS production upon infection, while we did not find any significant difference in ROS production.

Conclusion:
Our data show that rifampicin exposure of macrophages before *S. aureus* infection altered the capacity of the cells to respond to bacteria. Specifically, exposure of macrophages with rifampicin had an effect on the phagocytosis of *S. aureus*, intracellular killing capacity and nsSC formation. The decrease in intracellular killing and nsSC formation could be a consequence of the inhibition of RNS production in macrophages following rifampicin treatment. Indeed, RNS are known to have an antimicrobial function and, more recently, they were found to be involved in *S. aureus* persistence inside macrophages. Nevertheless, further investigations are needed to verify these results. Considering the prominent role of *S. aureus* persistence in antibiotic treatment failure, this translational project has the potential to advance the current understanding as well as develop new strategies aimed to curb recurrent *S. aureus* infections.

619

J. Bär[1], SGV. Charlton[2], A. Tarnutzer[1], GS. Ugolini[2], E. Secchi[2], AS. Zinkernagel[1]

Single-cell Staphylococcus aureus agr quorum-sensing dynamics during signal pulses and community interactions

Department of Infectious Diseases and Hospital Epidemiology, University Hospital Zurich, University of Zurich, Zurich, Switzerland[1], Institute of Environmental Engineering, ETH Zurich, Zurich, Switzerland[2]

Introduction:
The *accessory gene regulator* (*agr*) quorum sensing system (QS) of *Staphylococcus aureus* is critical for virulence regulation and plays a pivotal role in the transition from a colonizing to an invasive state. Understanding this system is mandatory for virulence management in patients especially due to the increasing challenge of antibiotic resistance and persistent infections. The four known *agr* types are distinguished by the amino acid sequence of the QS signal called autoinducing peptide (AIP) and cross-inhibit each other.

Methods:
We used four *agr* prototype lab strains and exposed them to specific concentrations of synthetic AIPs in mother-machine microfluidic devices, creating chemically stable environments without accumulation of self-produced AIP. Additionally, we employed innovative microfluidic chips with large chambers connected by nanochannels allowing chemical interactions between communities while preventing cell translocation. Through microscopy and deep-learning image analysis for cell segmentation and tracking, we quantified *agr* activity from a fluorescent reporter plasmid, achieving unparalleled single-cell resolution.

Results:
We uncovered notable differences in AIP sensitivity among the *agr* types, elucidating a complex picture of quorum sensing modulation. *Agr* type *II* notably displayed heightened sensitivity to AIPs and a distinctive increase in the time between cell divisions upon AIP stimulation, hinting at a unique physiological response. We also observed a remarkable intergenerational stability of the *agr* response within bacterial lineages, suggesting a phenotypically heritable component to how bacteria respond to their community's signals. This could indicate a persistent memory effect in bacterial behavior, an insight with profound implications for understanding chronic infections and treatment failure. The observed differences in AIP sensitivity and the unique generation time increase of *agr-II* could however not be explained by differential gene expression of known regulators of the *agr* system but may be linked to differences in genetic background among the tested strains. Our analysis further confirmed the antagonistic cross-inhibition typical of heterologous AIPs at a single-cell level, adding depth to our understanding of *agr* interactions. Diving deeper, we explored how different *agr* types interact within larger microbial communities utilizing coupled microfluidic chambers. Our findings revealed a spectrum of interaction dynamics. While one *agr* type often dominated the other, our data unveiled instances of dual-activation and dynamic switching of *agr* activation states. Importantly, these interactions exhibited variability based on the *agr* type combination and were influenced by early *agr* states and community sizes.

Conclusion:
This nuanced understanding of *agr* dynamics opens new avenues for targeted therapeutic strategies. By deciphering the conditions and interactions that regulate virulence, we can develop interventions that disrupt pathogenic behavior without resorting to traditional antibiotics. Such strategies might involve designing synthetic inhibitors or leveraging the natural antagonistic compounds produced by other bacterial species. Our work not only advances the fundamental understanding of bacterial communication and virulence regulation but also lays the groundwork for innovative approaches to treat and manage *S. aureus* infections, addressing a critical need in the era of rising antibiotic resistance.

620

E. Gorica[1], S. Costantino[1, 4], A. Elkhal[5], O. Dzemali[1, 2, 3], F. Paneni[1, 4], H. Rodriguez Cetina Biefer[1, 2, 3]

NAD+ Supplementation as a Potential Therapeutic Approach in Cardiotoxicity

Center for Translational and Experimental Cardiology (CTEC), Department of Cardiology, Zurich University Hospital and University of Zürich, Zürich, Switzerland[1], Department of Cardiac Surgery, Municipal Hospital of Zurich-Triemli, Zurich, Switzerland[2], Department of Cardiac Surgery, University Hospital of Zurich, Zurich, Switzerland[3], Department of Cardiology, University Heart Center, University Hospital Zurich, University of Zurich, Zürich, Switzerland[4], NAD, Immunology Laboratory, Huntington Medical Research Institutes, Pasadena, CA, USA[5]

Introduction:
Doxorubicin (DOX) is an effective chemotherapeutic treatment known for its severe side effect of cardiotoxicity, which can lead to heart failure. The mechanisms behind DOX-induced cardiotoxicity (DIC) are not fully understood but are often associated with oxidative stress and inflammation. Recent studies suggest that nicotinamide adenine dinucleotide (NAD^+) and other derivatives could prevent or reduce this cardiotoxicity. Therefore, in this study, we aim to evaluate the cardioprotective effects of NAD^+ in mitigating the side effects of DOX treatment in cancer patients. This study investigates the potential cardioprotective effects of nicotinamide adenine dinucleotide (NAD^+) in mitigating DIC.

Methods:
H9c2 rat cardiomyocytes underwent a 48-hour NAD^+ pretreatment at 100µM, a 24-hour exposure to 500nM DOX, and a subsequent 48-hour NAD^+ treatment at 100µM. The MTT assay determined cell viability, while mitochondrial reactive oxygen species (ROS) production was quantified with the MitoSOX assay. Gene expression relevant to cardiac cell development and function was analyzed via quantitative polymerase chain reaction (RT-PCR). Western blotting (WB) assessed the modulation of oxidative stress and apoptosis markers.

Results:
NAD+ treatment maintained myocardial cell viability in the presence of DOX and modulated gene expression beneficial for cardiac function, including downregulation of pro-inflammatory cytokines such as IL1b and TNF-a. Furthermore, it reduced oxidative stress markers, decreased levels of pro-apoptotic Caspase 3, and increased levels of the antioxidant SOD2, potentially via an upregulation of Sirt1.

Conclusion:
Our findings highlight the critical importance of a multidisciplinary research approach to elucidate the cardioprotective capacity of NAD^+ against DIC, potentially paving the way for new targeted strategies in oncological therapies.

621

K. Krebs[1], A. Rossi[1], S. Jurisic[1], M. Gajic[1], T. Albertini[1], P. Heiniger[1], A. Galafton[1], A. Pazhenkottil[1], P. Kaufmann[1], R. Buechel[1], D. Benz[1], A. Giannopoulos[1]

Effect of Image Reconstruction Algorithms in Pericoronary Adipose Tissue Attenuation obtained with Coronary CT Angiography

Department of Nuclear Medicine, Cardiac Imaging, University Hospital Zurich[1]

Introduction:
Pericoronary adipose tissue (PCAT) attenuation measured at coronary CT angiography (CCTA) can detect vascular inflammation and is a useful diagnostic and prognostic marker. Modern iterative and artificial-intelligence-based CCTA reconstruction methods can affect image noise and overall image quality. We aimed to investigate the potential influence of different CCTA image reconstruction algorithms on PCAT attenuation measurements.

Methods:
Patients referred for clinically indicated CCTA between March 2015 and June 2016 were retrospectively included. Datasets were reconstructed with filtered back projection (FBP), with adaptive statistical iterative reconstruction-Veo (ASiR-V) and with deep-learning image reconstruction (DLIR). In all three reconstructions, mean PCAT was evaluated in the three major epicardial coronary arteries using dedicated software (QAngio CT Research Edition version 3.2.0.13, Medis Medical Imaging Systems) and was defined as the area with an attenuation between − 30 and − 190 Hounsfield Units (HU) within a radial distance from the outer vessel wall equivalent to the diameter of the vessel. The proximal 40 mm segments of the left anterior descending artery (LAD) and left circumflex artery (LCx) and the proximal 10–50 mm segment of the right coronary artery (RCA) were analyzed. Using FBP ($PCAT_{FBP}$) as reference standard, correlation and agreement of PCAT estimates using ASIR-V ($PCAT_{ASIR\text{-}V}$) and DLIR ($PCAT_{DLIHR}$) reconstructions were assessed.

Results:
In 39 patients (mean age 57.9±11.2 years, 90% men), 117 arteries were analyzed. Mean $PCAT_{FBP}$ attenuation of the overall population was -79.9 ±9.4 HU and did not differ significantly compared to $PCAT_{ASIR\text{-}V}$ and to $PCAT_{DLIR}$ (-80.9±8.9 HU and -78.5±9.5 HU, respectively; p_{ANOVA}=0.123). Correlation was excellent for all comparisons [$PCAT_{FBP}$ vs. $PCAT_{ASIR\text{-}V}$; r=0.99, (y=4.68+1.046x, p<0.001), $PCAT_{FBP}$ vs. $PCAT_{DLIR}$; r=0.99 (y=-3.57+0.973x, p<0.001)]. Intraclass correlation coefficient was excellent for all reconstructions [$PCAT_{FBP}$ vs. $PCAT_{ASIR\text{-}V}$; 0.99 (95% confidence interval: 0.98-0.99), $PCAT_{FBP}$ vs. $PCAT_{DLIR}$; 0.98 (95% confidence interval: 0.98-0.99), all p<0.0001]. Agreement with Bland-Altman analysis was high with small mean absolute differences and relatively narrow limits of agreement [$PCAT_{FBP}$ vs. $PCAT_{ASIR\text{-}V}$; Bias: 1.0 HU (95% limits of agreement: -1.4 – 3.3), $PCAT_{FBP}$ vs. $PCAT_{DLIR}$; Bias: -1.5HU (95% limits of agreement: -4.4 – 1.4)].

Conclusion:
CCTA-derived PCAT measurements using advanced iterative image reconstruction– and deep-learning image reconstruction–algorithms have excellent correlation and high agreement compared to conventional image reconstruction algorithms and could be potentially interchangeably used.

622

I. Miescher[4], J. Rieber[4], T. Schweizer[2], M. Orlietti[3], A. Tarnuter[3], F. Andreoni[3], G. Meier Buergisser[4], P. Giovanoli[4], M. Calcagni[4], J. Snedeker[1], A. Zinkernagel[3], J. Buschmann[4]

In vitro assessment of Bacterial Adhesion and Biofilm Formation on Novel Bioactive, Biodegradable Electrospun Fiber Meshes Intended to Support Tendon Rupture Repair

Balgrist University Hospital Zurich[1], Department of Dermatology, University Hospital Zurich[2], Department of Infectious Diseases and Hospital Epidemiology, University Hospital Zurich[3], Plastic Surgery and Hand Surgery, University Hospital Zurich[4]

Introduction:
Surgical repair of ruptured tendons faces challenges: increased fibrous adhesion, inferior mechanical properties, and bacterial attachment to implants, hindering recovery and causing severe infections. A novel implant material, known as DegraPol® (DP), which has previously demonstrated a reduction in fibrous adhesion *in vivo* was used. To further enhance the healing process and mechanical properties, insulin-like growth factor-1 (IGF-1) was incorporated. Implant-associated infections pose significant challenges due to biofilm formation at the implant-tissue interface. The initial reversible bacterial adhesion is mediated by matrix components, and the material's chemical composition and surface characteristics play a crucial role. In orthopedics, both Gram-positive and Gram-negative bacteria can infect implants, leading to complications. To address this issue, implants were coated with silver (Ag) nanoparticles to mitigate the development of biofilms. Two novel materials, using hyaluronic acid (HA), known for anti-angiogenic and anti-inflammatory properties and PEO in 1:1 and 1:4 ratios were included as well. All materials were tested for biofilm formation with common surgical bacterial species with a total of ten different strains.

Methods:
Solutions were prepared; HA was mixed with respective amount of PEO and water, DP was mixed with Chloroform and hexafluoro-2-propanol and IGF-1 was added for one group. All the solutions were electrospun into a tube and punched into 5 mm circles. Some of the pure DP patches were submerged in an Ag nanoparticle solution overnight. By scanning electron microscopy (SEM) the fiber diameter and pore size were determined. The static and dynamic water contact angles were measured for surface characterization. Bacterial adhesion assays were conducted using 4 bacterial species; Staphylococcus aureus, Staphylococcus epidermidis, Pseudomonas aeruginosa and Enterococcus faecalis, and bacterial surface hydrophobicity was assessed through hexadecane-water partitioning.

Results:
DP-IGF-1 demonstrated the lowest water contact angle, indicating lower hydrophobicity. The bacterial strains exhibited varying hydrophobicity levels, with Staphylococcus aureus. being the most hydrophobic and P. aeruginosa the least. After 24 hours of incubation, biofilm formation significantly varied among the ten strains. However, the significance of these differences was not consistent across all strains within the same species. Generally, a reduced adherence to DP-IGF-1 compared to pure DP was observed. Although Ag treatment showed a trend towards reducing biofilm formation in four bacterial strains after 24 hours of incubation, none of these differences reached statistical significance. SEM images of bacterial adhesion of S. aureus SA1, revealed colonization not only on fibers but also within the pores.

Conclusion:
In this in vitro study, five electrospun materials (pure DP, DP-Ag, DP-IGF-1, HA:PEO 1:1, and HA:PEO 1:4) were assessed for bacterial adherence and biofilm formation. Pure DP meshes with higher hydrophobicity, exhibited higher biofilm formation than DP-IGF-1, while silver treatment showed a potential reduction in bacterial burden. The two HA:PEO blends showed similar biofilm formation. Despite proper sterilization and sterile surgery practices, bacterial proliferation and biofilm formation on all materials highlight the need for further optimization.

623

V. Ntinopoulos[1], H. Rodriguez Cetina Biefer[1], I. Tudorache[1], N. Papadopoulos[1], D. Odavic[1], P. Risteski[1], A. Haeussler[1], O. Dzemali[1]

Data extraction from unstructured medical records with the GPT-4 chatbot

University Hospital of Zurich[1]

Introduction:
This study presents a novel approach for using GPT-4 (generative pre-trained transformer 4) as a tool for data extraction from unstructured medical records and assesses its performance on this task.

Methods:
Fifty fictitious patient medical records were drafted in German language and GPT-4 was provided with instructions, on how to process each one. Data extraction involved text-mining and classification tasks for nine variables. The accuracy, recall, precision, and F1-Score of the GPT-4 model were assessed for each requested variable.

Results:
The accuracy of GPT-4 in data-mining tasks was 100% for all requested variables (patient identifier, EuroSCORE 2, admission and exit date). GPT-4 exhibited the following performance in classification tasks for each requested variable: stroke (accuracy 96%, F1-Score 95.80%), cardiac tamponade (accuracy 100%, F1-Score 100%), pacemaker implantation (accuracy 100%, F1-Score 100%), atrial fibrillation (accuracy 100%, F1-Score 100%) and death (accuracy 100%, F1-Score 100%).

Conclusion:
GPT-4 exhibited excellent performance in both text-mining and classification tasks. Reliable data extraction from unstructured medical records seems possible with the GPT-4 chatbot.

624

L. Sazgary[1], E. Theano Samara[3], A. Stüssi[3], M. Guckenberger[2], F. Ruschitzka[1], T. Wolber[1], N. Molitor[1], G. Fu[1], G. Suna[1], D. Hofer[1], A. Breitenstein[1], CB. Brunckhorst[1], F. Duru[1], AM. Saguner[1]

The Impact of Clinical Audits on Patient Radiation Exposure for Device Procedures

Cardiology Department, University Hospital Zürich[1], Department of Radiation Oncology, University Hospital Zurich[2], Radiation Protection Unit, University Hospital Zürich[3]

Introduction:
Clinical audits aim to ensure ideal use of ionizing radiation in clinical practice. Since it became mandatory by Swiss law in 2018, such an audit also took place in our Cardiac Pacing and Electrophysiology Division at the University Heart Center. The purpose of our study was to establish local diagnostic reference levels (DRLs) for specific procedures and to examine if patient radiation exposure was reduced after the clinical audit.

Methods:
Retrospective cohort study including patients from October 2018 to October 2020 who underwent device implantation, including pacemakers, implantable cardioverter defibrillators (ICD), cardiac resynchronization therapy (CRT), or lead extraction / device explantation. Main measures to reduce radiation exposure after the audit were lower pulsed fluoroscopy frame rates and dose characteristics at baseline. Patient radiation exposure was evaluated with the dose-area product (DAP), cumulative dose, fluoroscopy time, and the number of cine acquisitions. Secondary endpoints included the effective dose, the acute procedural success rate and 30-day complications. Data were collected from a dose management system and cross-checked for accuracy with the patient information system. The third quartiles were set as local DRLs. Data before and after the clinical audit were compared.

Results:
A total of 541 patients (45.7 % before the audit, 54.3% after the audit) were included. 28.3% had a conventional pacemaker, 22.0% a leadless pacemaker, 21.1% an ICD, and 17.2% a CRT implantation. Lead extraction / device explantation was undergone by 11.5% of patients. The local DRLs (including all procedures before and after the audit) for the DAP were significantly lower as compared to national DRLs (6.2 dGy.cm^2 vs 300 dGy.cm^2 for conventional pacemakers; 7.6 dGy.cm^2 vs 200 dGy.cm^2 for ICDs, 203 dGy.cm^2 vs 570 dGy.cm^2 for CRTs). After the audit, DAP (Figure 1), cumulative dose, effective dose and the number of cine acquisition significantly decreased for conventional pacemakers (p-value ≤ 0.04), whereas no significant differences were observed for the other procedures. The acute procedural success rate (98.4 vs 98.9%) and the 30-day complications (4.0 vs 7.8%) were not significantly different before and after the audit.

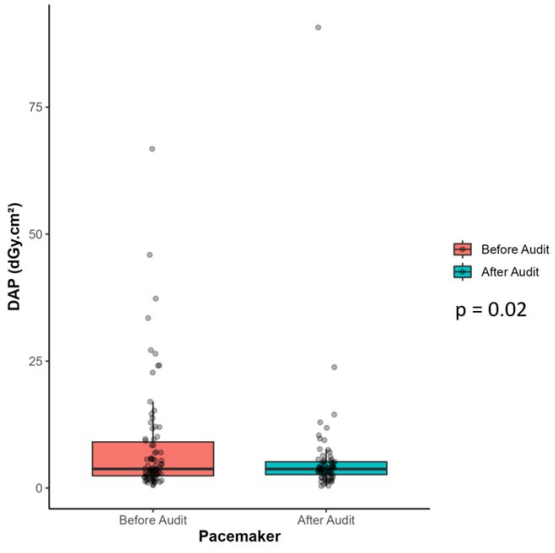

Figure 1: Dose area-product (DAP) for pacemakers before and after the audit

Conclusion:
The clinical audit in our institution led to a significant reduction of radiation exposure for patients during pacemaker implantations. Regarding DRLs, local values were far below national DRLs, which suggests that national DRLs need to be updated more regularly. Our study highlights the importance of clinical audits and the need for more research in this field.

627

Z. Steffek[1], D. Benz[1], T. Albertini[1], M. Gajic[1], S. Jurisic[1], A. Pazhenkottil[1], P. Kaufmann[1], R. Büchel[1], A. Giannopoulos[1]

Non-invasive Longitudinal Hemodynamic Phenotypes of Coronary Arteries with Atherosclerosis and Association with Myocardial Perfusion

Department of Nuclear Medicine, Cardiac Imaging, University Hospital Zurich[1]

Introduction:
CT-Simulated Pressure Loss Index (CT_{SPLI}) was developed as a coronary-artery-specific index based on computational longitudinal hemodynamics describing coronary artery disease (CAD) patterns as focal or diffuse using CCTA. We investigated the interplay between CAD phenotypes and arterial atherosclerotic burden and their association with myocardial perfusion defects.

Methods:
We retrospectively included 29 patients (23 men, 6 women; mean age 65.7±1.9 years) with suspected CAD that underwent hybrid CCTA and myocardial perfusion imaging (MPI; 25 with ^{99m}Tc-SPECT and 4 with ^{13}N-NH3-PET/CT) within 20 days. CAD was quantified at arterial-level in all coronaries with plaques and minimal lumen area stenosis of 25-99%, by assessing calcium score and percent atheroma volume. Hyperemic blood flow simulation was performed (XFFR, v1.6) and CT_{SPLI} was calculated in all coronaries with lesions and subtending ≥10% of the LV volume. MPI scans were assessed for presence of reversible perfusion defects and using fusion with CCTA, each defect was assigned to the respective coronary territories.

Results:
A total of 76 arteries with lesions (luminal area stenosis mean 65.6%±14.3) were analyzed and 38 of them subtended ischemic myocardium. CT_{SPLI} calculation was successful in all arteries (CT_{SPLI} mean 0.48±0.15, range 0.19-0.83). The 75th quartile was used to define CAD as focal (CT_{SPLI}>0.59) or diffuse (CT_{SPLI}≤0.59). Coronaries subtending ischemic myocardium had lower CT_{SPLI} values (0.43 vs. 0.52, p=0.015) and those with diffuse CAD more frequently subtended ischemic myocardium compared to those with focal CAD (x^2=5.68, p=0.017). Diffusely diseased coronaries had higher calcium score [277 AU (151-298) vs. 72 AU (13-128), p=0.046] and more percent atheroma volume than focally diseased (30.2% vs. 27.8%, p=0.033). No difference was observed in the presence of stenotic lesions between diffuse and focal arteries (81% vs. 73% p=0.52).

Conclusion:
CT_{SPLI} enables non-invasive assessment of CAD phenotypes. Coronaries with diffuse disease exhibit more global atherosclerotic burden and are more often associated with ischemia as compared to those with focal stenosis.

628

S. Makieva[1], M. Saenz-de-Juano[3], C. Almiñana[1], S. Bauersachs[4], S. Bernal-Ulloa[3], M. Xie[1], A. Velasco[1], N. Cervantes[1], M. Sachs[1], T. Cavazza[2], S. Ulbrich[3], B. Leeners[1]

The in vitro maturation rate of human oocytes is enhanced following uptake of extracellular vesicles originating from mature follicles.

Department of Reproductive Endocrinology, University Hospital Zurich, Zurich, Switzerland[1], Department of Reproductive Endocrinology, University of Zurich, Zurich, Switzerland[2], ETH Zurich, Animal Physiology, Institute of Agricultural Sciences, Zurich, Switzerland[3], Functional Genomics Group, Institute of Veterinary Anatomy, Vetsuisse Faculty Zurich, University of Zurich, Switzerland[4]

Introduction:
In vitro oocyte maturation (IVM) involves the culture of immature germinal vesicle (GV) oocytes under set laboratory conditions to allow for their transition to mature metaphase II (MII) stage, which is confirmed microscopically by the extrusion of the first polar body. Efficient IVM could circumvent controlled ovarian stimulation (COS) used for infertility treatment and requiring high doses of hormones to mature oocytes *in vivo.* Animal studies suggest that extracellular vesicles (EVs), membranous nanosized vesicles containing different molecular content (e.g. nucleic acids, proteins) are present in the ovarian follicles and could enhance oocyte maturation. The uptake of follicular fluid EVs (ffEVs) by bovine, equine and feline oocytes, but not human, has been demonstrated. We aimed to: a) identify differences in the protein cargo of ffEVs derived from human follicles containing mature versus (vs.) immature oocytes, b) demonstrate the capacity of human GV oocytes to internalize mature MII-ffEVs, and c) determine the effect of MII-ffEVs on human oocyte maturation.

Methods:
Women undergoing transvaginal oocyte retrieval after COS (n=83) were recruited to donate follicular fluid (n=54, women) and/or immature oocytes (n=95, GV). The study was ethically approved (BASEC-Nr. 2018-00797). EVs were isolated from follicular fluid samples containing a single MII (n=10) or GV (n=5) oocyte by ultracentrifugation. The ffEVs protein content was analyzed by LC-MS/MS. The uptake of fluorescently labelled MII-ffEVs by GV oocytes (n=15) was assessed by confocal microscopy. The impact of ffEV on oocyte maturation was evaluated after GV oocytes were supplemented with MII-ffEVs (n=45, treated group) or without (n=40, control group) during IVM culture in a timelapse incubator, by confirming the extrusion of the polar body.

Results:
Successful isolation of ffEVs was confirmed by transmission electron microscopy, followed by characterization for known EVs markers by Western blotting (TSG101 and CD63). Mass spectrometry identified a total of 1340 proteins across ffEVs samples. Statistical analysis revealed differentially abundant proteins (DAPs) in ffEVs: 61 in MII-ffEVs vs. GV-ffEVs (FDR<0.2). Among the 61 DAPs, 7 proteins that showed a fold change >2 in MII-ffEVs vs. GV-ffEVs have been related to oocyte maturation, lipid accumulation, calcium binding, and coagulation cascade (e.g., FABP5, S100A9, F12, SERPINA10). Confocal microscopy confirmed the internalisation of MII-ffEVs by GV oocytes after 24 hours of co-incubation. Supplementation of IVM culture with MII-ffEVs for 48 hours significantly increased the oocyte maturation rate by more than 22.8% ± 9.4 in treated oocytes (77.8% mature oocytes) compared to control (55% mature oocytes) (P-value=0.0372).

Conclusion:
Our findings pave the way for further mechanistic studies on the role of ffEVs in supporting oocyte maturation and inspire the development of clinical IVM supplements that could reduce the cost associated with ovarian stimulation and broaden the repertoire of infertility treatments.This study was supported by EMDO-Stiftung founds and FAN grant from the University of Zurich.

629

K. Michalek[1], S. Bhattacharjee[1], T. Loosli[1], K J. Metzner[1]

Elucidating the role of cellular factors in the formation of defective HIV-1 proviruses

University Hospital Zurich, Department of Infectious Diseases and Hospital Epidemiology,[1]

Introduction:
The human immunodeficiency virus type 1 (HIV-1) poses a significant threat to global health, with over 39 million people with HIV-1 (PWH) worldwide as of 2022. Although antiretroviral therapy is an effective treatment, a proper cure for this epidemic remains elusive. This is due to the ability of HIV-1 to remain latent inside the host cells as a provirus, via integration of its genome into the host genome. These proviruses can become reactivated later on, leading to the production of progeny HIV-1 virions, and thereby requiring life-long treatment of PWH. However, it has been observed that majority of HIV-1 proviruses harbor large internal deletions (LIDs), rendering them replication incompetent. Currently, the formation of these deletions in HIV-1 proviruses is assumed to be caused by erroneous template switching by viral reverse transcriptase, but surprisingly studies by our group has shown that LIDs are also formed following CRISPR/Cas9-mediated integration of HIV-1 based vectors and HIV-1, i.e. in the absence of viral enzymes. In line with these findings, we hypothesize that, besides viral factors, host cellular factors play an important role in the formation of LIDs.

Methods:
In order to identify cellular factors responsible for the formation of large internal deletions (LIDs) in HIV-1 proviruses, we are performing three types of human genome-wide CRISPR/Cas9 screens: CRISPRko (knockout), CRISPRi (interference), and CRISPRa (activation) screens to inhibit, reduce, or activate expression of every gene in the human genome, respectively. In the first steps, monoclonal (d)Cas9 expressing cells will be generated and used for infection with lentiviral pooled CRISPRko, CRISPRi, and CRISPRa libraries. We will then integrate HIV-1 based dual-fluorophore vector LTatCL[M] into the (d)Cas9 CRISPR cells as a readout of the CRISPR screens. In this vector, mCherry is constitutively expressed from a human promoter while the expression of Cerulean is dependent on the HIV-1 promoter. Based on the mCherry and Cerulean expression, cells will be FACS sorted into two populations - Cerulean+/mCherry+ cells harboring intact LTatCL[M] vector and mCherry+ cells with integrated defective vector containing LIDs. The gRNAs in these cell populations will be sequenced using next generation sequencing (NGS) technology and a gRNA enrichment analysis will be performed in order to obtain a ranked list of potential cellular factors involved in the LIDs formation.

Results:
Firstly, we stably integrated (d)Cas9 constructs - pLX_311-Cas9 (CRISPRko screen), pLX_311-KRAB-dCas9 (CRISPRi screen), and lenti dCAS-VP64_Blast (CRISPRa screen) into the genomic safe harbor site 1 (GSH1) of Jurkat and HEK 293T cells. Afterwards, we selected polyclonal and monoclonal (d)Cas9 cell lines. We amplified all the genome-wide CRISPR screen libraries and assessed the gRNA diversity, showing that 1µg of each library is sufficient to cover all gRNAs. We packaged CRISPRko and CRISPRa libraries into lentivirus particles and optimized the lentivirus production protocol in order to obtain high lentivirus titer. Currently, we are optimizing puromycin selection of (d)Cas9 CRISPR cells and integration of LTatCL[M] vector in cell line models.

Conclusion:
A vast majority of the HIV-1 proviruses in vivo are defective, containing large internal deletions (LIDs) and hypermutations. Despite LIDs being the most common defect, the mechanism of their formation is unclear. We hypothesize that the cellular factors are involved in the formation of the LIDs, most likely DNA repair proteins triggered during HIV-1 integration. In order to identify these factors, we are performing human genome-wide CRISPR/Cas9 screens. Our findings will initiate further research into the role of the identified host proteins, potentially compromising a novel antiviral defense mechanism, and have implications for the lentivirus-mediated gene delivery and HIV-1 cure strategies.

630

CC. Chang[1], A. Gomez Mejia[1], E. Cauwenberghs[2], S. Shambat[1], S. Brugger[1]

Adjuvant microbiota-transplantation to cure chronic and recurrent bacterial infections

University Hospital Zurich[1], University of Antwerp[2]

Introduction:
Colonization with pathogens, such as *S. aureus*, in the upper respiratory tract (URT) is linked to chronic inflammatory conditions such as sinusitis. Standard antibiotic therapies disrupt the human microbiome and pose the risk of antimicrobial resistance development, often leading to recurrent infections and treatment failures. This project aims to develop a strategy to enhance the efficacy of antibiotic treatments and find effective ways to reshape the composition of the URT microbiota to prevent infectious diseases. The widely acknowledged beneficial roles of commensal bacteria in maintaining tissue homeostasis through interspecies and host-microbe interactions have led us to propose that an adjuvant treatment comprising commensal bacteria could synergistically boost antibiotic effectiveness. This strategy could potentially eradicate pathogens and help prevent recurrent infections by re-establishing a healthy microbiota and balanced tissue homeostasis.

Methods:
An immunocompetent humanized 3D-organotypic airway tissue model (ATM) , comprising fibroblasts and immune cells-embedded stromal matrix and stratified epithelium, is utilized to recapitulate the human airway barrier tissue anatomy. To mimic intravenous antibiotic administration in clinical settings, antibiotic treatment was performed by replacing the antibiotic-free medium in the lower chambers of the air-liquid interface system with an antibiotic-containing medium after *S. aureus* infection, followed by the addition of commensal bacteria in the upper chambers of the ATM. Then, the airway tissue and supernatant were collected to evaluate pathogen survival and cytokine release by colony-forming units enumeration and enzyme-linked immunosorbent assay, respectively.

Results:
Our findings show that using *D. pigrum* or *C. pseudodiphtheriticum* alongside antibiotics significantly improved the elimination of *S. aureus*. However, the heat-killed-commensal bacteria consisting of the cell wall components did not maintain this enhanced antibacterial effect, indicating that live and active interactions between bacterial species and with the host are essential to control survival of the pathogen. Notably, the adjuvant treatment with commensal bacteria was associated with increased release of pro-inflammatory cytokines, such as IL-8, IL-1β, and TNF-α . The change in the phenotypic properties like phagocytosis and antigen presentation of innate immune cells is currently being assessed by flow cytometry. Furthermore, the ATMs upon infection and after commensal treatment have been processed for performing transcriptomic analysis to identify the gene regulatory networks in the host and bacterial cells. Molecules attributed to the tight junction, and adherens junction of epithelial cells in the ATMs upon infection and after commensal treatment will also be examined to investigate if commensal adjuvant therapy can further improve the protection of barrier tissue integrity.

Conclusion:
Our results indicate that antibiotic treatments against *S. aureus* can be improved by adjuvant treatment with commensal bacteria. Furthermore, modelling bacterial colonization and invasion by utilizing the immunocompetent humanized-ATM can be a powerful platform for studying the role of commensal bacteria in microbiota dysbiosis and tissue homeostasis.

631

M. Rechsteiner[2], M. Kirschner[3], R. Werner[3], H. Moch[2], B. Sobottka-Brillout[2], J. Rüschoff[2], A. Curioni-Fontecedro[1], I. Opitz[3]

Optimization by site and time of liquid biopsy for CGP in early cancer detection: a technical evaluation

Department of Oncology, Cantonal Hospital Fribourg, 4University of Fribourg[1], Department of Pathology and Molecular Pathology, University Hospital Zurich[2], Department of Thoracic Surgery, University Hospital Zurich[3]

Introduction:
Nowadays, liquid biopsies are mainly used in patients with metastatic disease in order to monitor response or to detect emerging resistance mechanisms, while further uses such as early tumor detection are still under investigation. The major difficulty for assays is the low abundance of circulating tumor DNA (ctDNA) in early cancers which comes along with technical limitations. The aim of this study is to assess the technical limits of such an assay and to determine best practices for liquid biopsies concerning input, quality and finally sensitivity and specificity.

Methods:
Recently, a new highly sensitive liquid biopsy NGS assay, the Oncomine Precision Assay, was released, which allows for the detection of the most relevant altered genes in cancers, including amplifications, fusions and intra-genic exon skipping, in 24 to 48 hours. To optimize the detection of ctDNA, a cohort of stage I-III cancer patients was selected with liquid biopsies at three different time-points: blood from i) peripheral vein at resection, ii) tumor draining vein at resection, iii) peripheral vein at first radiological follow-up.

Results:
From a first set of liquid biopsies (n=24) the cfDNA has already been extracted. In average, the cfDNA concentration per ml blood-plasma derived from the peripheral vein at resection 0.91 ng/ul, from the tumor draining vein at resection 24.42 ng/ul, and from the peripheral vein at first radiological follow-up 0.7 ng/ul. Sequencing is ongoing on the Genexus platform using the Oncomine Precision Assay.

Conclusion:
The first set of data revealed higher yields of cfDNA derived in liquid biopsies taken from the tumor draining vein compared to peripheral blood. At the venue, we show data evaluating the impact of these sampling strategies on sensitivity and specificity of the results generated by the Oncomine Precision Assay on the Genexus platform.

632

F. Vasella[2, 3], R. Weber[2], A. Klimko[3], M. Silginer[3], M. Lamfers[1], M. Neidert[2], L. Regli[2], G. Schwank[4], M. Weller[3]

Targeting the IDH1R132H mutation in gliomas by CRISPR/Cas precision base editing

Department of Neurosurgery, Brain Tumor Center, Erasmus University Medical Center, Rotterdam, Netherlands[1], Department of Neurosurgery, Clinical Neuroscience Centre, University Hospital and University of Zurich, Switzerland[2], Laboratory of Molecular Neuro-Oncology, Department of Neurology, Clinical Neuroscience Centre, University Hospital and University of Zurich, Zurich, Switzerland[3], Laboratory of Translational Genome Editing, Institute of Pharmacology and Toxicology, University of Zurich, Switzerland[4]

Introduction:
Gliomas are the most frequent malignant primary brain tumors and lack curative therapies. Understanding glioma-specific molecular alterations is crucial to develop novel therapies. Among them, the biological consequences of the isocitrate dehydrogenase 1 gene mutation (*IDH1*^{R132H}) remain inconclusive despite its early occurrence and widespread expression, requiring novel approaches to further elucidate the functional consequences and therapeutic potential of *IDH1*^{R132H}.

Methods:
Clustered, regularly interspaced, short palindromic repeat (CRISPR)-Cas precision base editing systems enable the alteration of a specific base pair without suffering from off-target editing associated with double strand brake-inducing systems, making them a promising tool to revert the point mutation in *IDH1*^{R132H} gliomas. Various adenine base editors were tested in preclinical IDH-mutant reporter and patient-derived models.

Results:
CRISPR/Cas adenine base editing was applied to convert of *IDH1*^{R132H} mutation in primary patient-derived cell lines and organoids. Targeted editing only led to decreased IDH1^{R132H} protein levels and reduced 2-hydroxyglutarate production, as well as increased cellular proliferation. The precision base editing system was packaged into a dual adeno-associated virus (AAV) split intein system demonstrating high editing efficiencies and allowing gene editing both *in vitro* and *in vivo*.

Conclusion:
Taken together, our study offers a comprehensive strategy for precise genetic intervention targeting the *IDH1R132H* mutation. This approach not only facilitates the development of accurate models for examining the mutation's influence on glioma biology but also serves as a foundational framework to advance our understanding and potential treatment of gliomas by gene therapy.

633

L. Weidmann[1], C. Laux[1], K. Castrezana Lopez[1], D. Harmacek[1], B. George[1], S. von Moos[1], T. Schachtner[1]

Immunosuppression and transplantation-related characteristics affect the difference between eGFR equations based on creatinine compared with creatinine and cystatin C in kidney transplant recipients

University Hospital of Zurich, Department of Nephrology[1]

Introduction:
Previous studies have shown substantial heterogeneity when applying estimated glomerular filtration rate (eGFR) equations to kidney transplant recipients (KTRs). Furthermore, the impact of transplantation-related characteristics on eGFR equations based on creatinine (eGFRcr) compared with creatinine and cystatin C (eGFRcr-cys) remains insufficiently studied.

Methods:
We analyzed 596 KTRs at the University Hospital of Zurich. The performances (bias and precision) and accuracies (P30/P20 and correct classification, CC) of five eGFRcr equations (MDRD, CKD-EPI 2009 and 2021, EKFC 2021, KRS-GFR 2023) were compared with three eGFRcr-cys equations (CKD-EPI 2012 and 2021, EKFC 2023), and evaluated across multiple transplantation-related variables. Multivariate analysis identified transplantation-related characteristics independently associated with a smaller or greater difference between eGFRcr and eGFRcr-cys.

Results:
Taking eGFRcr-cys CKD-EPI 2012 as reference, eGFRcr KRS-GFR 2023 (median bias: -10.56 ml/min/1.73m2, precision: 26.12 ml/min/1.73m2, P30: 80.2%, P20: 64.9%, CC: 60.1%) had lower performance and accuracy than EKFC 2021 (median bias: -9.81 ml/min/1.73m2, precision: 19.02 ml/min/1.73m2, P30: 88.6%, P20: 75.8%, CC: 66.8%). Mean bias (linear regression model) decreased between eGFRcr and eGFRcr-cys equations with better GFR (all $p<0.05$). Upon multivariate analysis, living kidney donation and belatacept use were independent factors associated with a smaller difference between eGFRcr equations and eGFRcr-cys CKD-EPI 2012 (p between 0.001 and $p=0.031$). Prednisone use was independently associated with a greater difference between eGFRcr MDRD or CKD-EPI 2021 and eGFRcr-cys CKD-EPI 2012 ($p=0.006$ and $p=0.024$, respectively).

Conclusion:
More recent eGFRcr equations do not overcome the limitations of non-GFR determinants of creatinine in KTRs. However, European (i.e. EKFC) equations perform similar as established CKD-EPI equations in KTRs. Better GFR, as well as transplantation-related characteristics of the recipient, donor, and especially the immunosuppressive medication affect the differences between eGFRcr and eGFRcr-cys.

634

J. Tschumi[1], L. Jörimann[1], M. Zeeb[1], K. Neumann[1], M. Stöckle[4], E. Bernasconi[6], S. Yerly[7], M. Cavassini[5], A. Rauch[2], P. Schmid[3], R D. Kouyos[1], H F. Günthard[1], K J. Metzner[1]

Similar Changes in Proviral Landscapes Over 10 Years in People With Diverging HIV Reservoir Dynamics

Department of Infectious Diseases and Hospital Epidemiology, University Hospital Zurich, Zurich, Switzerland[1], Department of Infectious Diseases, Inselspital, Bern University Hospital, University of Bern, Switzerland[2], Division of Infectious Diseases and Hospital Epidemiology, Cantonal Hospital of St. Gallen, St. Gallen, Switzerland[3], Division of Infectious Diseases and Hospital Epidemiology, University Hospital Basel, Basel, Switzerland[4], Division of Infectious Diseases, Centre Hospitalier Universitaire Vaudois, University of Lausanne, Lausanne, Switzerland[5], Division of Infectious Diseases, Ente Ospedaliero Cantonale, Lugano, University of Geneva and University of Southern Switzerland, Lugano, Switzerland[6], Laboratory of Virology, Laboratory Medicine Division, University Hospital of Geneva, Geneva, Switzerland[7]

Introduction:
The HIV-1 reservoir was recently shown to be increasing in >25% of people with HIV (PWH) over years on efficient antiretroviral therapy (ART). Reasons and potential clinical implications of this HIV-1 reservoir increase remain unclear. In this study, we aimed to characterize the proviral landscape in four distinct groups of PWH, presenting either an increase or decrease of the HIV-1 reservoir over 10 years on ART and additionally experiencing or not experiencing intermittent viremia, to find potential differences explaining the contrasting long-term dynamics of the HIV 1 reservoir.

Methods:
Near full-length HIV-1 proviral NGS in bulk was applied to four longitudinal PBMC samples from 40 well characterized participants enrolled in the Swiss HIV Cohort Study (SHCS). After removing hypermutated reads, genetic distances and diversities were calculated and drug resistance mutations were assessed. Total, intact and unintegrated HIV-1 DNA and HIV-1 transcript were quantified using digital PCR.

Results:
A decrease of intact proviruses was observed independent of HIV-1 reservoir size dynamics. Genetic distances and diversities of individuals' proviral sequences did not increase over time in any group. While some non APOBEC-induced drug resistance mutations (DRMs) could be observed in proviral DNA of individuals in all groups, numbers were not significantly different among the groups. Low numbers of unspliced and multiply spliced RNA and 2-LTR circles were detected at low levels in all groups.

Conclusion:
Our results show no evidence of evolution of the HIV-1 reservoir, regardless of HIV-1 reservoir size dynamics and intermittent viremia over a follow-up period of 10 years on ART. These findings suggest that the increase of HIV-1 reservoir size observed in a substantial fraction of individuals is driven by an increase of defective proviruses, and that not low-level replication but other mechanisms, e.g. clonal expansion, are more likely responsible for the HIV-1 reservoir increase, largely independent of intermittent viremia.

635

E. Rho[2], C. Martinetti[2], B. George[2], T. Schachtner[2], F. Ruschitzka[1], M. Frank[1]

Patient characteristics and outcomes of an inter- and multidisciplinary nephrology and cardiology clinic

University Hospital Zurich, Division of Cardiology[1], University Hospital Zurich, Division of Nephrology[2]

Introduction:
The prevalence of cardiorenal syndrome is increasing due to the growing number of patients with chronic kidney disease (CKD) and heart failure (HF). To further improve outcomes in this high risk population, an interdisciplinary, evidence-based and patient-centered approach is advocated. Hence, it was the aim of this study to identify and describe the patient population which might profit from an inter- and multidisciplinary nephrology and cardiology clinic at a tertiary university hospital.

Methods:
We screened 552 patients who from 01.01.2015 and 30.06.2022 had been in the nephrology and in the cardiology outpatient clinics of the University Hospital of Zurich. Patients with kidney or heart transplantation or on dialysis were excluded. Out of the remaining patients, we identified 223 patients having CKD 2-5 and HF. Characteristics with respect to entity and cause of kidney and heart disease, cardiovascular risk factors, therapy, incidence of acute kidney injury (AKI), hospitalisations and patient survival were recorded.

Results:
The most common cause of CKD was a cardiorenal syndrome type 2 (42%, 95/223). 59/223 (26%) had at least moderate albuminuria. At the beginning of follow-up, 61/223 (26%) were in CKD2, 95/223 (42%) in CKD3a, 47/223(21%) in CKD3b, 6/223 (7%) in CKD4 1, 2/223 (1%) in CKD5. Ischemic cardiomyopathy was the most common cause of heart failure, (36%, 80/223 patients). 119/223 patients (53%) had HFrEF, 41/223 (19%) HFmrEF and 63/223 (28%) HFpE. 64/223 (28%) of the patients were treated with SGLT2i,159/223 (71%) with RASi of which 37 (17%) were on an ARNI. Patients under combined RASi and SGLT2i were younger (66 vs 73 years, p=0.005), were more likely to have diabetes (44% vs 30%), HFrEF rather than HFpEF (70% vs 7% p=0.002) and had a better kidney function at the beginning of follow-up (eGFR 65 vs 55 ml/min/1.73m2, p <0.001).
Hospitalization-rate due to HF and incidence of AKI were high with 0.6/patient/year and 4.8/patient/year respectively. 72/223 (32%) patients died during the mean follow-up of 3.1 years.

Conclusion:
We identified a high-risk patient population with cardiorenal disease that might particularly benefit from evidence-based and patient-centered interdisciplinary care. A cardiorenal outpatient clinic may have the potential to improve a personalized approach in more vulnerable patients.

636

A. Movasati[2, 3], C. Leemann[2], K. Neumann[2], R. Chen[2], R. Regös[1], K. Metzner[2, 3]

Comprehensive Characterization of HIV-1 Evolution in A Long-Term Experimental Evolution Study

ETH[1], University Hospital Zurich[2], University of Zurich[3]

Introduction:
Evolution is the gradual change in the heritable characteristics of organisms over successive generations. Evolutionary driving forces include mutagenesis, natural selection, genetic drift, and gene flow that work in tandem to improve fitness of organisms in their environment. Characterizing these processes and their interactions can help us form a better understanding of evolution. One of the popular laboratory methods to mimic evolution are the long-term experimental evolution (LTEE) studies. In an LTEE, a microorganism is passaged in a controlled laboratory condition for a long time period. HIV-1 is one of the microorganisms that has been subject to extensive evolutionary research due to its adaptation capabilities which is attributed to its rapid and error-prone replication. The high degree of adaptability enables the virus to escape immunity and acquire resistance to effective antiretroviral drugs, complicating containment of the virus.

Methods:
In our two ongoing LTEE experiments, named EXPIII and EXPIV, we have been passaging HIV-1 NL4_3 in two human T-cell leukemia cell lines for over 1200 generations. In both experiments, HIV-1 is propagating under no external adaptive pressure. Every 3-4 days (~2 generations) the virions are collected from the cell culture, and a fixed amount is transferred to the next cell culture. At every tenths transfer, the viral genome is extracted from the virions and used for whole-genome sequencing of the virus. In EXPIII we are propagating HIV-1 in two independent replicates in two human T-cell lines, namely MT-2 and MT-4, while in EXPIV the virus is being propagated in four replicates in MT-2 cells. Another experimental design difference between EXPIII and IV is that while at each transfer of EXPIII an abundant amount of virus is collected and used for infecting the next cell culture, in EXPIV we have introduced a viral titer bottleneck which limits the amount of transferred virus. The genomic sequencing data is then processed to obtain annotated variants. The annotated variants are then used to perform a plethora of downstream analyses.

Results:
The preliminary analyses of EXPIII genomic data reveals significant differences between viral lines propagating in MT-2 and MT-4. These differences are evident both in rate of mutation fixation and supply. We observe higher and linear supply of mutations in MT-4 infecting HIV-1 populations, while in MT-2 lines that rate reaches a plateau at around transfer 230. On the other hand, the rate of mutation fixation is significantly lower in MT-4 compared to MT-2 infecting HIV-1 populations. In EXPIV, we see that the population diversity in terms of minority mutations in EXPIV is maintained at a low level since newly acquired mutations either quickly reach majority or are omitted from the population by chance. Additionally, we have observed so far that the neutrality of evolution in our experiments increases over time, as evident by increasing values of dN/dS throughout the genome.

Conclusion:
So far we have observed stark differences in the evolutionary dynamics between viral populations propagating in MT-2 and MT-4 lines. These differences are most likely stemming from distinct environmental pressures that the virus is exposed to. Furthermore, we are able to confirm that the introduced bottleneck on viral transfer titration in EXPIV is effective and has led to significant changes in the evolutionary landscape of the viral population. Our observation is in accordance with the theory that the lower the population size, the more pronounced the activity of genetic drift is. Last but not least, in all our viral lines, selection seems to play a more important role in driving evolution in the initial phase (up to passage 100) of the experiments, while subsequently we see more neutrality in evolution. This is probably due to the fact that after some time the viral lines are sufficiently adapted to their environment and have reached a local or global fitness peak.

637

A. Gomez-Mejia[1], S. Mairpady Shambat[1], E. Sosa[1], M. Huemer[1], A. Zinkernagel[1]

Staphylococcus aureus adaptation to antibiotic stress modulates tolerance and survival

Department of Infectious Diseases and Hospital Epidemiology, University Hospital Zurich, University of Zurich[1]

Introduction:
Beyond the ability of *Staphylococcus aureus* to survive the current treatment strategies, there is a complex and efficient regulatory network tasked to provide the necessary queues to promote adaptation in different environments. As the result of a successful adaption, *S. aureus* is capable of causing difficult-to-threat infections, eluding the host immune response of the host and overcoming the action of antibiotics.

Methods:
Two strains of *S. aureus* were exposed to four different classes of antibiotics in physiological media. A proteomic analysis was performed to identify changes in the abundance of virulence factors upon antibiotic exposure. The consequences of the observed phenotype and secretome profile changes were explored by antibiotic persister assay and intracellular survival assays with human primary monocyte derived cells in conjunction with live imaging using fluorescence microscopy.

Results:
We identified the most noteworthy changes when the *S. aureus* strains were exposed for four hours to 40x MIC of rifampicin and clindamycin with a drastic reduction in the abundance of secreted toxins, chaperones, stress response proteins and immune modulators. Furthermore, the surviving populations from both strains exposed to rifampicin and clindamycin showed different levels of antibiotic tolerance in a 24 hours persister assay against 40x MIC of antibiotics and an increased intracellular survival when challenged against human primary monocyte derived cells. Finally, using the NARSA transposon-insertion mutants for the regulator rot and the chaperones *clpB*, *htrA* and *tig*, we could demonstrate that these proteins are involved in the successful adaption of *S. aureus* towards antibiotic induced stress and their abundance in the secretome suggest an important role in the extracellular milieu.

Conclusion:
Exposures as short of 4 hours to high antibiotic concentrations produce adaptive changes in *S. aureus* leading to a modification of its secretome profile in response to stress and initiates a survival strategy leading to changes in its antibiotic tolerance and intracellular survival.

638

M. Kirschner[1], F. Schläpfer[1], M. Meerang[1], I. Opitz[1]

Dysregulated microRNAs contribute to chemotherapy-resistance of pleural mesothelioma

Department of Thoracic Surgery, University Hospital Zurich[1]

Introduction:
Dysregulated expression of microRNAs has been shown to contribute to response to chemotherapeutic agents in several cancers, including pleural mesothelioma (PM). Following identification of several microRNAs which tissue-expression might correlate with patient's response to cisplatin-pemetrexed, we here evaluate how altering their expression in cell lines in vitro, affects cell growth and response to chemotherapy.

Methods:
PM cell lines MSTO-211H (biphasic), H28, Meso-1, Mero-82 (epithelioid) and non-malignant MeT-5A were reverse transfected with synthetic microRNA mimics for 15 candidates. Following transfection, cell growth, colony forming ability, migratory potential and induction of apoptosis were assessed using standard assays. In addition, transfected cells were exposed to increasing concentrations of cisplatin and pemetrexed (alone or in combination) to evaluate sensitivity to these drugs.

Results:
Overexpression of seven of the candidates resulted in varying degrees of growth inhibition in all investigated PM cell lines five days post transfection. The strongest effects were observed for miR-380-5p, miR-221-3p, miR-210, miR-625-3p, and miR-19b, which reduced cell growth to 30-60% of that of untransfected cells. Growth of non-malignant MeT-5A cells remained largely unaffected. Overexpression of both microRNAs in addition resulted in a strong reduction of colony forming ability of at least 50%, while an effect on the wound healing capacity (migration) of the cells could not be observed. FACS analysis then further revealed that overexpression of miR-380-5p, miR-221-3p and miR-625-3p significantly increased the proportion of apoptotic/dead cells from <10% to up to 40%. Preliminary data suggest that in some cases this may be accompanied by a downregulation of anti-apoptotic BCL-2 gene expression. Finally, we were able to show that especially overexpression of miR-221-3p, miR-625-3p and miR-19b was able sensitise cells towards cisplatin, with the strongest effect observed in MSTO-211H for miR-221-3p (IC50 from 17.6µM to 2.7µM) and miR-19b (IC50 from 17.6µM to 0.7µM), and in Mero-82 for miR-625-3p (IC50 from 3.75µM to 0.8µM).

Conclusion:
We were able to show that overexpression of several microRNAs has the potential to alter PM cell growth and colony forming ability, and can result in a strong induction of apoptosis. Furthermore, microRNA overexpression can sensitise cells towards cisplatin, although the degree of sensitisation varies between different cell lines. Current analyses focus on the response towards the cisplatin/pemetrexed doublet and on the effect on cell cycle and expression of associated genes. Furthermore, we will also evaluate the effect of simultaneous re-expression of several candidates.

639

M. Kirschner[1], V. Orlowski[1], F. Schläpfer[1], M. Meerang[1], I. Opitz[1]

Novel microRNAs are associated with presence of pleural mesothelioma and response to chemotherapy

Department of Thoracic Surgery, University Hospital Zurich[1]

Introduction:
Various studies have shown that dysregulation of microRNA expression contributes to pleural mesothelioma (PM), including its resistance to chemotherapy. In addition, microRNAs have been proposed as diagnostic and prognostic biomarkers. While the majority of studies focused on well-annotated microRNAs, in 2019 previously unknown microRNAs were identified, which distinguished TCGA-MESO from TCGA lung cancer samples with high accuracy. Here we are evaluating these microRNAs in PM, non-PM and lung cancer tissue using PCR as alternative detection approach.

Methods:
We used archived FFPE tissue from an increased cohort of 51 PM (39 epithelioid, 9 biphasic, 3 sarcomatoid) collected prior to chemotherapy, 16 pleural biopsies from non-PM, and 14 lung cancer cases (9 adenocarcinomas). The non-PM cases consisted of 9 patients with benign inflammatory reaction, and 7 pleural metastases. Novel microRNAs were measured using self-designed PCR primers. Independent samples t-test was used to assess expression differences between groups.

Results:
We found significantly elevated expression of mpm-miRs-72, -18 and -58 in PM compared to both non-PM and lung cancer, while there was no significant difference between non-PM and lung cancer. Further subdividing our non-PM cases, we found that expression differences remained significant between PM and benign tissue with the highest expression difference found for mpm-miR-72 (5.4-fold, $p=0.01$). Expression of all three microRNAs was highest in biphasic PM cases, reaching statistical significance for mpm-miR-18 (1.9-fold, $p=0.036$;). Similarly, we did not observe significant expression differences between adenocarcinoma and squamous cell carcinoma. Since microRNAs have been shown to influence response to chemotherapy, we also compared expression differences based on chemotherapy response for the 33 PM patients for whom RECIST data was available. Indeed, all three microRNAs showed highest expression in patients with progressive disease, with an expression difference compared to partial responders of 2.8-fold for mpm-miR-58 reaching statistical significance ($p<0.001$).

Conclusion:
Our current findings support a diagnostic potential of novel microRNAs in PM for differentiation from benign lesions and lung cancer. Higher expression of all three microRNAs in patients with progressive disease suggests a contribution of these microRNAs to chemoresponse, which warrants further investigation. At present, we are reevaluating all samples using a second PCR approach, which is also able to detect additional mpm-miR candidates.

640

S. Hertegonne[1], A. Tarnutzer[1], S. Mairpady Shambat[1], A. Zinkernagel[1]

Staphylococcus aureus induces differential functional responses in neutrophils during acute infection

Department of Infectious Diseases and Hospital Epidemiology, University Hospital Zurich, University of Zurich, Zurich, Switzerland[1]

Introduction:
Staphylococcus aureus is a pathobiont that can intermittently colonize as well as causes mild to severe invasive infections in humans. Currently, *S. aureus* infections are often difficult-to-treat as a result of emergence in antibiotic resistance and an increase in antibiotic tolerance. Antibiotic tolerance is a transient phenomenon where the bacterial population can withstand high antibiotic concentrations which are otherwise lethal. Under certain conditions during infection due to host-mediated as well as antibiotic mediated stress, a subpopulation of bacterial cells enter the dormant phase that can survive and tolerate high concentrations of antibiotics due to the formation of so-called persister cells. While persister cells are naturally present in a bacterial population, several environmental stressors, such as acidic pH, abscess environment, immune cell mediated stress, nutrient limitation and post-antibiotic stress, can induce their formation. The inability to clear persistent bacteria can lead to chronic and relapsing infections, characterized by recurring abscess formation. In order to treat these abscesses, surgical debridement is needed, which can be a challenging and adds to the overall health care associated costs. Previously we have shown that acidic pH and neutrophil mediated stress, two characteristics from abscess environment, can induce the formation of non-stable small colonies (nsSCs), which are a proxy for persister cells. However, it remains unclear whether persister cells modulate the neutrophil functional responses allowing the bacteria to better withstand neutrophil mediated killing.

Methods:
Aiming to dissect the interplay between stress adaptation in *S. aureus* and neutrophil functional responses during infection, we used a neutrophil *ex vivo* co-culture model. Multi-parametric flow cytometry and confocal microscopy were used to quantify the kinetics and dynamics of neutrophil functional responses, such as phagocytosis, degranulation, regulated cell death, and neutrophil extracellular trap formation.

Results:
We showed that acid-stressed bacteria induced regulated cell death in neutrophils, accompanied by an increased bacterial survival. This increased neutrophil cell death could be linked to a lower phagocytosis percentage of acid-stressed *S. aureus.* Moreover, degranulation of primary granules was enhanced, seen by increased CD63 expression and intracellular myeloperoxidase levels. On the other hand, bacterial supernatant containing released virulence factors did not induce this pattern, suggesting that the bacterial cell surface plays an important role in inducing degranulation of neutrophils. Additionally, kinetics of granule release indicate that this response occurs within the first ten minutes of infection.

Conclusion:
These findings provide initial insights into differential functional responses of neutrophils during different physiological state of *S. aureus* infections, which in turn influences the neutrophil effector response. Furthering our understanding of this interplay and the hierarchy of the responses will allow us to develop effective therapeutic strategies to tackle severe invasive *S. aureus* infections. Furthermore, elucidating the surface expression of Fc and chemokine receptors could help us understand the underlying nature of the neutrophil response. Considering the high rate of treatment failure linked to *S. aureus* infections and the many questions concerning neutrophil heterogeneity in the context of infectious diseases, this project has great potential of furthering our understanding of host-pathogen interactions as well as developing new treatment strategies to treat recurring bacterial infections.

641

J. Mengers[2], M. Haberecker[1], M. Kirschner[2], N. Bosbach[2], O. Lauk[2], i. Opitz[2], M. Meerang[2]

Low Ki-67 Positive Index is a Prognostic Factor for Better Survival Outcomes of Patients Treated with Intracavitary Cisplatin-Fibrin

Department of Pathology and Molecular Pathology, University Hospital Zürich[1], Department of Thoracic Surgery, University Hospital Zürich[2]

Introduction:
Novel therapeutic approaches are needed for patients with pleural mesothelioma (PM). Our phase I and II clinical trials for localized chemotherapy with cisplatin-fibrin after surgery investigated safety and efficacy of this novel approach. Here, we aimed to identify biomarkers associated with disease outcomes.

Methods:
Tissues collected at diagnosis (pre-CTX) were available from 5 patients. We collected tumor tissues at surgery (post-CTX), before start of localized treatment, from all patients enrolled (n=25). FFPE tissues were immunohistochemically stained for p21 (cisplatin resistance), and Ki-67 (proliferation)1. Using Qupath software, we classified tumor cells from stroma. Number of positive cells (%) were automatically counted. For p21, we also acquired H-score (sum of intensity x % positive cells) for p21. The association of marker expression with disease outcomes including progression free survival (PFS) and overall survival (OS) from surgery was analysed by SPSS software.

Results:
Ki-67 staining index (%) ranged from 1.2 – 60.8 (median 12.8). p21 staining index and H–score (range (median)) are 0 - 96 (21) and 0 - 225 (32), respectively. High Ki-67 labelling index was significantly associated with shorter PFS (p=<0.001, median (95% CI): 25.1 (11.3 – 39) vs 8.5 (6.8 -10.2) months) and OS (p<0.001, 37.8 (26.7 – 48.8) vs 16 (12.6 – 19.3) months) (figure 1). There was no association between clinical parameters with Ki-67 or p21 staining. p21 staining index and H-score showed no association with disease outcomes. For 5 patients of whom pre- and post-CTX tissues were available, we observed reduction of Ki-67 index after CTX in 3 cases. Whether the change in Ki-67 was associated with response to CTX and intracavitary treatment is still under investigation.

Conclusion:
Although a small patient cohort, Ki-67 showed significant association with disease outcomes for patients receiving localized cisplatin-fibrin. Ki-67 may be useful for the selection of patients for this treatment regimen.

642

A. Astourian[1], L. Fabbella[1], M. Hartmann[1], V. Vongrad[1], D. Rodriguez Gutierrez[1], B. Leeners[1]

Human Endometrial Assembloids: A Tool for Studying Cellular Interplay in Endometriosis

Department of Reproductive Endocrinology, Universitätspital Zurich, Zurich, Switzerland[1]

Introduction:
Endometriosis is a chronic disease that affects 6-10% of women of reproductive age globally and is associated with severe pelvic pain and infertility. Due to the unclear etiology and pathogenesis of endometriosis, there are limited pharmacological treatments besides hormones. At a cellular level, fibroblasts considered to play a central role in endometriosis lesions due to the observed fibrotic nature of the tissue. The two-dimensional monolayer cell culture has been classically used in endometriosis research. However, this system fails to mimic the natural endometriosis microenvironment with complex cellular communication (cell-cell and cell-matrix) and obtained results cannot be fully translated into clinical research. To overcome these limitations, three-dimensional culture systems like spheroids and organoids are being increasingly developed as a suitable alternative and might become essential tools for endometriosis research. In a one step further, organoids can be used to generate assembloids by the combination of an organoid with additional cell types. Patient-derived 3D assembloids have an extraordinary potential to model and highlight mechanism of cell interaction and invasiveness in endometriosis lesions.

Methods:
Primary epithelial endometrial cells were enzymatically isolated from endometriosis patient tissue fragments and characterized by the presence of epithelial cell marker EpCAM via flow cytometry and Immunofluorescence. EpCAM positive cells were incubated in low attachment wells with conditioned medium to generate human endometrial organoids (HEOs). HEOs were further expanded in 3D Matrigel cultures. Confluent organoid cultures were released from the Matrigel and resuspended in a collagen I/hydrogel solution mixed with stromal cells and complete medium. Subsequently, the mixture was seeded in a drop within an Akura 96-well Microplate plate and allowed to gelate. The structure was added with complete medium and cultured in low attachment conditions, allowing for cells self-assembling into an endometriosis assembloid. After 10 days of maturation, the assembloids were characterized by the expression of stromal and epithelia markers (CD90, CD10, ER-α,ER-β, vimentin, and EpCAM) by immunostaining.

Results:
We successfully generated endometriosis organoids from epithelial cells. When combined with ectopic stromal cells in a 3D matrix environment, cells interacted among each other to form human endometriosis assembloids. Immunostaining analysis of the assembloids confirmed a multilayer structure organization of the culture similar to physiological tissue, with spherical formations of EpCAM positive epithelial cells surrounded by CD10 and Vimentin positive stromal cells.

Conclusion:
This proof-of-concept study offers a novel approach for endometriosis research, able to mimic complex conditions of the physiological microenvironment of lesions, and represent an excellent platform for high-throughput screening of therapeutic and diagnostic solutions in a personalized manner.

643

J. Trepl[2], C. Pasin[1, 3], D. Schneidawind[2], N. Mueller[1], M. Manz[2], A. Bankova[2, 4], I. Abela[1, 3]

Evaluating Tixagevimab/Cilgavimab Prophylaxis in Allogeneic Hematopoietic Cell Transplantation Recipients for COVID-19 Prevention

Department of Infectious Diseases and Hospital Epidemiology, University Hospital Zurich, Switzerland[1], Department of Medical Oncology and Hematology, University Hospital Zurich, Switzerland[2], Institute of Medical Virology, University of Zurich, Switzerland[3], National Specialized Hospital for Hematological Diseases, Sofia, Bulgaria[4]

Introduction:
The COVID-19 pandemic, caused by the severe acute respiratory syndrome coronavirus 2 (SARS-CoV-2), has presented substantial challenges to global healthcare systems. Allogeneic hematopoietic cell transplantation (allo-HCT) recipients exhibit an increased risk of COVID-19 infections, particularly in the early post-transplant phase, due to insufficient vaccine responses. Therefore, additional preventive strategies such as monoclonal antibody (mAb) preexposure prophylaxis (PrEP) might play an important role in reducing the incidence of SARS-CoV-2 infections until protective vaccine responses develop. In 2021 the Food and Drug Administration issued emergency use authorization for tixagevimab/cilgavimab, a monoclonal antibody combination that neutralizes the SARS-CoV-2 virus, based on the placebo-controlled PROVENT study. However, limited real-world data exist regarding the efficacy of T/C against Omicron sublineages circulating in 2022 in immunocompromised patients following allo-HCT.

Methods:
We conducted a retrospecitve study from January 2022 to June 2023 investigating the incidence of SARS-CoV-2 infection in allo-HCT recipients who received tixagevimab/cilgavimab preexposure prophylaxis (T/C PrEP) compared to those who did not. T/C was administered as a single intramuscular injection of 300/300mg within 1 to 3 months post allo-HCT from April 2022. COVID-19 diagnosis was confirmed through a positive RT-PCR test. Univariable and multivariable logistic regressions were used to assess risk factors associated with COVID-19 infection, and Cox proportional hazards models were employed to evaluate risk factors associated with the time from transplant to COVID-19 infection.

Results:
Logistic regression, adjusted for sex, age, SARS-CoV-2 vaccination status, and immunosuppressive treatment, revealed a significant reduction in the likelihood of SARS-CoV-2 infection risk with T/C PrEP (adjusted odds ratio aOR = 0.26 [0.07, 0.91]). Kaplan-Meier analysis of the time to SARS-CoV-2 infection revealed a trend toward a longer time to infection in patients who received T/C compared to those who did not. Using a Cox-model for survival analysis, we confirmed a trend for a lower hazard of infection in the group of patients under T/C (adjusted hazard ratio (aHR) = 0.36, 95% CI = [0.12;1.06]).

Conclusion:
Our study contributes relevant evidence that mAb PrEP can be successfully implemented in the early posttranspant period and reduces the risk of SARS-CoV-2 infection before sufficient vaccination responses can be expected. It also highlights the ongoing vulnerability of patients after allo-HCT to symptomatic infections and emphasizes the continued importance of a comprehensive strategy for preventing SARS-CoV-2, which includes a combination of active and passive immunization measures.

644

N. Jucker[2], D. Alceste[2], M. Serra[2], HAJ. Meijer[3], A. Thalheimer[2], RE. Steinert[2], AC. Spector[1], D. Gero[2], M. Bueter[2]

Effect of Roux-en-Y Gastric Bypass on Microstructural Parameters of Ingestive Behavior in Adult Females with Obesity during a Four-Bottle Preference Test.

Florida State University, USA[1], University Hospital Zurich[2], University of Groningen, Netherlands[3]

Introduction:
Metabolic bariatric surgery, particularly Roux-en-Y gastric bypass (RYGB), has proven effective in obesity treatment, surpassing non-surgical methods in numerous health outcomes. Recent research, including our latest studies, has shifted focus from traditional dietary metrics to the microstructure of ingestive behavior. With a four-bottle test we found that the RYGB reduced the absolute but not the relative macronutrient intake of patients with obesity one year after surgery, thereby confirming the results of other similar studies with cafeteria and residential settings. Furthermore, we could also confirm previous results about the postoperative reduction of meal duration and eating rates. The aim of this study was to extend this investigation to the microstructural changes of ingestive behavior one year after RYGB.

Methods:
This study compares the microstructural parameters of ingestive behavior between adult females with obesity undergoing RYGB (n = 23) and adult females with obesity not scheduled for surgery (n = 24) during a four-bottle preference test, where adult females with normal body weight were included for test stability purposes (n = 11). The four bottles were isocaloric milks with different concentrations of sugar, maltodextrin, and cream: high-fat/high-sugar, high-fat/low-sugar, low-fat/high-sugar, and low-fat/low-sugar. Using a drinkometer device, data about burst size, burst duration, burst rate, number of sucks per burst, and overall microstructural parameters from the most preferred bottle were collected. The measurements were performed at five different time points over the first postoperative year.

Results:
The study found significant postoperative changes for various ingestive behavior parameters in the population with RYGB compared to baseline and the population with Obesity. Notably, reductions in suck size (–9 kcal, $p < 0.01$), suck rate (–3.6 kcal/s, $p < 0.001$), burst size (–81.0 kcal ($p < 0.001$), burst rate (–2.3 kcal/s, $p < 0.05$), burst duration (–5.6 s, $p < 0.01$), and number of sucks per bursts (–2.5 u, $p < 0.001$) were observed twelve months after RYGB compared to the population with Obesity.

Conclusion:
This study revealed new insights into the effect of RYGB on the microstructure of ingestive behavior, highlighting the need to shift focus from traditional dietary intake to a detailed analysis of ingestive behavior. While RYGB patients show reduced food intake compared to non-operated individuals with obesity, this is not due to changes in macronutrient-based food preferences. Instead, RYGB appears to exert a deeper, mechanistic effect on the microstructure of ingestive behavior. These findings underscore the importance of a standardized, unified approach to studying these microstructural changes, crucial for a comprehensive understanding of the multifaceted impact of RYGB on obesity treatment.

645

M. Serra[2], D. Alceste[2], H. Hauser[2], N. Jucker[2], PJM. Hulshof[4], HAJ. Meijer[3, 4], A. Thalheimer[2], RE. Steinert[2], PA. Gerber[2], AC. Spector[1], D. Gero[2], M. Bueter[2]

Validity Assessment of the SNAQ App for Estimation of Daily Energy Intake in Adult Females with Normal Weight and Obesity.

Florida State University, USA[1], University Hospital Zurich, Switzerland[2], University of Groningen, Netherlands[3], Wageningen University, United Kingdom[4]

Introduction:
Dietary intake assessment is crucial in nutritional research and clinical practice. The SNAQ app, an image-based food-recognition tool based on computer vision, has emerged as a novel method for evaluating dietary intake. This research aimed to assess the validity of SNAQ in estimating daily energy intake compared to the doubly labelled water (DLW) technique and a traditional method, such as the 24-hour dietary recall (24HR), in adult females with normal body weight and obesity.

Methods:
Two studies were conducted, each focusing on a different cohort. In both studies, the participants were asked to record their dietary intake in free-living conditions with the SNAQ app over seven consecutive days. Each participant received a dose of DLW and the isotopic concentration was measure in the urine with a two-point method. The first studyinvestigated adult females with normal body weight. In this population, the energy intake estimated by SNAQ was compared against the measurements obtained from DLW and 24HR. The methodological approach included a comprehensive set of statistical and descriptive analyses, consistent across both studies. To answer the primary research question, a Bland-Altman analysis was performed to assess pairwise the agreement and bias between SNAQ, DLW, and 24HR. The second study investigated adult females with obesity. Similar to the first study, it compared thevalidity of SNAQ against DLW and 24HR. The analytical methods employed were the same as those in the first study, ensuring consistency in the evaluation approach.

Results:
For adult females with normal weight (n = 30), the energy intake estimated with SNAQ was closer to DLW measurements than that from 24HR, with an underestimation of –12.8% at the group level. Bland-Altman analysis indicated a smaller bias for SNAQ compared to 24HR. However, for adult females with obesity (n = 20), SNAQ and 24HR both differed significantly from DLW estimates. The standard deviation of SNAQ estimates was three times larger than 24HR, indicating greater variability. Overall, the bias of agreement was more considerable in females with obesity(−817.3 kcal/day) compared to those with normal weight (−329.6 kcal/day).

Conclusion:
SNAQ might offer more accurate energy intake estimates than 24HR in adult females with normal weight. However, its accuracy diminishes in females with obesity. Both studies highlight the potential and limitations of image-based dietary assessment tools like SNAQ. Further research is necessary to enhance the accuracy and reliability of dietary assessment tools based on computer vision for clinical and research applications, considering individual variations in dietary reporting and the technological limitations of image-based assessments.

646

A. Mongelli[1], S. Mohammed[1], E. Gorica[1], A. Mengozzi[1], M. Telesca[1], C. Matter[1], F. Paneni[1], F. Ruschitzka[1], S. Costantino[1]

Long non-coding RNA PANDA drives diabetic vascular dysfunction by promoting endothelial senescence and oxidative damage

Center for Translational and Experimental Cardiology (CTEC),Department of Cardiology, University Hospital Zurich, University of Zurich, Switzerland[1]

Introduction:
ROS and inflammation are major features of diabetic vasculopathy, yet the underlying mechanisms remain elusive. Long non-coding RNAs (lncRNAs) are emerging as important players in the pathogenesis of cardiovascular disease. Recent work has shown that PANDA, a newly identified lncRNA, is a key regulator of cellular senescence and apoptosis

Methods:
Human aortic endothelial cells (HAECs) were exposed to normal (NG, 5 mmol/L) and high glucose concentrations (HG, 25 mmol/L). PANDA depletion in HG-treated HAECs was obtained by siRNA transfection. Expression of PANDA was assessed by real time PCR. RNAs sequencing (RNA-seq) and bioinformatic analysis (network perturbation amplitude, NPA) were leveraged to unveil transcriptional changes upon PANDA depletion. PANDA RNA immuno-precipitation (RIP) was performed to check its binding to relevant transcriptional factor. Western Blots was used to investigate on NRF2 protein and its products. Beta-galactosidase staining was used to detect endothelial senescence while, migration and tube formation were employed to evaluate angiogenic properties of HAECs. ROS production and NRF2 localization were investigated by fluorescence staining

Results:
PANDA expression was significantly increased in HAECs exposed to HG as compared to NG. Transcriptomic analysis revealed dysregulation of several genes upon PANDA silencing with the antioxidant gene heme oxygenase-1 as the top-ranking transcript in HG-treated cells. NPA analysis showed a strong involvement of PANDA in senescence, DNA damage, NRF2 signaling, hypoxic stress response and proliferation. Under HG conditions PANDA perturbed the pathway of the transcription factor NRF2, thus inhibiting the expression of NRF2-dependent pro-survival and anti-aging gene. Indeed, silencing of PANDA in HG-treated HAECs reduced the apotosis and senescence. PANDA depletion in HG improved endothelial migration and tube formation, while ROS production was reduced. In HG, there was an increasing of PANDA-NRF2 binding. Interesting, in HG NRF2 was more present in the cytosol, while PANDA siRNA allowed its translocation into the nucleus where it can promote the transcription of HMOX1.

Conclusion:
The hyperglycemia induced the upregulation of PANDA driving endothelial senescence and impairing angiogenic properties. PANDA depletion in HG-treated HAECs rescued maladaptive transcriptional changes enhancing NRF2 pathway. Of note, targeting PANDA in the diabetic vasculature was able to rescue endothelial dysfunction. These results indicate PANDA as a novel molecular target in the setting of diabetic vascular disease.

647

L. Ihm[1], R. Speck[1], N. Kadzioch[1]

The pathogenic significance of USP18 in HIV pathogenesis

Universitätsspital Zürich[1]

Introduction:
Interferon (IFN) signaling is a major defense against viral infection such as with Human Immunodeficiency Virus (HIV). However, chronic immune activation, as during the latent phase of HIV infection, contributes to immune cell exhaustion and therefore the decline of CD4+ T cells – a hallmark of HIV pathogenesis. Ubiquitin specific peptidase 18 (USP18) is a key negative regulator of IFN signaling. Functionally, it binds the inner domain of IFN receptor (IFNAR) α subunit 2 and inhibits Jak/STAT signaling and subsequent transcription and translation of IFN stimulated genes (ISGs). USP18, being an ISG itself is a feedback inhibitor. During chronic HIV infection however, USP18 is somehow unable to desensitize cells to IFN stimulation and therefore ISG production. A second role of USP18 is its ability to deconjugate ISG15, a key anti-viral effector, from its target proteins. Previous studies in monocytes and T cells, as well as in mouse models, showed a clear link between a downregulation of USP18 and decreased HIV replication capacity as well as improved immune cell maintenance. As such, the role of USP18 in HIV pathogenesis requires further study.

Methods:
This project aims to deepen the understanding of the USP18/ISG15/IFN signaling axis by studying gain and loss of function of USP18 in the context of HIV infection. First, in vitro cell lines and primary cells will be used and subsequently in vivo studies in humanized mice will allow the placing of results in a physiological context. USP18 was previously knocked out in Jurkat, SupT1, and THP1 cells. Variants of the protein with a range of functional modifications reconstituted were under a tet-on promoter, which allows for temporal control of gene expression. The next steps are aimed to elucidate the functional significance of each of the major function of USP18 (negative regulation of IFN signaling/ deISGylation) in the context of IFN stimulation as well as HIV infection. Characterization of the cell lines will be done using a variety of methods: cell viability will be monitored using XTT assay and Annexin V staining; Proliferation will be monitored by CFSE5 labelling; Selected ISGs (IFIT1, CXCL10, IFI16, MX1 and ISG15) will be quantified by real-time PCR; ISGylation will be analyzed using Western Blot analysis with antibodies against ISG15; STAT-phosphorylation will also be assessed via Western Blotting.

Results:
Initial analysis has confirmed the functionality of the tet-on promoter system in the cell lines. Furthermore, interesting results were regarding cell viability of USP18-/- cells following IFN stimulation: a strong decrease in cell viability – further found to be due to apoptosis – occurs in USP18-/- cells following stimulation with IFNα2. Lastly, tissue expression levels of USP18 in humanized mice was quantified for the first time both at baseline and following IFN stimulation.

Conclusion:
The IFN system is pivot for the innate as well as the adaptive immune system. For this, and to avoid excess activation, the IFN system must be highly fine-tuned. Its dysfunction has also major effects on neoplasia as well as autoimmune diseases. USP18 is a key negative regulator of the Jak/STAT pathway. Its clinical significance underlined by the devastating interferonopathies in patients with impaired USP18 functioning. USP18 is upregulated in HIV infection and there is a clear link between USP18, IFN signaling, and HIV pathogenesis. This project will help shed light on the mechanism underlying this known link and hopefully contribute to the development of novel ways to enhance the immune response against HIV.

648

LV. Heeb[1], A. Gupta[1], L. Huynh-Russo[1], E. Breuer[1], P. Clavien[1]

Assessing the therapeutic potential of immunotherapies to control colorectal cancer metastasis in the regenerating liver

Department of Surgery and Transplantation, University Hospital Zurich[1]

Introduction:
Due to the livers remarkable capacity to regenerate, the gold standard to treat liver cancer is the surgical resection of malignant tissue (hepatectomy). However, if the future liver remnant is too small, regeneration is impaired and consequently leads to liver failure, thus limiting intervention at advanced cancer stages. Furthermore, during regeneration, nonresectable occult micrometastases can start to regrow leading to cancer relapse, probably due to the growth-inducing microenvironment of the regenerating liver. Therefore, tumor-targeting treatments that do not impair liver regeneration are needed.

Methods:
Here we use tumor-specific immunotherapies during the perioperative window (before, during and after surgery) after liver resection in a murine liver regeneration and tumor model. To mimic liver regeneration due to tumor resection, we developed a mouse model, which combines the injection of tumor cells into the portal vein with partial hepatectomy. This allows us to study the dynamics of cancer relapse due to regenerative processes. By using specific knockout mouse lines of immunomodulatory molecules such as PD-L1, PD-1 and LAG-3 and administering blocking antibodies to wildtype mice, we study the effect of immunotherapy on liver regeneration, liver metastases and immune cells.

Results:
Our results show that liver metastases grow faster after partial hepatectomy and show an increased expression of PD-L1. Blocking of PD-1 and LAG-3 does not impair liver regeneration and administration of such blocking antibodies during liver regeneration in micrometastases-carrying mice reduces tumor growth. Furthermore, immunohistochemical and flow cytometric analysis reveals that tumor-infiltrating immune cells are mostly myeloid cells and CD8+ T cells show a less activated and less cytotoxic phenotype in the regenerating liver.

Conclusion:
Our data suggests that the immunomodulatory molecules PD-1, PD-L1 and LAG-3 can be safely blocked during liver regeneration to target liver metastases. Overall, this project aims to prevent cancer relapse during liver regeneration.

649

M. Determann[6], L. Luise[6], M. Schwarzfischer[6], A. Niechcial[6], M. Wilmink[6], M. Walker[6], D. Pöhlmann[6], MR. Spaliner[6], Y. Morsy[6], F. Sella[7], M. Levesque[7], VH. Koelzer[4], AL. Frei[8], S. Buch[5], J. Hampe[5], C. Datz[1], C. Schafmayer[3], M. Heikenwälder[2], M. Scharl[6], S. Blümel[6]

Hepatic cytotoxic T cells in metabolic dysfunction-associated steatohepatitis are regulated by protein tyrosine phosphatase non-receptor type 2

General Hospital Oberndorf, Teaching Hospital of the Paracelsus Medical University Salzburg, Department of Internal Medicine, Salzburg, Austria[1], German Cancer-Research Center, Department Chronic Inflammation and Cancer, Heidelberg, Germany[2], University Hospital Rostock, Department of General Surgery, Rostock, Germany[3], University of Basel, University Hospital Basel, Institute of Medical Genetics and Pathology, Basel, Switzerland[4], University of Technology Dresden, University Hospital Dresden, Medical Department I, Dresden, Germany[5], University of Zurich, University Hospital Zurich, Departement of Gastroenterology and Hepatology[6], University of Zurich, University Hospital Zurich, Department of Dermatology, Zurich, Switzerland[7], University of Zurich, University Hospital Zurich, Department of Pathology and Molecular Pathology, Zurich, Switzerland[8]

Introduction:
Obesity and its complications, including metabolic dysfunction-associated steatohepatitis (MASH), cirrhosis, and hepatocellular carcinoma are a growing global epidemic. MASH development is characterized by hepatic recruitment of cytotoxic CD8+ T cells, which correlates with liver damage and fibrosis. Protein tyrosine phosphatase non-receptor type 2 (PTPN2) attenuates CD8+ T cell responses to self-antigens, tumors and inflammation. Thus, PTPN2 is involved in pathways, affecting MASH development and may therefore be crucial in MASH pathogenesis by modulating CD8+ T cell functionality. Here, we studied the impact of T cell-specific PTPN2 on MASH development and disease progression in a translational project with human samples and mouse models.

Methods:
The impact of human hepatic PTPN2 expression on MASH development was analyzed from (1) mRNA data from the sequence read archive (SRA) database (n = 32 control, 48 Metabolic Dysfunction-associated Steatotic Liver Disease (MASLD), 26 MASH patients); (2) protein expression in liver biopsies using multicolor immunofluorescence staining (n = 7 control, 12 MASH patients); (3) the presence of the single nucleotide polymorphism (SNP) rs2542151, which results in PTPN2 dys-function, in an Austrian and German MASLD cohort (n = 251 control, 672 MASLD, 73 MASH patients). To understand how PTPN2 in T cells is connected to MASH development, mice with conditional PTPN2-knock-out in T cells (KO, PTPN2fl/fl x CD4Cre) and their wild-type (WT, PTPN2fl/fl) littermates (n = 4-19 mice per group) were fed 28 weeks with western-style fast food diet (FFD), starting at 8 weeks of age. The mice were investigated regarding their MASH characteristics.

Results:
In human livers, PTPN2 mRNA-expression was increased in MASLD and MASH patients compared to healthy controls, and in MASH compared to MASLD ($p < 0.05$). PTPN2 expression in patients with non-alcoholic fatty liver disease (NAFLD) activity score (NAS) 5 and NAS 6 was higher compared to patients with NAS 0 ($p < 0.05$). Immunofluorescence analysis revealed increased numbers of PTPN2+, CD3+ PTPN2+ and CD8+ PTPN2+ cells in MASH patients compared to controls ($p < 0.05$). Of note, the frequency of severe liver fibrosis in MASH patients with the SNP rs2542151 was reduced (minor allele frequency (MAF) for F3/4 fibrosis and cirrhosis = 0.108-0.139 vs. fibrosis F0/1-MAF = 0.156). The FFD-fed PTPN2fl/fl x CD4Cre had a lower body weight than their WT littermates ($p < 0.05$) with no differences in water or food consumption. In contrast to their WT littermates, the FFD-fed KO mice were protected from MASH and fibrosis (mean WT-NAS 6 vs. KO-NAS 4; mean WT-fibrosis F2 vs. KO-fibrosis F0). In flow cytometry, livers of FFD-fed KO mice had higher amounts of exhausted and central memory CD8+ T cells ($p < 0.05$), while all other immune cell groups were not different between genotypes.

Conclusion:
We observed increased PTPN2 mRNA and protein expression in human MASH livers, suggesting a disease aggravating effect of PTPN2. The SNP analyzes and in vivo data indicated a protective effect of PTPN2 deficiency against MASH most likely mediated by intrahepatic CD8+ T cell functionality. The mechanism of how these T cells influence hepatic lipogenesis and fibrogenesis has yet to be investigated.

650

Y. Chen[1], S. Steiner[1], C. Hagedorn[1], S. Kollar[1], A. Pliego-Mendieta[1], M. Haberecker[1], J. Plock[2], C. Britschgi[1], L. Planas-Paz[1], C. Pauli[1]

Acquired NF2 mutation confers resistance to TRK inhibition in an ex vivo LMNA::NTRK1 rearranged soft tissue sarcoma cell model

Department of Pathology and Molecular Pathology, USZ[1], Department of Plastic Surgery and Hand Surgery, Kantonsspital Aarau & Department of Plastic Surgery and Hand Surgery, USZ[2]

Introduction:
The neurotrophic receptor tyrosine kinase genes (NTRK1, NTRK2, and NTRK3) belong to a family of nerve growth factor receptor genes encoding a single transmembrane receptor tyrosine kinase (RTK) protein. Rearrangements of NTRK genes often results in sustained cancer cell proliferation through the activation of MAPK and AKT downstream pathways. The first generation TRK inhibitors larotrectinib and entrectinib showed excellent clinical respnse in NTRK fusion tumors. However, the occurence of drug resistance is a major obstacle. There is a need to delineate underlying resistance mechanism and improve clinical therapeutic regime. Patient-derived *ex vivo* cell models have shown to better recapitulate the genotype and phenotype of patient tumor. NTRK fusion mutation is observed in over 90% of infantile fibrosarcoma, but due to the rarity of soft tissue sarcoma (STS), well-established cell model is extremely limited and functional studies are therefore sparse. We here established a patient-derived LMNA::NTRK1-rearranged STS cell model with an *ex vivo* acquired resistance to entrectinib. Molecular analysis revealed an acquired point mutation in the NF2 gene, and increased activation of the MAPK and mTOR/PI3K/AKT pathways. Our model provides new insight into the biology of acquired drug resistance in LMNA::NTRK1-rearranged soft tissue sarcomas and allows us to discover potential therapeutic strategies to overcome the resistance and guide further patient care.

Methods:
Tissue processing and ex vivo cell model establishment
Histology assessment and immunohistochemistry
Molecular characterization
Functional analysis
Induction of acquired resistance
Western blot
Bioinformatics analysis

Results:
We established an ex vivo STS cell model with an oncogenic LMNA::NTRK1-rearrangement from a 16-year-old female patient. The model faithfully recapitulated patient tumor characteristics, confirmed by immunohistochemistry and molecular profiling. Resistance was induced by escalating entrectinib exposure from 0.6 µM to 5 µM over 6.5 months, resulting in biobanked resistant clones. Dose response curves to TRK inhibitors indicated reduced sensitivity in resistant clones compared to parental cells. Genomic profiling revealed a newly acquired NF2 splice site mutation in all resistant clones, correlating with decreased NF2 expression and upregulation of MAPK pathway regulators. Western blot confirmed elevated pERK, pAKT, and pS6 signal in resistant clones, suggesting MAPK and mTOR pathway upregulation due to NF2 loss. Functional investigation involved inhibiting MAPK and mTOR pathways with rapamycin and trametinib. Trametinib monotherapy exhibited increased potency in resistant clones, and combination drugging showed synergy between entrectinib and trametinib or rapamycin. Sarco-spheres were subjected to medium-throughput mono- or combination drug screens, identifying histone deacetylase inhibitor romidepsin and fibroblast growth factor receptor inhibitors infigratinib and futibatinib as potent monotherapies or in combination with entrectinib among 80 tested drugs.

Conclusion:
In summary, we developed a model of drug resistance in an LMNA::NTRK1-rearranged soft tissue sarcoma and broadened the understanding of acquired drug resistance to targeted TRK therapy. Furthermore, we identified single and combination compounds to overcome acquired drug resistance and potentially guide patient care.

651

N. Han[3, 4], T. Loosli[3, 4], A. Hauser[4, 8], J. Josi[3, 4], L. Johnson[1], R. Lessells[2, 6], H. Günthard[3, 4], M. Egger[2, 5, 7], R. Kouyos[3, 4]

The impact of long-acting cabotegravir and rilpivirine on the HIV epidemic and resistance dynamics in South Africa – a modelling study

Centre for Infectious Disease Epidemiology and Research, University of Cape Town[1], Centre for the AIDS Programme of Research in South Africa (CAPRISA)[2], Department of Infectious Diseases and Hospital Epidemiology, University Hospital Zurich[3], Institute of Medical Virology, University of Zurich[4], Institute of Social and Preventive Medicine (ISPM), University of Bern[5], KwaZulu-Natal Research Innovation and Sequencing Platform (KRISP), University of KwaZulu-Natal[6], Population Health Sciences, Bristol Medical School, University of Bristol[7], Sorbonne Université, INSERM U1136, Institut Pierre Louis d'Epidémiologie et de Santé Publique (IPLESP)[8]

Introduction:
Long-acting cabotegravir and rilpivirine (CAB/RPV-LA) is the first long-acting antiretroviral therapy (LA-ART), shown in various clinical trials to be an effective switching option for people with viral suppression. However, there is a risk of acquiring integrase strand transfer inhibitor (INSTI) resistance upon failure or discontinuation of CAB/RPV-LA, particularly where people are 'lost-from-care' (LfC), given the long pharmacokinetic tail of LA-ART. Long-term perspectives on the impact of implementing CAB/RPV-LA treatment and its association with LfC on drug resistance are unclear, especially in resource-limited settings.

Methods:
We extended the MARISA (Modelling Antiretroviral drug Resistance in South Africa) model to include a complex INSTI resistance layer, CAB/RPV-LA treatment cascade, and LfC dynamics. This mechanistic model captures the HIV epidemic and drug resistance in South Africa from 2005 with dolutegravir (DTG) roll-out in 2020. We implemented the following hypothetical scenarios: (1) no CAB/RPV-LA (all first-line treatment with DTG-based regimens); (2) CAB/RPV-LA as either switching option for people with viral suppression or both switching and new first-line initiators starting in 2023. We further explore varying assumptions of CAB/RPV-LA treatment efficacy, tail phase dynamics, and access depending on resistance mutations. Two levels of retention in care were modelled: full retention in care, and partial retention, in which a fraction of people may become LfC, with the option of re-entering care). Drug resistance for CAB/RPV-LA and DTG was modelled considering the same major drug resistance mutations and acquisition patterns. For CAB/RPV-LA, however, we assumed a lower genetic barrier, resulting in a faster mutation acquisition, and decreased susceptibility due to resistance to CAB/RPV-LA, according to the Stanford HIV Drug Resistance Database genotypic resistance interpretation system. During the simulation, we assumed that CAB is not used as pre-exposure prophylaxis but only as ART in the form of CAB/RPV-LA.

Results:
Using the extended MARISA model, we find that introducing CAB/RPV-LA as ART is associated with an increase in INSTI drug resistance at the population level; in particular, when individuals are only partially retained in care and when CAB/RPV-LA is implemented as both switching and ART initiation option. Implementing CAB/RPV-LA is also expected to reduce NRTI (nucleoside reverse transcriptase inhibitor) resistance on the population level, but to increase RPV resistance. The increase in INSTI resistance depends on the frequency of CAB/RPV-LA usage and the degree of care retention. The predicted trends of increasing population level drug resistance are robust to varying LA-ART-related parameters including treatment efficacy, eligibility criteria regarding drug resistance at initiation or switch, and the length of the tail phase.

Conclusion:
Our model suggests that introducing CAB/RPV-LA as antiretroviral treatment in South Africa may lead to a substantial increase in HIV drug resistance at the population level. Based on our findings, we suggest that the implementation of CAB/RPV-LA should be accompanied by additional considerations, such as access to LA-ART and viral load monitoring to minimize the risk of resistance evolution and transmission.

652

J. Duran Ramirez[1, 8], K. Kusejko[1, 8], K. Metzner[1, 8], M. Huber[8], Y. Martin[3], . Stöckle[6], A. Calmy[5], L. Decosterd[4], M. Cavassini[4], E. Bernasconi[2], P. Schmid[7], H. Günthard[1, 8], D. Braun[1], S. SHCS[1]

Uptake and Discontinuation of the Long-Acting Duo in The Swiss HIV Cohort Study: Preliminary Analysis on Cabotegravir Plus Rilpivirine

Department of Infectious Diseases and Hospital Epidemiology, University Hospital Zurich, University of Zurich, Zurich, Switzerland[1], Department of Infectious Diseases, Ente Ospedaliero Cantonale, Lugano, University of Geneva and University of Southern Switzerland, Lugano, Switzerland[2], Department of Infectious Diseases, Inselspital, Bern University Hospital, University of Bern, Bern, Switzerland[3], Department of Infectious Diseases, Lausanne University Hospital, University of Lausanne, Lausanne, Switzerland[4], Department of Infectious Diseases, University Hospital Geneva, University of Geneva, Geneva, Switzerland[5], Division of Infectious Diseases & Hospital Epidemiology, University Hospital Basel, University of Basel, Basel, Switzerland[6], Division of Infectious Diseases, Cantonal Hospital St Gallen, St. Gallen, Switzerland[7], Institute of Medical Virology, University of Zurich, Zurich, Switzerland[8]

Introduction:
Routine clinical data on the uptake and discontinuation of cabotegravir plus rilpivirine long-acting (CAB+RPV-LA) is scarce. We present data from the Swiss HIV Cohort Study (SHCS) more than one year after market authorization (March 2022) in Switzerland.

Methods:
We assessed sociodemographic, clinical, and behavioural baseline characteristics of all SHCS participants initiating the CAB+RPV LA regimen since March 2022. Moreover, we describe reasons for CAB+RPV-LA discontinuation.

Results:
From 9,479 active SHCS participants, 264 (2.8%) initiated CAB+RPV-LA, with a peak of 35 participants starting in June 2022. The median age was 48 years, and the median body mass index was 25.4 kg/m2. The majority of individuals were male (n=216;82%), of white ethnicity (n=186;71%), acquired HIV through men-who-have-sex-with-men (MSM) sexual contacts (n=169;64%), had higher education (n=134;51%), were in a steady partnership (n=156;61%) and highly adherent (n=207;81%) to the previous antiretroviral therapy (ART) regimen. Albeit 59% (n=156) of participants were recruited in larger university hospitals, recruitment also took place in private practices (n=73;28%) and affiliated hospitals (n=35;13%). 29% (77/264) had prior exposure to RPV, and most participants switched from bictegravir/ emtricitabin/ tenofovir alafenamide (n=77;29%) to CAB+RPV-LA. Eight individuals (3%) discontinued the CAB+RPV-LA regimen: reasons for discontinuation were participant's wish (n=1), death (n=1), injection site reactions (n=2), moving to a foreign country without access (n=1), loss to SHCS care (n=1), confirmed virological failure (n=1, two consecutive measurements of >50 RNA copies/mL plasma), and low RPV blood concentration (n=1).

Conclusion:
After more than one year of market authorization, only a small proportion of SHCS participants switched to the CAB+RPV-LA regimen, and most of them were middle-aged white MSM with high educational levels. The vast majority of participants switched from an integrase strand transfer inhibitor-based regimen, with a high proportion having prior exposure to RPV. CAB+RPV-LA discontinuation and confirmed virological failure (0.4%) were low.

653

L. Jones[2], H. Rodriguez[1], R. Katzschmann[2], O. Dzemali[1]

Using Metamaterials and Cardiac Tissue Engineering to engineer Robust and Contractile Cardiac Tissue Patches

Klinik für Herzchirurgie, Universitätsspital Zürich[1], Soft Robotics Lab, ETH Zurich[2]

Introduction:
Ventricular Septal Rupture (VSR) is a challenge in cardiac medicine with a high mortality rate of 45-60%. Current treatment methods use bovine pericardial patches (BPPs), which are non-contractile, tend to calcify over time, and fail to integrate effectively with the myocardium. Therefore, patients do not fully recover cardiac function.

Methods:
We are engineering a cardiac tissue patch that uses human stem cell-derived cardiomyocytes in hydrogel, reinforced with a metamaterial lattice. This approach allows us to tune the patch's mechanical properties and contractility while enabling stable implantation within the intraventricular space.

Results:
Here, we will showcase our current results on metamaterial design and manufacturing, mechanical characterization (tunable stiffness and anisotropic ratio), and biological characterization (biocompatibility, cell maturation, and tissue contractility).

Conclusion:
In summary, we will show how metamaterials can be combined with engineered cardiac tissues to fabricate centimetre scale, three dimensional, and implantable cardiac tissues.

654

FG. Beltrami[1], KGP. Boyle[1], C. Brunckhorst[2], F. Duru[2], CM. Spengler[1, 3], AM. Saguner[2]

Ventricular arrhythmia burden during different physical activities in patients with Arrhythmogenic Right Ventricular Cardiomyopathy: Preliminary Analysis

ETH Zürich[1], University Heart Center Zürich[2], Zurich Center for Integrative Human Physiology (ZIHP), University of Zurich[3]

Introduction:
Patients suffering from arrhythmogenic right ventricular cardiomyopathy (ARVC) should avoid intense endurance exercise to reduce the risk of adverse cardiac events and disease progression. While an active lifestyle would be preferable to a sedentary one, evidence for safe levels of physical activity in ARVC, however, is scarce. This study aimed to describe the ventricular arrhythmia burden experienced during exercise and immediate recovery - estimated as the prevalence of premature ventricular contractions (PVC) - of different exercise modalities and intensities on ARVC patients.

Methods:
This preliminary analysis includes four (1 female, age 33±12 years, body mass index 24±4 kg/m2) ARVC patients harboring a pathogenic plakophilin-2 variant and carrying an implantable cardioverter-defibrillator that performed different exercises while monitored via 12-lead ECG. All exercise bouts were performed within a single visit. Resistance exercises included two-legged squats and single arm biceps curls (each with 20 repetitions and totalizing 2 min duration). Endurance exercise included 5 min of treadmill walking and 3-min cycling bouts at heart rates (HR) of 80, 100 and 120 bpm, as well as cycling at 120 bpm with 2 additional min of active cool down, where power output was reduced by 50%. Blood lactate concentration was assessed after each cycling bout. The order of modalities was randomized and participants instructed to stop when surpassing perceived exertion of 15 on the Borg 6-20 scale.

Results:
No adverse cardiac event or early termination for medical reasons occurred. During walking (HR 76 ± 8 bpm), PVC burden was 11 ± 6% (range 4 – 18%). Cycling at 82 ± 4 bpm induced a PVC burden of 7 ± 5% (range 3 – 14%), which increased to 13 ± 8% (range 3 – 21%) at 93 ± 2 bpm and increased further to 16 ± 16% (range 7 – 37%) at 105 ± 3 bpm. In all three intensities the PVC burden was higher in the first 3 min of recovery than during the activity itself. Adding a 2-min active cool down increased the PVC burden to 25 ± 16% (range 6 – 45%). 2-legged squats (HR 101 ± 15 bpm) had a PVC burden of 9 ± 12%, which increased to 19 ± 14% at recovery. One arm biceps curls (HR 75 ± 13 bpm) had a PVC burden of 4 ± 3% during the activity and 9 ± 5% during recovery, even though perception of effort was similar to that seen during moderate/intense cycling (average 13.8, range 11 – 15). Perception of effort varied widely when cycling at 80 bpm (range 6 – 12) or 100 bpm (range 8 – 14), but less so at 120 bpm (range 13 – 15). Blood lactate concentration when cycling at 120 bpm ranged between 2.2 and 3.5 mmol/L, typically associated with exercise in the “heavy” intensity domain.

Conclusion:
PVC burden was high and seemingly intensity-dependent during exercise and immediate recovery, except when a very small muscle mass was used, when the relationship between intensity and PVC burden was attenuated. The wide range of PVC burden for physiological or subjective markers of effort call for personalized recommendations on physical activity. Exercises with small muscle mass such as biceps curls seem to minimize the PVC burden, thus, training the different muscles separately could be an interesting avenue to maintain physical fitness in ARVC patients.

655

D. Wimmersberger[2], K. Kusejko[2, 4], S. Brugger[2], D. Haerry[5], M. Stöckle[7], J. Notter[1], A. Calmy[8], M. Cavassini[9], E. Bernasconi[6], E. Colin-Benoit[3], H. Günthard[2, 4], D. Braun[2, 4]

Acceptance of doxycycline post-exposure prophylaxis and four-component meningococcal B vaccine for the prevention of bacterial sexually transmitted diseases in men who have sex with men and transgender women living with HIV in Switzerland

Cantonal Hospital St Gallen, St Gallen, Switzerland[1], Department of Infectious Diseases and Hospital Epidemiology, University Hospital Zurich, University of Zurich, Zurich, Switzerland[2], Inselspital Bern, Bern, Switzerland[3], Institute of Medical Virology, University of Zurich, Zurich, Switzerland[4], Patient and Public Involvement (PPI), Swiss HIV Cohort Study[5], Regional Hospital Lugano, Lugano, Switzerland[6], University Hospital Basel, Basel, Switzerland[7], University Hospital Geneva, Geneva, Switzerland[8], University Hospital Lausanne, Lausanne, Switzerland[9]

Introduction:
Bacterial sexually transmitted diseases (STDs) cause a substantial disease burden and stigma among men who have sex with men (MSM) and transgender women (TGW) living with HIV. There is growing evidence that event-driven doxycycline post-exposure prophylaxis (dPEP) and the four-component serogroup B meningococcal vaccine (4CMenB) can reduce the incidence of the major bacterial STDs (i.e. syphilis, gonorrhea, and *Chlamydia trachomatis*).

Methods:
From May 15th to December 15th, 2023, we conducted a survey exploring the acceptance of the off-label use of dPEP and 4CMenB among participants of the Swiss HIV cohort study at highest risk for STDs, i.e. MSM and TGW diagnosed with ≥ 1 STI within the preceding 3 years and/or reporting condomless sex with ≥ 1 occasional partner within the preceding 6 months. The participants were asked if they had already heard about dPEP and 4CMenB as STD prevention strategies and if they consider their use.

Results:
637 out of 2129 eligible persons answered the questionnaire of whom 122 (19.2%) and 49 (7.7%) had already heard about dPEP and 4CMenB used for STD prevention, respectively. 340 (53.4%) and 305 (47.9%) consider the off-label use of dPEP or 4CMenB, respectively. Proportions of acceptance were highest in individuals younger than 35 years of age (58.7% and 53.3% for dPEP and 4CMenB, respectively). Acceptance for both interventions was highest in patients who had an STD in the previous year as compared to people with the last STD episode > 1 year ago or no STD history (dPEP 65.1% vs. 49.1%; 4CMenB 61.5% vs. 42.9%; $p < 0.001$). In centers of the French and Italian speaking parts of Switzerland, acceptance for dPEP was higher than in German speaking regions (64.7% vs. 50.5%; $p = 0.001$), whereas 4CMenB was more accepted in Swiss German centers (45.1% vs. 49.0%; $p = 0.03$).

Conclusion:
People living with HIV in Switzerland at highest risk for bacterial STDs show high acceptance for the off-label use of dPEP and 4CMenB to prevent bacterial STDs. Clinicians should become familiar with these preventive interventions and consider their use as an adjunct to standard screening, counseling, and treatment efforts in persons at highest risk for STDs.

656

K.D. Raghvendra[1], G. Azzarito[1], M. Rosselli[1], B. Leeners[1]

Transcriptomic Profiling of SARS-CoV-2 Spike Protein S1 Subunit Mediated Changes in Human Vascular Endothelial cells, -Pericytes, -Smooth Muscle Cells and Lymphatic Endothelial cells: Evidence for Differential Gene Regulation

University Hospital of Zurich[1]

Introduction:
SARS-CoV-2 S1 spike protein (S1-SP) plays a critical role by actively facilitating host & virus interaction via ACE2 to mediate the deleterious effects of COVID19. Evidence suggests that SP devoid of virus is not latent & modulate pro-inflammatory actions. Circulating SP levels increase in subjects receiving mRNA vaccines & those who develop post-vaccination myocarditis. However, the mechanism(s) involved remain unclear. Since interaction between circulating factors and vascular cells play a key role in the pathophysiology of cardiovascular complication, using microarrays we assessed the modulatory effects of S1-SP on genes of key human vascular cells (lymphatic and vascular endothelial cells (VECs; LECs), -pericytes (PCs), & –smooth muscle cells (SMCs)).

Methods:
Cells (PCs; VECs; LECs; SMCs) grown to 80% confluence in cell specific culture medium were treated with 10ng/ml recombinant SARS-CoV2 spike protein full length S1 subunit (Val16-Gl690; Ray Biotech). Briefly, cells were fed cell-specific basal medium containing or lacking S1-SP for 60 min under serum free condition. Subsequently FCS was added to a final concentration of 2.5% and the cells allowed to grow for 36 hours and RNA or total protein extracted for either Microarrays & Transciptomic Analysis, Protein Arrays or Western Blotting.

Results:
CoV-2 S1-SP activates multiple genes in a cell specific and ACE-2 independent manner. Majority of genes were differentially modulated by S1 in PCs & VECs. The top 20 genes (up/down) varied in LECs & VECs, moreover, only 8 down- and 2 up-regulated genes were common between PCs, VECs & LECs. The gene modulatory actions of S1-SP were not ACE-2 dependent as S1-SP failed to modulate genes in SMCs, which expressed ACE2. Moreover, S1-SP modulated genes in VECs, which expressed little or no ACE-2. Since S1 activates TGB-β by interacting with cell surface Integrins, Lectins, Glycosaminoglycans, they may, in part contribute to S1 mediated gene expression. In Bioplanet analysis, TGF-β pathway was highly regulated in PCs, VECs and LECs. S1-SP significantly modulated genes for P-selectin, vWF as well as genes implicated in myocarditis, COVID-19 infection, inflammation & metabolism.

Conclusion:
The comparative transcriptomic profiling of S1-SP induced changes in vascular PCs, VECs, LECs and SMCs, provides important insights to elucidate the mechanisms mediating the deleterious cardiovascular actions of circulating S1-SP associated with COVID-19 and/or mRNA vaccine.

657

C. Pellegrino[3], N. Favalli[5], L. Volta[3], R. Benz[3], S. Puglioli[5], G. Bassi[5], K. Zitzmann[4], CJ. Auernhammer[4], S. Nölting[1], C. Magnani[3], D. Neri[5], F. Beuschlein[1, 2, 6], MG. Manz[3]

Peptide-Guided Adaptor-CAR T-Cell Therapy for the Treatment of SSTR2-expressing Neuroendocrine Tumors

Department of Endocrinology, Diabetology and Clinical Nutrition, University Hospital Zürich (USZ), Zürich, and University of Zürich (UZH) Switzerland.[1], Department of Internal Medicine IV and Interdisciplinary Center of Neuroendocrine Tumors of the GastroEnteroPancreatic System (GEPNET-KUM), Ludwig Maximilian University, LMU Klinikum, Munich, Germany[2], Department of Medical Oncology and Hematology, University Hospital Zürich (USZ) and University of Zürich (UZH); Zürich, Switzerland. Comprehensive Cancer Center Zürich, Zürich, Switzerland[3], Department of Medicine II, University-Hospital Munich-Grosshadern, University of Munich, Germany[4], Philochem AG; Otelfingen, Switzerland[5], The LOOP Zurich - Medical Research Center, Zürich, Switzerland[6]

Introduction:
Somatostatin receptor type 2 (SSTR2) is one of five subtypes of somatostatin receptors and is overexpressed on the surface of most gastro-entero-pancreatic (GEP) NETs, pituitary tumors, paraganglioma, meningioma, as well as hepatocellular carcinoma and breast cancer. Chimeric antigen receptor (CAR) T-cells are genetically engineered to express an artificial, T-cell activating binder, leading upon ligation to biocidal activity against target-antigen expressing cells. Adaptor-CAR T-cells recognize, via the CAR, a tag on an antigen-binding molecule, building an activating bridge between the CAR and the target cell.

Methods:
We hypothesized that a novel generated fluorescent-peptide antagonist of SSTR2, called Octo-Fluo, in combination with anti-FITC adaptor (AdFITC(E2)) CAR T-cells, may function as an on-off tunable activating bridge between the CAR and SSTR2 expressing target cells.

Results:
In vitro studies confirmed the binding of Octo-Fluo to Bon1-SSTR2 mCherry-Luc cells without evidence of internalization. AdFITC(E2)-CAR T-cells were activated and efficiently induced Bon1-SSTR2 cell death in vitro, in an Octo-Fluo concentration-dependent manner. In vivo, AdFITC(E2)-CAR T-cells in combination with Octo-Fluo efficiently infiltrated and eliminated Bon1-SSTR2 tumors in immunodeficient mice in therapeutic settings. Both, AdFITC(E2)-CAR T-cell tumor infiltration and biocidal activity, were Octo-Fluo concentration-dependent.

Conclusion:
Our findings demonstrate preclinical efficacy of AdFITC(E2)-CAR T-cells with Octo-Fluo as a versatile, on-off tunable bispecific adaptor for targeted CAR T-cell immunotherapy against SSTR2-positive NETs.

658

A. Kraft[1, 2, 5], M. Meerang[2], MB. Kirschner[2], V. Boeva[1, 3, 4, 5], I. Opitz[2]

A Comparative Analysis of Secreted miRNAs Reveals Candidate Biomarkers for Pleural Mesothelioma Detection

Department of Computer Science, Institute for Machine Learning, ETH Zurich, Zurich, Switzerland[1], Department of Thoracic Surgery, University Hospital Zurich, Zurich, Switzerland[2], ETH AI Center, ETH Zurich, ZUrich, Switzerland[3], INSERM, U1016, Cochin Institute, CNRS UMR8104, Paris Descartes University, Paris, France[4], Swiss Institute of Bioinformatics (SIB), Zurich, Switzerland[5]

Introduction:
Recent research demonstrated that microRNAs released by tumour cells through exosomes or in non-encapsulated form, can promote tumour growth and treatment resistance. These findings underscore the immense potential of tumour-secreted miRNAs as a promising avenue for discovering novel biomarkers and treatment targets. Although specific miRNA dysregulation was linked with pleural mesothelioma (PM), limited knowledge exists about miRNAs secreted in this devastating disease. Here, we want to fill this gap by exploring secreted miRNAs differentially expressed in PM primary cells compared to non-PM ones.

Methods:
We established primary cell cultures from pleural effusion of 12 PM and 7 non-PM patients. For each cell line, we profiled two types of secreted miRNAs: (1) total secreted miRNA in cell culture supernatant (Sup), and (2) exosomal (Exo) miRNAs. Exosomes were extracted using iZON qEV columns, followed by RNA extraction with mirVana PARIS kit. Small RNA sequencing libraries were prepared using the QIAseq miRNA Library Kit (Qiagen). After sequencing, we mapped the cleaned reads on the mature miRNA sequences from MirBaseDB. We identified differentially expressed miRNAs using DESeq2. Survival analysis was done using the survival package. MiRNA target genes were selected using MirDB and functionally annotated using DAVID.

Results:
We compared the miRNA profile of PM and non-PM primary cells in supernatants and exosomes. Our analysis identified 309 and 84 deregulated miRNAs in PM-Exo and PM-Sup, respectively (p-value <0.05). Among the up-regulated miRNAs, we found let-7c-3p and miR-16-5p, which are known tumour suppressors, and miR-23a-3p and miR-30a-5p. Interestingly, miR-30a-5p belongs to the same family as miR-30e-5p, which together with miR-23a-3p was previously identified as part of the long survival signature in PM. Additionally, we identified 11 miRNAs that showed up-regulation in both PM-Exo and PM-Sup. Further analysis of these candidate miRNAs revealed that exosomal expression of miR-30a-5p was a significant predictor of patient survival. Finally, we identified potential target genes of the 11 up-regulated miRNAs and characterised their biological function. The target genes were significantly associated with transcriptional regulation and cell division (p-value <0.05).

Conclusion:
Our comparative analysis of secreted miRNAs in early passage primary cultures identified 11 candidate miRNA biomarkers for PM. The differential enrichment of miRNAs in supernatants (total) and exosomes, suggests selective packaging of miRNAs into exosomes. Our findings emphasise the importance of the PM secretome in advancing our understanding of mesothelioma biology and discovering novel cell-free biomarkers. Further in-depth analyses are currently underway.

659

L. Rings[1], A. Häussler[2], L. Mavrova-Risteska[2], V. Ntinopoulos[1, 2], P. Fleckenstein[1], M. Tanadini[3], H. Rodriguez Cetina Biefer[1, 2], O. Dzemali[1, 2]

Lactate dehydrogenase is not a reliable postoperative marker for hemolysis in paravalvular leakage for sutureless valves

Department of Cardiac Surgery, City Hospital of Zurich – Site Triemli, Zurich, Switzerland[1], Department of Cardiac Surgery, University Hospital Zurich, Zurich, Switzerland[2], Zurich Data Scientists GmbH, Sihlquai 131, 8005, Zurich, Switzerland[3]

Introduction:
Lactate dehydrogenase (LDH) is a standard postoperative marker for hemolysis in the presence of paravalvular leakage (PVL) after aortic valve replacement (AVR). LDH is elevated in certain valves by a fluttering phenomenon. Data suggested a correlation between microparticels (MP) and LDH elevation after AVR. Thus, we analyze the postoperative relevance of LDH after AVR with either transapical transcatheter aortic valves (TA-TAV) or rapid deployment valves (RDV).

Methods:
We performed a retrospective analysis of the data of patients receiving an AVR with RDV-Group and TA-TAV-Group between 2015-2018. We compared PVL and LDH levels before and after surgery, transvalvular gradients, heart block requiring pacemaker implantation, and 30-day mortality.

Results:
138 consecutive patients were selected for the study; 79 patients in RDV-Group (37 Sorin® Perceval valve, 42 Edwards® Intuity valves) and 59 in the TA-TAV-Group (Edwards® Sapien valve). TA-TAV-group were older (median 10 years ($P < 0,0001$) and with a higher incidence of PVL (22.8%, n=13 vs. 2.5 %, n=2; p=0.04). Interestingly, TA-TAV-Group showed lower levels of LDH despite higher rates of PVL. Of note, the Perceval valve trended towards higher LDH values. Moreover, RDV-Group showed an increased arrhythmia profile (p=0.0041); however, no difference in pacemaker implantation was observed. 30-day mortality was similar between groups.

Conclusion:
Our data do not support the correlation between hemolysis and PVL despite elevated LDH in sutureless valves. Our results suggest that LDH might be a marker of extreme heart muscle output or fluttering phenomena and not a marker for hemolysis after sutureless AVR.

660

A. Hülsmeier[1]

The atypical sphingolipid C18SOΔ14Z is a biomarker for DEGS1 related hypomyelinating leukodystrophy

University Hospital Zurich[1]

Introduction:
Sphingolipids (SL) represent a structurally diverse class of lipids that are central to cellular physiology and neuronal development and function. Defects in the sphingolipid metabolism are typically associated with nervous system disorders. The C4-dihydroceramide desaturase (DEGS1) catalyzes the conversion of dihydroceramide to ceramide, the final step in the SL *de-novo* synthesis. Loss of function mutations in DEGS1 cause a hypomyelinating leukodystrophy, which is associated with increased plasma dihydrosphingolipids (dhSL) and with the formation of an atypical C18SOΔ14Z metabolite.

Methods:
We use clinical examination, magnetic resonance imaging and sphingolipid profiling in plasma, utilizing liquid chromatography coupled multi-reaction monitoring mass spectrometry.

Results:
Here, we characterize two novel DEGS1 variants of unknown significance (VUS), provide a structural model with a predicted substrate binding site and propose a regulatory link between DEGS1 and fatty acid desaturase 3 (FADS3). Both VUS involve single amino acid substitutions near the C-terminus within conserved regions of the enzyme. Patient 1 (p.R311K variant) shows severe progressive tetraspasticity, intellectual disability, and epilepsy in combination with brain magnetic resonance imaging (MRI) findings, typical for DEGS1-related leukodystrophy. Patient 2 (p.G270E variant) presents with delayed psychomotor development, oculomotor apraxia, and a normal brain MRI. Plasma from the p.R311K carrier showed a significantly elevated dhSL species and the presence of C18SOΔ14Z, while the plasma SL profile for the p.G270E variant was not altered. This suggests the p.R331K variant is pathogenic, while the p.G270E appears benign.

Conclusion:
As an increase in dihydroSL species is also seen in other pathological disorders of the SL metabolism, the C18SOΔ14Z seems to be a more specific biomarker to discriminate between pathogenic and benign DEGS1 variants.

661

M. Gort[1], S. Arni[2], J. Schumacher[2], T. Aigner[2], K. van Tilburg[2], S. David[2], G. Lang[2], M. Kirschner[2], M. Meboldt[1], I. Schmitt-Opitz[2]

Silicone Additive Manufacturing of Artificial Lungs

ETH Zürich[1], USZ[2]

Introduction:
The vision is a mini extra-corporal membrane oxygenator (ECMO) for outpatient use. With silicone additive manufacturing (SAM) now available, the objective is to evaluate the feasibility of SAM artificial lungs (AL) and how the blood flow path should be designed for SAM. Inferior silicone hemocompatibility favoured the development of polymethylpentene ECMO systems, but silicone remains a great platform to study optimized additively manufactured artificial lung designs. Further, knowledge gained with SAM could be later transferred to newly developed materials.

Methods:
Three silicone designs were additively manufactured with 1.3 mL priming volume, 0.5 mm membrane thickness, 22 mm^2 cross-sectional area at the gas exchange level, and a minimal channel diameter of 1 mm. The perfusate oxygenation and CO2 removal performance of the three designs were compared using anti-coagulated bovine whole blood (ACD citrate, HTK 32%, aseptic) at flow rates of 5, 10, and 15 mL/min. All parts in contact with blood were heparinized. Blood parameters (pH, pCO2, pO2, T) were continuously recorded with a blood monitoring system. Positive ventilation was applied with a rat-sized in-vitro lung perfusion system. Finally, all designs have been scanned with a micro computer tomography (µCT) pre- and post-perfusion to assess the different designs, check for thrombus formation, damage, and adsorption.

Results:
Designs A, B, and C had surface area to volume ratios of 2.7 mm^{-1}, 1.8 mm^{-1}, and 2.5 mm^{-1}, respectively. Design C excelled in oxygenation, while design A was most efficient in CO2 removal. Design A exhibited the lowest pressure drop followed by C and B with 0.4 kPa, 0.9 kPa, and 1.3 kPa, respectively at a flow rate of 15 mL/min. However, in design B 13 of 27 channels were not manufactured correctly and clogged.

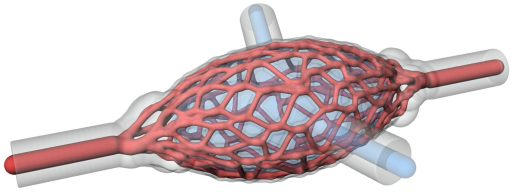

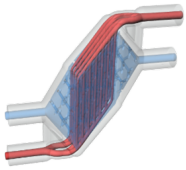

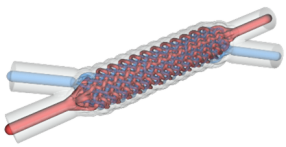

	Design A			Design B			Design C		
Flow [ml/min]	ΔpCO2 [kPa]	ΔpO2 [kPa]	Δp [kPa]	ΔpCO2 [kPa]	ΔpO2 [kPa]	Δp [kPa]	ΔpCO2 [kPa]	ΔpO2 [kPa]	Δp [kPa]
5	**-0.5**	0.9	**0.26**	-0.3	2.8	1.29	-0.1	**5.3**	0.44
10	-0.1	**0.5**	0.33	-0.1	1.3	0.91	-0.1	2.8	0.69
15	-0.2	0.8	0.43	**0**	1.2	**0.56**	**0**	1.5	0.91

Conclusion:
Small-scale SAM AL are feasible and are at least short-term hemocompatible. To become clinically viable, SAM must improve towards creating smaller channel diameter and thinner membranes and allow to print AL similar in size to human lungs.

662

L. Ilcheva[2], V. Ntinopoulos[1, 2], A. Häussler[1, 2], I. Tudorache[1, 2], P. Risteski[1, 2], H. Rodriguez Cetina Biefer[1, 2], O. Dzemali[1, 2]

Early and long-term outcomes of mitral valve surgery after transcatheter edge-to-edge repair: two center experience over 5 years

Department of Cardiac Surgery, City Hospital Triemli[1], Department of Cardiac Surgery, University Hospital of Zurich[2]

Introduction:
The percutaneous edge-to-edge mitral valve (MV) repair with MitraClip, is increasingly favored for high-risk or “inoperable” patients, a term presently defined ambiguously, with unverified long-term efficacy. This study aims to evaluate the early and mid-term outcomes of MV surgery after percutaneous edge-to-edge MV repair in patients deemed “inoperable”.

Methods:
Retrospective two-center study analyzing patients who had received MV repair or replacement after failed transcatheter edge-to-edge repair between 2018 and 2023. Primary endpoints were all-cause mortality at 30 days, 90 days, one year, and postoperative morbidity during index hospitalization. Secondary endpoints were freedom from severe mitral regurgitation (MR), improved clinical (New York Heart Association (NYHA) stage), and left ventricular ejection fraction (LVEF) at 30 days, 90 days, and one year postoperatively.

Results:
32 patients were analyzed. The mean age was 77±6 years, and the median Euroscore II was 8.4 (3.8-17.1). The all-cause mortality rates revealed survival rates of 90% at 30 days, 87% at 90 days, and 87% at one year. Postoperatively, there was a significant reduction in median LVEF from 53% preoperatively to 48% ($p<0.05$), yet the median LVEF remained stable when comparing the 30-day, 90-day, and one-year postoperative marks (53% (49%-61%) vs 48%(41%-57%) vs 48%(40-55%), $p>0.05$). MV function remained stable, with a complete absence of severe mitral regurgitation observed after both 90 days and one year. Additionally, there was significant improvement in the NYHA functional class ($p<0.05$) and freedom from the NYHA IV during postoperative follow-up.

Conclusion:
Patients defined as inoperable by the time they underwent transcatheter edge-to-edge repair show a survival rate of 90% in the first 30 days and 87% in one year after high-risk MV surgery. Therefore, it is essential to critically reassess and engage in interdisciplinary discussions regarding the definition of "inoperable" to facilitate optimal treatment selection.

664

L. Ilcheva[2], V. Ntinopoulos[1, 2], N. Papadopoulos[1, 2], A. Häussler[1, 2], H. Rodríguez Cetina Biefer[1, 2], O. Dzemali[1, 2]

Five years of single-center experience in performing transapical transcatheter aortic valve implantation

Department of Cardiac Surgery, City Hospital Triemli[1], Department of Cardiac Surgery, University Hospital of Zurich[2]

Introduction:
Percutaneous transcatheter aortic valve implantation (TAVI) is widely regarded as the optimal therapeutic modality for high-risk patients afflicted with severe aortic stenosis (AS). However, severe calcification or tortuosity in the femoral vessels poses a significant contraindication for utilizing this approach. Consequently, transapical TAVI (TA-TAVI), which had previously been a commonly employed technique, fell out of favor due to concerns regarding its notably elevated rates of complications. This study aims to investigate the contemporary outcomes associated with TA-TAVI.

Methods:
A database retrospective analysis of patients receiving TA-TAVI between 2018 and 2023 was performed. Primary endpoints were intraoperative and in-hospital mortality and major adverse cardiac and cerebrovascular events (MACCE). Secondary endpoints included intraoperative conversion to median sternotomy, rethoracotomy rates, and the incidence of definitive pacemaker implantation.A database retrospective analysis of patients receiving TA-TAVI between 2018 and 2023 was performed. Primary endpoints were intraoperative and in-hospital mortality and MACCE. Secondary endpoints included intraoperative conversion to median sternotomy, rethoracotomy rates, and the incidence of definitive pacemaker implantation.

Results:
Fifty-one consecutive patients were identified. The mean age was 82±7 years, with a dominant male population constituting 76.5%. The median Euroscore II score was 4.6 (2.3-7.5). The in-hospital all-cause mortality was estimated to be 3.9%(n=2) and 0% intraoperative mortality. Perioperative myocardial infarct occurred in 1.96 %(n=1) of the cases. There were no cases of postoperative stroke. The most common postoperative complication was new-onset atrial fibrillation (25.5 %), and rates of postoperative pacemaker implantation were established at 7.8% (n=4). The intraoperative conversion rate to median sternotomy was 0% and the rethoracotomy rate was 5.9 % (n=3). Additionally, no new dialysis cases were observed; no significant differences in left ventricular ejection fraction pre- and postoperatively were observed.

Conclusion:
Despite previously observed poor outcomes in TA-TAVI, our study demonstrates TA-TAVI as an excellent alternative in the contemporary era of TAVI. Our findings reveal significantly low in-hospital mortality rates and minimal MACCE, highlighting TA-TAVI as a viable therapeutic option for patients characterized by severe calcification or tortuosity in the femoral vessels.

665

M. Labarile[1, 6], J. Fellay[7, 9, 11], CW. Thorball[9], K. Kusejko[1, 6], A. Calmy[5], M. Stöckle[4], A. Rauch[2], B. Surial[2], M. Cavassini[10], E. Bernasconi[8, 12], J. Notter[3], HF. Günthard[1, 6], J. Nemeth[1], PE. Tarr[13], C. Pasin[1, 6], RD. Kouyos[1, 6]

Genetic and non-genetic risk factors affect the risk of Type 2 Diabetes in the Swiss HIV Cohort Study

Department of Infectious Diseases and Hospital Epidemiology, University Hospital Zurich, Zurich, Switzerland[1], Department of Infectious Diseases, Inselspital, Bern University Hospital, University of Bern, Bern, Switzerland[2], Division of Infectious Diseases and Hospital Epidemiology, Cantonal Hospital St Gallen, St Gallen, Switzerland[3], Division of Infectious Diseases and Hospital Epidemiology, University Hospital Basel, University of Basel, Basel, Switzerland[4], HIV/AIDS Unit, Division of Infectious Diseases, Geneva University Hospitals, Geneva, Switzerland[5], Institute of Medical Virology, University of Zurich, Zurich, Switzerland[6], Precision Medicine Unit, Lausanne University Hospital and University of Lausanne, Lausanne, Switzerland[7], Regional Hospital Lugano, Ente Ospedaliero Cantonale, Lugano, Switzerland[8], School of Life Sciences, École Polytechnique Fédérale de Lausanne, Lausanne, Switzerland[9], Services of Infectious Diseases, Lausanne University Hospital, University of Lausanne, Lausanne, Switzerland[10], Swiss Institute of Bioinformatics, Lausanne, Switzerland[11], Università della Svizzera italiana, Lugano, Switzerland[12], University Department of Medicine and Infectious Diseases Service, Kantonsspital Baselland, University of Basel, Bruderholz, Switzerland[13]

Introduction:
Type-2 Diabetes (T2D) is one of the most frequent comorbidities in people with HIV (PWH), and occurs more often than in people without HIV. Previous work suggests a link between HIV-specific factors, such as antiretroviral drugs and pre-treatment CD4-cell counts, and the risk of developing T2D. In the general population, T2D has been shown to have a strong genetic component, which can be summarized in polygenic risk scores (PRS). It is unknown whether HIV-specific factors impact or interact with the genetic component of T2D.

Methods:
We used incidence density sampling to match 688 participants with a diagnosis of T2D to 2475 controls within the Swiss HIV Cohort Study. Cases and controls were matched for age, study registration year, and study center. Conditional logistic regression was used to evaluate risk factors for T2D, including two PRSs (one for T2D and one for BMI). We further adjusted the models for age, sex, ethnicity, BMI, waist-hip ratio, ART-regimen, and CD4-cell count and fitted multiple alternative models for sensitivity analyses. We assessed the impact of including a PRS as a predictor on prediction accuracy via leave-one-out cross-validation and computing the area under the receiver operator characteristic (ROC) curve.

Results:
We found a clear dose-response relationship between the PRS for T2D and the risk of developing T2D, with participants in the highest PRS quintile having an over three-times larger risk of developing T2D (odds ratio, OR [95%-CI], 3.41 [2.61, 5.11]) compared to the first quintile. This effect size is comparable to having a BMI in the overweight (OR [95%-CI], 2.40 [1.85, 3.11]) or obese range (OR [95%-CI], 4.29 [3.05, 6.02]). CD4-cell count at T2D diagnosis was not associated with the risk of T2D (OR [95%-CI], 1.02 [0.947, 1.10]). Compared to an NNRTI-based ART-regimen, an INSTI-based regimen was associated with an increased T2D risk (OR [95%-CI], 2.35 [1.63, 3.40]), as was a PI-based regimen (OR [95%-CI], 1.68 [1.21, 2.33]). Neither the pre-ART CD4-cell count nadir (OR [95%-CI], 1.16 [1.00, 1.35]), nor CD4/CD8 ratio (OR [95%-CI], 0.920 [0.813, 1.04]) were significantly associated with the risk for T2D. When evaluating clinical and demographical characteristics at each participant's first available timepoint, the effect of PRS remained stable. Consistent with previous results, we found a positive, but not statistically significant association between a previous infection with Mycobacterium tuberculosis and the risk of T2D (OR [95%-CI], 1.32 [0.869, 2.01]). Removing the PRS as a predictor reduced the area under the ROC curve from 0.816 to 0.802. Adding a PRS for BMI as a predictor did not significantly increase prediction accuracy (area under the ROC curve 0.806).

Conclusion:
In a large population of PWH, we found a strong dose-response relationship between a PRS for T2D and the diagnosis of Type-2 Diabetes. This association was stable even when evaluating time-dependent variables at baseline. PI and INSTI-based ART regimens were associated with an increased risk for T2D. Thus, PRSs represent an option for targeted long-term preventive measures to mitigate the risk of T2D in PWH.

666

T. Loosli[7, 13], A. Hauser[7, 13], J. Josi[7, 13], N. Han[7, 13], S. Ingle[16], A. van Sighem[18], L. Wittkop[3, 11, 19], J. Vehreschild[4, 5, 10], F. Ceccherini-Silberstein[6], G. Maartens[9], M. Gill[8, 17], C. Sabin[12], L. Johnson[1], R. Lessells[2, 15], H. Günthard[7, 13], M. Egger[1, 14, 16], R. Kouyos[7, 13]

Predicting Dolutegravir resistance in South Africa: A modelling study

Centre for Infectious Disease Epidemiology and Research, School of Public Health, University of Cape Town, Cape Town, South Africa[1], Centre for the AIDS Programme of Research in South Africa (CAPRISA), Durban, South Africa[2], CHU de Bordeaux, Service d'information Médicale, INSERM, Institut Bergonié, CIC-EC 1401, Bordeaux, F-33000, France[3], Department I of Internal Medicine, Faculty of Medicine and University Hospital Cologne, University of Cologne, Cologne, Germany[4], Department II of Internal Medicine, Hematology/Oncology, Goethe University, Frankfurt, Frankfurt Am Main, Germany[5], Department of Experimental Medicine and Surgery, University of Rome Tor Vergata, Rome, Italy[6], Department of Infectious Diseases and Hospital Epidemiology, University Hospital Zurich, Zurich, Switzerland[7], Department of Medicine, University of Calgary, Calgary, AB, Canada[8], Division of Clinical Pharmacology, Department of Medicine, University of Cape Town, Cape Town, South Africa[9], German Centre for Infection Research (DZIF), Partner Site Bonn-Cologne, Cologne, Germany[10], INRIA SISTM Team, Talence, France[11], Institute for Global Health, University College London, UK[12], Institute of Medical Virology, University of Zurich, Zurich, Switzerland[13], Institute of Social and Preventive Medicine (ISPM), University of Bern, Bern, Switzerland[14], KwaZulu-Natal Research Innovation and Sequencing Platform (KRISP), University of KwaZulu-Natal, Durban, South Africa[15], Population Health Sciences, Bristol Medical School, University of Bristol, UK[16], Southern Alberta Clinic, Calgary, AB, Canada[17], Stichting hiv monitoring, Amsterdam, the Netherlands[18], Univ. Bordeaux, INSERM, Institut Bergonié BPH U1219, CIC-EC 1401, Bordeaux, F-33000, France[19]

Introduction:
HIV drug resistance is a significant challenge for sustainable antiretroviral therapy. In response to the exponentially rising levels of NNRTI resistance, millions of people have recently been switched to Dolutegravir (DTG)-based ART. Data on DTG resistance are limited, and DTG-resistant HIV has rarely been reported. However, given the frequency of use and the recency of the DTG rollout, rates of DTG resistance may increase. Understanding the dynamics of future DTG resistance for medium- and long-term health policy planning is essential. Here we develop DTG-MARISA, a compartmental model that considers the cascade of care, gender, disease progression and resistance genotype to predict DTG resistance in South Africa up to 2040.

Methods:
MARISA (Modelling Antiretroviral drug Resistance In South Africa) is a deterministic compartmental model consisting of the four layers: cascade of care, disease progression, sex, and drug resistance. It has been shown to reproduce the HIV epidemic in South Africa, as well as NNRTI acquired drug resistance (ADR) and transmitted drug resistance (TDR) – see Hauser et al. PLoS Comp Biol 2019. MARISA distinguished between susceptible and resistant HIV strains, disregarding the complex genetics of HIV resistance that are crucial for high genetic barrier drugs such as DTG. We expanded the resistance genotype as follows: NRTI and NNRTI resistance are classified as either susceptible or resistant. For DTG resistance, we include the key mutations (E138K, G140SR, Q148HR, N155H, R263K) observed in people experiencing failure on DTG-based ART.

Results:
Based on DTG-MARISA, we model acquired and transmitted drug resistance among people living with HIV in South Africa up to 2040. We explore different scenarios regarding mutation acquisition rates, the impact of resistance on treatment, and NRTI backbone drug resistance on DTG resistance. We investigate how these factors will affect the emergence of DTG resistance by 2040. The model predicts that with the introduction of DTG-based ART in 2020, DTG TDR will increase over time and could reach the 10% threshold by 2040, and DTG ADR to increase strongly in the coming years.

Conclusion:
Despite high efficacy of DTG at the individual level, a DTG resistance epidemic is likely in the coming years as more and more people are treated with DTG-based therapies. However, the frequency of DTG resistance is highly variable and dependent on treatment and surveillance strategies, and may be particularly high in settings where pre-existing NRTI resistance is more common, and resources for HIV-1 RNA monitoring, and resistance testing or switching to alternative ART regimens are limited.

667

D. Basu[2], H. Bolck[2], J. Theurillat[1], H. Moch[2]

Development of a Mechanistic Understanding and Therapeutic Strategy for TFE3-Rearranged Renal Cell Carcinoma

Università della Svizzera italiana[1], University Hospital Zurich[2]

Introduction:
TFE3-rearranged renal cell carcinoma (TFE3-tRCC) is a recently identified rare subtype of RCC harboring gene fusions that trigger oncogenic activation of TFE3 transcription factor. Importantly, TFE3-tRCC can show aggressive behavior with rapid progression and little-to-no response to the drugs commonly used for RCC. It has been established that TFE3 is a bHLH/LZ domain containing transcription factor, which mostly binds to E box sequences. Thus, it regulates a wide range of cellular process i.e. pluripotency, lysosomal biogenesis, autophagy, stress response etc. In tRCC, the C-terminal DNA binding domain of TFE3 is fused with an N-terminal regulatory domain of a fusion partner. More than 20 fusion partners with distinct biological functions have been described that likely impact on the dysregulation of the chimeric protein and drive tumorigenesis. However, our understanding of the molecular and clinical consequences of the different TFE3 fusions remains limited. A major obstacle towards the development of targeted therapeutic strategies for TFE3-tRCC is our incomplete understanding of its molecular landscape and clinical consequences of the fusions. In this scenario of unmet clinical needs, we want to propose a novel theranostic approach for tRCC.

Methods:
We have developped an RNA based targeted NGS panel to determine the fusion and their putative partners in patient samples. Following these results, we will investigate the downstream molecular events affected by the TFE3 fusions and delineate their consequences with regard to the specific fusion partner by ChIP-Seq approach. Moreover, we generated patient-derived organoid (PDO) and patient-derived xenograft (PDX) models for TFE3-tRCCs. Finally, we aim to perform combination drug screens in these models in order to suggest novel personalized treatments for patients with this aggressive cancer.

Results:
In our internal archive, we have identified 16 RCC cases, which had been diagnosed as TFE3-rearranged RCC on the basis of TFE3 overexpression and/or fusion by IHC or FISH/NGS respectively. Next, we used a newly developed targeted NGS panel, named RCC FusionPlex to detect the breakpoints and fusion partners for each case. After sequencing, we have identified fusion events in 13 out of 16 samples. Also we could determine the corresponding fusion partners (7 different fusion partners): PRCC, RBM10, etc. Next, we want to investigate the downstream transcriptional regulation and signaling events of different TFE3 fusions by ChiP-seq. For technical reasons, we decided to perform this analysis in TFE3-tRCC cell lines first. Nevertheless, several steps were required to be standardized before the sequencing assay. Following these preliminary tests, I carried out a first ChIP experiment using different TFE3-tRCC cell lines where the band intensities were found to be higher in ChIPed samples compared to negative control after PCR, that indicates towards the success of the chromatin IP experiment. Moreover, we developped 3D models from three commercially available TFE3-tRCC cell lines as well as a patient derived organoid (PDO) model harboring TFE3 fusions. From this PDO, our collaborator succesfully generated a patient derived xenograft (PDX) model in BALB/c mice. Viably frozen tissue was stored to re-develop the PDX model in future again. With Help of these tools, we aim to perform targeted drug testing in order to propse novel treatment strategy for TFE3-tRCC.

Conclusion:
Taken together, we seek to define the molecular features of TFE3-tRCC, thereby uncovering specific vulnerabilities of tumor cells that prompt the development of new therapeutic strategies.

668

S. Kuoni[2, 4], R. Steiner[3], L. Saleh[3], R. Lehmann[1, 4], N. Ochsenbein-Kölble[2, 4], AP. Simões-Wüst[2, 4]

Safety assessment of the SGLT2 inhibitors empagliflozin, dapagliflozin and canagliflozin during pregnancy: An ex vivo human placenta perfusion and in vitro study

Department of Endocrinology, University Hospital Zurich, CH-8091 Zurich, Switzerland[1], Department of Obstetrics, University Hospital Zurich, CH-8091 Zurich, Switzerland[2], Institute of Clinical Chemistry, University Hospital Zurich, CH-8091 Zurich, Switzerland[3], University of Zurich, CH-8091 Zurich, Switzerland[4]

Introduction:
Although uncontrolled hyperglycaemia during pregnancy can cause complications for both the mother and her offspring, pharmacological treatment options for gestational and type 2 diabetes in pregnancy are still limited. Empagliflozin (EMPA), dapagliflozin (DAPA) and canagliflozin (CANA) are three sodium glucose co-transporter 2 (SGLT2) inhibitors, a newer group of oral antidiabetics that are well established in the treatment of type 2 diabetes mellitus in non-pregnant patients. To date, no data regarding their placental transfer and safety in pregnant woman are available.

Methods:
Four *ex vivo* human placental perfusions (n=4, term placentae, creatinine and antipyrine as connectivity controls) were performed independently to evaluate the transplacental transfer of EMPA, DAPA and CANA across the placental barrier and assessed their influence on the secretion of two placental peptide hormones, leptin and b-human chorionic gonadotropin (β-hCG). The influence on the peptide hormone secretion was additionally assessed *in vitro,* using BeWo cells (originated from gestational choriocarcinoma cells) as a model for cytotrophoblasts.

Results:
We discovered that all three SGLT2 inhibitors cross the placental barrier and attained maximal foetal to maternal concentration ratios of 0.38 ± 0.09 (EMPA), 0.67 ± 0.05 (DAPA) and 0.62 ± 0.05 (CANA) within the tested 360 min. A moderate but statistically significant decrease in placental leptin – but not β-hCG – secretion was observed during perfusions with SGLT2 inhibitors, which was confirmed in experiments performed with human placental BeWo cells.

Conclusion:
SGLT2 inhibitors are able to cross the human placental barrier and seem to interfere with placental leptin production. These observations should be considered in the ongoing discussion on the optimal treatment for gestational diabetes and type 2 diabetes mellitus in pregnancy.

669

K. Arnke[1]

Diversity of bone derifed skeletal stem-cells – New targets for clinical applications

Traumatology[1], University Hospital Zurich

Introduction:
The mechanistic and cellular processes underlying bone growth, homeostasis and repair are complex and precisely controlled. Recently, the stem cell regulation and hierarchical organization of skeletal progenitor cells has been questioned. The group around Chan described for the first time in a mouse model a new type of bone stem cells, so-called skeletal stem cells (SSC). They could even divide these cells type in two further subgroups: perivascular- (pv) and osteochondral- (oc) SSCs. Those subpopulations showed different cell marker profiles and differed in their differentiation potentials. The ocSSCs were more localized in the growth plate and periosteum of the young mice and showed no adipogenesis, while the pvSSCs in the bone marrow were more pronounced and showed a weaker osteochondrogenic differentiation ability and a good adipogenic differentiation. Duchamp de Lageneste also described a cell type in the periosteum of mice that showed higher osteochondrogenic differentiation potential then bone marrow stem cells. Dysfunction of these SSCs could be a contributor to many different skeletal pathologies such as delayed fracture repair or diseases like osteoporosis.

Methods:
Most studies in this area are conducted in murine models. Thus, we focused on human SSCs in our study. For that reason, we collected bone marrow and tissue from fractured bones from patients with healthy and osteoporotic bones. Cells were isolated either directly from the bone marrow (BM) or from the spongiosa (SP) and cortex (CB) of bone pieces. The different cell types were analyzed for SSC marker expression mentioned previously by Chan as well as neural crest stem cell (NCSC) marker using FACS-analysis and RT-qPCR and for their ability to trilineage differentiate.

Results:
We have characterized these cells and tested for their trilineage differentiation potential. We observed major differences in differentiation capacity between healthy and diseased cells. The most pronouncing difference was that in the healthy patients, the osteogenic differentiation capacity was the weakest in BMs and the strongest in CBs while in the diseased patients the order was invers. The cortical bone-derived cells even seem to be barely able to differentiate into osteoblasts. We could observe an inversed reciprocal behaviour between healthy and diseased patients in the adipogenic differentiation.While in healthy patients BM cells were the dominant group in adipogenesis, in the diseased patients CB cells showed the highest capability for it. Next to the different differentiation behaviour, we observed also differences in cell marker expression pattern specific for SSCs and NCSCs. In all cell types in osteoporotic patients genes, which were supposed to be negative in SSCs (CD90 and CD146), were upregulated when compared to cells from healthy patients. PDPN, on the other hand, was positive and highly expressed in healthy patients but strongly downregulated in BM and SP cells from diseased patients. NCSC markers like NOTCH1 and SOX9 were strongly upregulated in all cell types in diseased patients. BM cells showed a downregulation in CD271 and CSPG4 in osteoporotic patients compared to healthy ones while these genes were higher expressed in SP and CB cells in diseased patients than in healthy patients.

Conclusion:
Overall, in our preliminary study we were able to demonstrate that different regions of human bone harbour different types of SSC or stem cells with different gene expressions and *in vitro* differentiation capacities. Furthermore, we observed pathological alterations in the gene expression and differentiation ability of these three cell types in patients with osteoporosis or low bone density.

670

I.S. Martinez Lopez[2], B. Battilana[2], M. Haberecker[1], D. Kračun[2], M. Kirschner[2], I. Opitz[2]

Understanding the contribution of different cell types in the development of chronic thromboembolic pulmonary hypertension (CTEPH)

Department of Pathology and Molecular Pathology, USZ[1], Department of Thoracic Surgery, USZ[2]

Introduction:
Chronic Thromboembolic Pulmonary Hypertension (CTEPH) is a rare and severe form of pulmonary hypertension marked by persistent obstruction in pulmonary arteries (PA) caused by fibroobstructive tissue (FO), which may originate from unresolved thromboembolic material. The precise triggers for inadequate resolution of pulmonary emboli in CTEPH are not understood. The only curative treatment is the removal of FO and diseased intima by Pulmonary Endarterectomy (PEA). The FO in CTEPH may result from intimal damage, prompting mesenchymal transition and fibroblast proliferation. Understanding CTEPH development necessitates a focused exploration and characterization of the involved cell types was the aim of the present project.

Methods:
The fully organized FO and diseased intima, were resected during PEA. Thereafter, tissues were macerated, digested, and obtained cell suspensions were cultured in a medium sustaining the growth of ECs. Propagated cell populations were analyzed for their cyto-morphological properties (shape size, morphology) by light microscopy.

Results:
Analysis of the obtained cultured primary cell populations from FO identified four different morphologies solely or in combination: fibroblast-, cobblestone-, squamous- and dendritic-like cells. Interestingly, on a limited number of resected intimal tissues we could identify a mixture of mainly cobblestone- and squamous cell-like cells.

Conclusion:
As expected, cells isolated from intimal tissue contained more epithelioid cell types, while FO tissue predominantly contained fibroblast-like cells. These data imply that different cells populations are contributing to development of FO in CTEPH pathogenesis, pointing to their complex interactions being a key for deciphering the development of CTEPH. Further studies in this direction are warranted, in which the obtained cell types will be characterized, with an ultimate goal of establishing primary cell lines for further therapy studies either solely or in co-culture.

671

M. Van Hemelrijck[1], J. Sromicki[1], P. Risteski[1], I. Tudorache[1], A. Häussler[1], M. Frank[1], B. Hasse[1], H. Rodriguez Cetina Biefer[1], O. Dzemali[1]

Aortic graft infection after surgery for acute aortic syndrome

University Hospital Zurich[1]

Introduction:
Aortic graft infection (AGI) after surgery for acute aortic syndrome remains a dreaded complication with mortality rates of up to 20%. Nevertheless, specific risk factors remain largely unknown. This study aims to describe incidental rates and predisposal characteristics of AGI patients after surgical repair for acute aortic syndrome.

Methods:
Retrospective analysis from a single-center cohort of patients using the MAGIC criteria for diagnosis of AGI. Early infection occurred <4 months after surgery, whereas late infections occurred >4 months. Fisher's exact and Mann-Whitney-U-Test were used for categorical and continuous variables

Results:
We identified 611 patients from 01/2010-12/2020. Of these, 6% (37) were diagnosed with an AGI during a median follow-up of 2.5 years (0.25 – 5.7). Overall, late infections were predominant at 72.9% (27/37). There were no statistically significant differences in baseline characteristics. There were more male AGI patients, 81.1% (30/37) vs. 67.6% (388/574), and they were older, 65.8 (56.2-69.9) vs. 64.5 (55-73.5) years. Comorbidities that were more likely found in AGI patients were coronary or peripheral artery disease (10.8% (4/37) vs. 8.9% (51/574); 8.1% (3/37) vs. 5.2% (30/574)) and connective tissue disorders (2.7% (1/37) vs. 1.6% (9/574)). DeBakey Type I was more commonly found in AGI-patients (78.4% (29/37) vs. 65.2% (374/574)), and these received more composite graft replacement: bio 24.3% (9/37) vs. 17.6% (101/574); mechanical 21.6% (8/37) vs. 16.7% (96/574); and total aortic arch replacement: 16.2% (6/37) vs. 7.8% (45/574). Surgery-, CPB- and aortic-cross-clamp times were longer in AGI-patients: 337min vs 332min, p=0.675; 198min vs 192min, p=0.818; and 117min vs 104min, p=0.959. Re-thoracotomy due to bleeding was more commonly performed in AGI-group (27% (10/37) vs 20.6% (118/574), p=0.403). Staphylococci were the most common microorganism in 27% (10/37).

Conclusion:
The present study reports an incidence rate of 6% for Acute Gastrointestinal Injury (AGI) in the studied population. Our findings indicate that longer operation times and re-thoracotomy are potential risk factors contributing to AGI's development. Furthermore, our analysis suggests that patients with a higher burden of comorbidities and those requiring complex repairs may be at a greater risk of developing AGI. However, further investigations are warranted to validate these findings on a larger scale and explore potential mechanisms underlying the observed associations.

672

J. Jang[1], R. Werner[1], M. Kirschner[1], M. Honegger[1], E. Casanova Zimmermann[1], S. Märsmann[1], P. Cinelli[1], W. Jungraithmayr[1], I. Opitz[1]

A novel 3D culture of lung adenocarcinoma cells with mesenchymal stromal cells

University Hospital Zürich[1]

Introduction:
Lung cancer is the second most diagnosed cancer and a leading cause of cancer-related death worldwide. The stromal environment involving activated fibroblast or cancer-associated fibroblast (CAF) is known to support tumor growth, metastasis, and therapy resistance in lung cancer. Those stromal fibroblasts mostly originated from multipotent mesenchymal stem cells (MSC) of the lung. Although therapeutic purposes of MSC for lung diseases gained attraction, a potential benefit and key regulation modality of MSC against lung cancers remain elusive. Recently we found that lung adenocarcinoma expression of CD26/dipeptidyl peptidase 4 (CD26) was significantly correlated with the survival of patients and the inhibition of CD26 decreased the growth of lung tumors in animal models. To investigate the role of MSC in lung cancer, we were able to perform a 3-dimensional (D) primary cell culture and detect the expression of CD26 not only in lung cancer cells but also in MSCs.

Methods:
Surgically resected tumor and normal lung tissue were chopped and digested by collagenase for 3D culture, which was maintained in Matrigel with hEGF, hFGF, and Rock inhibitor supplement. Following enzymatic dissociation of tissue, suspended cells after the filtration (40μm) were sorted for cancer organoid formation, while non-filtered tissue was embedded in Matrigel for MSC culture. Outgrown MSCs were moved to T25 flask (Fig. 1) with the support of 10% FBS in DMEM and subculture until the 10th passage. The mesenchymal characteristic expressions of CD73, CD90, and CD105 at 3rd passage of MSCs were assessed by flow cytometry. The phenotypic and replicative pattern was defined by alpha-smooth muscle actin (α-SMA) immunohistochemistry (IHC) when MSCs are unable to admit the subculture. For 3D tumor culture, we tested assembloid concept, which allows a spatial construct with tumor cells and stromal cells. The cell lines of mouse lung cancer (LLC) and primary human adenocarcinoma (Mai9 and Gon8) were mixed with MSCs on agarose agarose-coated plates. The production of CD26 was measured by ELISA from the culture supernatant and IHC.

Results:
Three surface markers of mesenchymal linage cells were highly positive (Fig. 2) among all MSCs from cancer and normal lung tissue. The capability of replication of MSCs was significantly decreased in cMSC (n=32) compared to nMSC (21) (Fig. 3). α-SMA IHC showed positive expression only on non-replicative MSCs (Fig. 4). While mono-culture of cancer cell lines were not able to form a spheroidal structure, mixed-culture of cancer cell line with MSCs successfully establish assembloid on no adhesive culture plate (Fig. 5). Lung adenocarcinoma expressed CD26 was detected by IHC and ELISA, but MSC produced CD26 was measured only in the culture supernatant (Fig. 6).

Conclusion:
3D cell culture method has been developed to provide close circumstances of in vivo. However, there have been technical obstacles including optimization of media and finding suitable matrix. From the experience of tumor organoid culture, essential nutrients were successfully suggested by researchers and tested by us as well. Now, we found an enhanced 3D culture method for lung cancer as a form of assembloid. We deem this novel 3D culture system can considerably contribute to the development of personalized precision medicine.

673

J. Baum[2, 3], C. Boggon[1], R. Nora[2, 3], L. Isa[1], SD. Brugger[2, 3]

Microbiota engineering for the eradication of S. aureus

ETH Zurich[1], University Hospital of Zurich[2], University of Zurich[3]

Introduction:
Staphylococcus aureus is a pathobiont mainly colonizing the upper respiratory tract (URT). Colonization is a major risk factor for infection and transmission; thus, measures are taken to decolonize at risk patients and reduce the risk of infection. However, all of them are tedious and resistance to common decolonization agents has been described highlighting the need for better and sustained decolonization strategies. One novel approach to decolonization is to reengineer the microbiome to exclude S. aureus colonization. Metagenomic analysis of the URT microbiome has revealed a negative correlation between pathobiont and certain commensal species. In vitro agar based interaction studies of pathobiont and commensals have revealed a direct inhibition of S. aureus by Dolosigranulum pigrum. The nature of this inhibition as well as the single cell interactions between different members of the URT microbiome is yet unknown. Here we quantitatively describe the negative interaction between S. aureus and D. pigrum on a macroscopic and on a microscopic level. For the microscopic assays we use a novel technique called capillarity assisted particle assembly (CAPA) to pattern bacteria on a polydimethylsiloxane (PDMS) template with high precision. This allows us to evaluate the effect of the inhibition on a single cell level.

Methods:
We use co-culture assays where one species is spotted next to another on an agar plate to screen the inhibition capacity of different D. pigrum strains against different S. aureus strains. Additionally, we use CAPA to deposit bacteria and evaluate the inhibition on a single cell level. After the bacteria are deposited on a PDMS template we place a nutrient containing agar pad, that has been pre-conditioned with the commensal bacteria, on top of the template. The bacteria are then placed under a microscope where we can take time lapse images of the growing bacteria. From the time-lapse images parameters such as deposition yield, lag time as well as growth rate of single bacteria can be extracted and compared. To evaluate the nature of the inhibition we extract and quantify S. aureus cells from the inhibition zone.

Results:
We show that all D. pigrum isolates tested inhibit S. aureus to varying extend. Pre-conditioning agar with C. pseudodiphtheriticum prior to co-cultivation increases the inhibition of S. aureus by D. pigrum. We were not able to recover viable bacteria from the inhibition zone indicating, that the inhibitory factor produced by D. pigrum is killing S. aureus. When analyzing the inhibition on a single cell level we see that there is a distance dependent inhibition gradient when deposited S. aureus cells are grown on D. pigrum pre-conditioned agar.

Conclusion:
Here we investigate the negative interaction of S. aureus with the commensal D. pigrum. We quantify the inhibition on a macroscopic as well as on a microscopic level. In addition, we further analyze the effect of the inhibitory factor on S. aureus and find that S. aureus is likely being killed by D. pigrum. This data supports the theory that D. pigrum is a key part of an URT microbiome that is colonization resistant to S. aureus. The technique used here to investigate the inhibition on a single cell level can be further expanded to model minimal microbial compositions and investigate interactions between more than two species. Ultimately, patterning multiple species on the same template this technique will allow us to model minimal microbiota and identify communities that are predictive for stable decolonization and communities that are resilient to pathobiont colonization.

674

L. Volta[3, 5], R. Myburgh[3], C. Pellegrino[3, 5], C. Koch[3], M. Maurer[3], F. Manfredi[3], M. Hofstetter[3], A. Kaiser[3], F. Schneiter[2], J. Müller[3], M. Buehler[4], R. De Luca[6], N. Favalli[6], C. Magnani[1, 3], T. Schroeder[2], D. Neri[5, 6], M. Manz[1, 3]

Efficient Combinatorial Adaptor-Mediated Targeting of Acute Myeloid Leukemia with CAR T-Cells

Comprehensive Cancer Center Zurich (CCCZ); Zurich, Switzerland[1], Department of Biosystems Science and Engineering, ETH Zurich; Basel, Switzerland[2], Department of Medical Oncology and Hematology, University Hospital Zurich and University of Zurich; Zurich, Switzerland[3], Department of Pathology and Molecular Pathology, University Hospital Zurich; Zurich, Switzerland[4], Institute of Pharmaceutical Sciences, Department of Chemistry and Applied Biosciences, ETH Zurich; Zurich, Switzerland[5], Philochem AG; Otelfingen, Switzerland[6]

Introduction:
Chimeric Antigen Receptor (CAR) T-cell therapies have demonstrated remarkable efficacy in the treatment of B- and plasma-cell malignancies by targeting cell-of-origin antigens. While these therapies effectively eradicate both tumor cells and healthy counterparts, the resulting loss can be mitigated through immunoglobulin substitution until cells regenerate from hematopoietic stem and progenitor cells (HSPCs). A similar on-target, off-tumor cell-of-origin elimination would be detrimental in the context of HSPC-derived malignancies like acute myeloid leukemia (AML), as CAR T-cell activity might lead to terminal ablation of hematopoiesis. In addressing this challenge, we developed adaptor-mediated CAR T-cells designed to bind to fluorescein, conjugated to antigen-binding adaptors. The administration of these tagged adaptors, characterized by a short half-life, serves as a safety switch for controlled CAR T-cell activity. In addition, combinatorial use of multiple adaptors with different antigen specificities might enhance target selectivity.

Methods:
We engineered second-generation CAR T-cells to display a fully human anti-fluorescein single-chain variable fragment, denoted as AdFITC-CAR T-cells. We further generated site-specific fluorescein-labeled adaptors in diabody format (Db-FM), directed against the AML markers CD117 and CD33. Cytotoxicity elicited by adaptors, individually or in combination, was evaluated in vitro against cell lines and primary patient samples. Pharmacokinetic studies were performed to determine the serum half-life of adaptor molecules and AML-xenograft mouse models were generated to assess on-tumor residence time of the adaptors as well as the therapeutic efficacy when administered with AdFITC CAR T-cells.

Results:
In vitro, combinatorial staining of antigen-positive cells with CD117 and CD33 Db-FM increased fluorescein decoration of target cells, thus enhancing AdFITC-CAR T-cell target density. Coculture of AdFITC-CAR T-cells with cell lines or patient-derived AML blasts demonstrated that dual adaptor use improved tumor cell lysis compared to equimolar concentrations of single adaptors. Live-cell imaging revealed that the addition of both CD117 and CD33 Db-FM accelerated tumor cell lysis with a more rapid and durable engagement of CAR T-cells with target cells.
We then performed pharmacokinetic studies and evaluated the on-tumor residence time of Db-FM to optimize the schedule of adaptor administration and ensure continuous labeling of tumor cells. In therapeutic xenogeneic mouse models with cell lines or primary AML blasts, AdFITC-CAR T-cells in combination with CD117 or CD33 Db-FM, administered singularly, demonstrated efficacy comparable to direct CAR T-cells targeting the same antigens. Injection of AdFITC-CAR T-cells along with both CD117 and CD33 Db-FM effectively inhibited tumor growth, outperforming monotherapies and, in some instances, leading to complete AML elimination in the bone marrow.

Conclusion:
We here tested an adaptor CAR T-cell approach using multiple adaptors to modulate CAR T-cell activity and enhance their selectivity, focusing on AML as a relevant disease model with a high clinical need for therapeutic improvement. The high antigen heterogeneity on AML cells supports a combinatorial targeting strategy, individualized based on the respective AML immunophenotype. Due to their small molecular weight, diabody-based adaptors are rapidly cleared from the body, allowing for rapid control over AdFITC-CAR T-cell on-off activity. We envision that this approach has the clinical potential for AML elimination and controlled HSPC abrogation. Once CAR T-cell activity is terminated, HSPC transplantation can facilitate hematopoietic recovery, offering a viable alternative for patients unable to tolerate radiation and high-dose chemotherapy.

675

T. Obenhuber[1], T. Scheier[1], T. Stutz[1], M. Hug[1], D. Fontein[2], A. Kaiser[3], S. Schoene[4], P. Steiger[4], S. Brugger[1], W. Zingg[1], P. Schreiber[1]

An outbreak with multidrug-resistant Acinetobacter baumannii on a burn ICU and its control with multifaceted containment measures

Department of Infectious Diseases and Hospital Epidemiology, University Hospital Zurich and University of Zurich, Zurich, Switzerland[1], Department of Plastic Surgery and Hand Surgery, University Hospital Zurich, Zurich, Zurich, Switzerland[2], Institute for Anaesthesiology, University Hospital Zurich and University of Zürich, Zurich, Switzerland[3], Institute of Intensive Care Medicine, University Hospital of Zurich, Zurich, Switzerland[4]

Introduction:
Patients in burn centres are at high risk of acquiring multidrug-resistant pathogens due to reduced skin barrier and long hospital stay.

Methods:
We report the investigation and control of an outbreak due to multidrug-resistant*Acinetobacter baumannii* in a burn centre. The 27 patients hospitalized in the centre during the outbreak were regularly screened and a total of 132 environmental samples were performed to identify a potential source. Fourier-transform infrared (FT-IR) spectroscopy and multilocus sequence typing (MLST) were applied to characterise the outbreak strain.

Results:
Between August and November 2022, the outbreak affected eight patients with eleven infections and three potentially related fatal outcomes. An interdisciplinary and multiprofessional outbreak team implemented a bundle strategy with repetitive admission stops, isolation precaution measures, patient screenings, enhanced cleaning and disinfection, and staff education. FT-IR spectroscopy suggested that the outbreak started from an index patient, who was repatriated one month before from a country with high prevalence of MDR *A. baumannii*. Environmental sampling did not identify a common source. Acquisition of the outbreak strain was associated with larger burn lesions ≥ 2a (per percent increase odds ratio (OR) 1.05 (0.99-1.12), P=0.09), and inversely associated with a higher nurse-to-patient ratio (per 0.1 increase OR 0.34, 95%CI 0.10-1.12, P=0.06).

Conclusion:
Burn patients with a large area of affected body surface, are at high risk for colonization and infection due to MDRO, particularly during periods of high workload. A multifaceted containment strategy can successfully control outbreaks due to MDR*A. baumannii* in a burn centre.

676

S. Traxel[1], C. Beerli[1], F. Schmidt[1], V. Dinh-Van[1], RF. Speck[1], S. Bredl[1]

Turning the tumor hot: Genetically engineered macrophages to disrupt the cold tumor microenvironment

Department of Infectious Diseases and Hospital Epidemiology, University Hospital Zurich, University of Zurich[1]

Introduction:
Triple negative breast cancer (TNBC) is an aggressive subtype of breast cancer and accounts for 40% of breast cancer deaths. The prognosis of TNBC patients is significantly influenced by the tumor microenvironment (TME). For example, patients with low T cell infiltration in the tumor that have a so-called cold TME are predicted to have a worse outcome due to a lack of an adaptive anti-tumor immune response. This anti-tumor immune response is further impacted by tumor-associated macrophages (TAMs), which highly infiltrate the TME of TNBC patients. Depending on the microenvironment, macrophages have different phenotypes: TAMs usually have an immunosuppressive phenotype and are induced by cytokines like IL-10 and TGFβ. They are associated with lower T cell infiltration, inhibit the anti-tumor immune response and promote tumor growth, migration and vascularization. Consequently, a high frequency of immunosuppressive TAMs in the TME are associated with worse outcome in TNBC. In contrast, macrophages with an inflammatory phenotype are induced by IFNγ. They have anti-tumoral activity through enhancing T cell infiltration, generating an anti-tumor immune response and by directly affecting tumor cell viability. Here, we aim to develop an adoptive cell therapy employing genetically engineered macrophages that express a chimeric cytokine receptor and are activated to an inflammatory phenotype by immunosuppressive cytokines in the TME. In the patient, we hypothesize that genetically engineered macrophages will migrate to the tumor, adopt an inflammatory phenotype, generate an inflamed TME by attracting T cells and directly affect tumor cell viability and thus the prognosis.

Methods:
To achieve a switch in macrophage phenotype in the TME, we will genetically engineer macrophages to express a chimeric cytokine receptor (ChCR). We designed the ChCR to induce an IFNγ-like signaling (STAT1) upon binding of immunosuppressive cytokines present in the TME. Here, we evaluated two ChCR variants activated by IL-10 and TGFβ, respectively. To engineer the macrophages, we transduced monocytes with lentiviruses to express the ChCR. Upon differentiation of transduced monocytes to macrophages, we assessed their phenotype by analyzing surface marker expression by flow cytometry and by analyzing their secretome. Moreover, we assessed their direct anti-tumoral activity using a WST1 assay.

Results:
We could successfully transduce macrophages at 80% and confirmed ChCR expression. Moreover, we show that both the IL-10 and TGFβ ChCR induce STAT1 signaling upon stimulation with IL-10 or TGFβ, respectively. Furthermore, stimulation of ChCR expressing macrophages by IL-10 or TGFβ switches them towards an inflammatory phenotype as analyzed by surface marker expression (HLA-DR, CD38, CD163). Moreover, ChCR expressing macrophages secreted IP-10 upon stimulation, a chemokine important for generating an inflamed TME. Finally, we assessed the direct anti-tumoral activity of ChCR expression. Importantly, we found that supernatant harvested from ChCR macrophages affected the viability of TNBC cell lines as measured by WST1 assay.

Conclusion:
We successfully engineer macrophages with high efficacy to express a ChCR that induced an inflammatory phenotype in macrophages in an immunosuppressive environment. Thus, ChCR macrophages represent a promising strategy to disrupt the immunosuppressive TME and have potential to turn a cold TME into an inflamed one.

677

R. Dal Bello[1], J. von der Grün[1], S. Tanadini-Lang[1], N. Andratschke[1], P. Balermpas[1], M. Guckenberger[1]

Technical preparation for a Phase I Clinical Study of e-FLASH Radiotherapy for Palliative Treatment of Superficial Skin Lesions of Malignant Melanomas

Department of Radiation Oncology, University Hospital Zurich and University of Zurich, Zurich, Switzerland[1]

Introduction:
Conventional photon or electron beam radiotherapy (CONV-RT) can dose-dependently cause high-grade acute and late toxic effects to normal tissue seriously impairing patient`s quality of life. Furthermore, local control rates for malignant melanomas are not yet satisfactory, despite the relatively high irradiation doses applied. However, treatment-related toxicity of CONV-RT currently limits further dose-escalation. Electron FLASH radiotherapy (FLASH-RT) with dose rates of > 40 Gy/s can potentially spare normal tissues while showing uncompromised tumor control rates in preclinical models. This broadening of the therapeutic ratio could allow isotoxic increase of tumor control or isoeffective toxicity reduction. We aim to conduct a phase I clinical trial to assess feasibility and safety of electron FLASH-RT using a converted linear accelerator in the palliative treatment of superficial skin melanomas. The planned clinical trial will be conducted as a single-arm, single-center phase I feasibility trial. Six patients with minimum two melanoma skin lesions each will be treated with a radiotherapy schedule of 3x 9Gy. One lesion will be treated with FLASH-RT (2x 9Gy) followed by CONV-RT (1x 9Gy) as experimental treatment. One lesion will be treated with CONV-RT (3x 9Gy) as internal control group. In this work, we present the technical conversion of the linear accelerator, which is planned to be used for the clinical trial.

Methods:
This study has been performed on a TrueBeam linac (Varian, USA), which after being in clinical operation from 2009 to 2022 was decommissioned, converted into a research platform and upgraded to deliver electron beams of 9 MeV in FLASH mode. Modifications included a software patch, thinner scattering foil and beam tuning. The dose rate, beam characteristics and reproducibility were measured at the linac isocenter.

Results:
The dose per pulse that can be achieved at isocenter reaches up to 1.05 Gy/pulse, corresponding to average and instantaneous dose rates up to 210 Gy/s and 2.3·105 Gy/s, respectively. Beam characteristics such as profiles and percentage depth dose were equivalent between 9 MeV FLASH and CONV for field sizes up to 10x10cm2. Dependence of the dose per pulse and profiles with gantry angle was excluded. The overall beam stability for the delivery of a fraction of 9 Gy was ±9%, this improved to ±4% after additional tuning of the klystron and a linac warmup. Finally, modulation of the dose per pulse was achieved by varying the pulse length or the pulse height. This allowed to reduce the average dose rate arbitrarily from 210 Gy/s down to the minimum dose rate for the FLASH effect of 40 Gy/s. The integral dose could be controlled by the number of delivered pulses.

Conclusion:
The converted linac characteristics are suitable for its potential application in the planned clinical trial. This study demonstrated dose rates within the ranges where the FLASH effect has been reported in preclinical models. Validation and testing, as well as approval for clinical investigation with a medical device will follow. This prospective single center phase I trials aims to assess feasibility and safety of FLASH radiotherapy for treatment of melanoma skin metastases. Feasibility will be defined as FLASH delivery with an accuracy of +/-10%, safety will be confirmed if maximum 30% of patients develop dose limited toxicity.

679

M. Rechsteiner[3], U. Wagner[3], A. Wethmar[1], S. Voglis[2], R. Reimann[1]

Fast-track CNV calling by Nanopore technology for meningioma classification

Department of Neuropathology, University Hospital Zurich[1], Department of Neurosurgery, University Hospital Zurich[2], Department of Pathology and Molecular Pathology, University Hospital Zurich[3]

Introduction:
Meningiomas represent the most common entity of primary intracranial tumors in adults. Recent publications show that, in addition to certain histologic information, like the number of mitotic figures, certain loss of heterozygosity (LOH) are of high prognostic significance with regard to recurrence free survival. This LOH can be detected by copy number variant (CNV) analysis. Most likely the next update of the fifth edition of the WHO classification of central nervous system tumor will include this LOH in the so-called 'integrated diagnosis'.

Methods:
Nanopore sequencing is an emerging technology that does not require a capture and/or amplification step like the next-generation sequencing solutions used in diagnostics today. Thus, its advantage lies not only in generating less PCR artefacts but as well in being more time-efficient. With the intention of offering a fast track LOH detecting system for meningiomas at the University Hospital Zurich, the Mk1C platform from Nanopore was set up with the transposase based whole genome library preparation protocol and DNA-isolates from fresh frozen tissue samples. Sequences were live monitored and the data further analyzed using the Epi2Me software from Nanopore.

Results:
For the initial implementation of the Nanopore CNV calling pipeline a fully anonymized sample was selected with a specific CNV profile (gains in chr4 and chr8 and LOH in chr6, 11, 14, and 15) known from previous analysis by Illumina Infinium MethylationEPIC Array. The sample was then sequenced by Nanopore and stopped after 384510 mapped reads. The CNV plot showed the expected gains and LOH. An additional focal amplification in chr12 was not detected with default settings but only with higher segment resolution. The reads were then down sampled to randomly composed datasets with only 50%, 20%, 10%, 5%, and 2.5% of reads. The CNV pattern was consistent until down-sampling to 10% (38451 reads). Furthermore, the performance of the same sample was tested in a multiplexed approach and a robust CNV pattern was obtained after 6h sequencing with five different barcodes and down to 45449 reads. Next, five fully anonymized samples from meningioma cases with different CNV patterns and varying tumor cell content (TCC) were tested. Compared again to the Infinium MethylationEPIC Array results, the CNV patterns were reproducible down to 70% TCC. A sample with 40% TCC did not give the expected CNV gain or loss, although it was visible to the eye in the plot.

Conclusion:
An emerging body of data points to the importance of LOH calling for the recurrence risk stratification in meningioma patients. The fast-track analysis by Nanopore delivered consistent CNV patterns compared to the Infinium MethlyationEPIC Array in a turnaround time of 2 days vs. 10 days. As a result, molecular information will be available at the first tumor board after surgery, allowing for a more personalized treatment plan. Further optimization of the workflow may be aimed at intraoperative CNV pattern analysis and thereby surgical decision support.

680

TA. Schweizer[2, 5], J. Würmli[2, 5], J. Prinz[5], M. Wölfle[7], R. Marti[1, 8], H. Koliwer-Brandl[8], R. Zbinden[8], A. Egli[8], H. Walt[4], L. Imhof[5], P. Bosshard[3, 5], Y. Achermann[3, 6, 9]

Photodynamic therapy with protoporphyrin IX precursors using artificial daylight improves skin antisepsis for orthopaedic surgeries

Analytica Medizinische Laboratorien AG, Zurich, Switzerland[1], Co-First Author[2], Co-Last Author[3], Department for Cranio-Maxillofacial and Oral Surgery, University Hospital Zurich, Zurich, Switzerland[4], Department of Dermatology, University Hospital Zurich, University of Zurich, Zurich, Switzerland[5], Department of Dermatology, University Hospital Zurich, University of Zurich, Zurich, Switzerland, Co-Last Author[6], Department of Infectious Diseases and Hospital Epidemiology, University Hospital Zurich, University of Zurich, Zurich, Switzerland[7], Institute of Medical Microbiology, University of Zurich, Zurich, Switzerland[8], Internal Medicine, Hospital Zollikerberg, Zollikerberg, Switzerland[9]

Introduction:
Preoperative skin antisepsis fails to completely reduce growth of skin-colonizing bacteria at time of arthroplasty. We hypothesize that reduced cutaneous bacterial burden at time of arthroplasty surgery would decrease the incidence of postoperative infections. We previously investigated and showed that photodynamic therapy (PDT) with red light (633nm, 40 J/cm2) and the pre-photosensitizer methyl-aminolevulinate (MAL; 160mg/g, 3h incubation) in combination with skin antisepsis led to absence of bacterial growth on the skin in 10/10 healthy participants. However, we observed local skin erythema, posing an obstacle for immediate orthopaedic surgery.

Methods:
In this study, we explored whether artificial day-light PDT (PDT-DL: 350–900nm, 10 J/cm2) instead of red light improves skin antisepsis without side effects. Healthy participants were allocated to the PDT-DL group receiving either 5-aminolevulinic acid (5-ALA-PDT-DL, n=10; 8mg, 4h incubation) or MAL (MAL-PDT-DL, n=10; 160mg/g, 1h incubation) before antisepsis with povidone-iodine/alcohol. The contralateral leg of each participant served as control with antisepsis only. Additionally, 10 independent participants were allocated to the control group (n=30). Skin swabs were taken at baseline, after PDT and after antisepsis in the groin to cultivate bacteria. After three days, bacterial cultures were repeated before and after antisepsis without PDT. In selected participants with MAL-PDT-DL, 16S rRNA-based metagenomics was performed.

Results:
All participants showed bacterial colonization at baseline. In the control group, 16 participants (55%) showed bacterial growth post antisepsis. PDT combined with antisepsis led to 46% and 82% reduction with 5-ALA-PDT-DL and MAL-PDT-DL as compared to control, respectively After three days, a non-significant effect (46% reduction) post antisepsis was observed for both arms as compared to control. Side effects were reported in 6 participants with 5-ALA-PDT-DL, while none were reported with MAL-PDT-DL.

Conclusion:
MAL-PDT-DL with skin antisepsis significantly improved bacterial reduction on the skin without side effects. However, reduction did not persist for 3 days post-treatment. The results of this study provide the fundament for a prospective study of patients with orthopaedic surgery to investigate safety and efficacy of MAL-PDT-DL.

681

E. Voloviceva[2, 3], S. Kakava[2, 3], S. Sandra[1], A. von Eckardstein[2, 3], J. Robert[2, 3]

Role of apolipoprotein E in the cerebrovasculature

ETH Zurich[1], University Hospital Zurich[2], University of Zurich[3]

Introduction:
Alzheimer's disease (AD) is the leading cause of dementia in elderly adults, with 55 million cases recorded worldwide in 2019. This number is expected to almost triple by 2050. The economic burden of the disease is estimated to reach 2.8 trillion USD by 2030. The role of apolipoprotein E (apoE) in AD is well recognized but the underlying mechanisms remain to be explained. It is known that genetic variations of APOE affect the likelihood of AD development and the age of onset, with APOEε4 allele being detrimental, APOEε3 neutral, and APOEε2 protective. In the central nervous system, apoE particles are secreted by various cell types, including astrocytes, pericytes, and microglia. However, it is not yet known if the protein and lipid compositions and functions of apoE particles are cell-type dependent. We hypothesize that protein and lipid composition of apoE particles depend on the cell type they originate from. These lipidome and proteome signatures then influence apoE functions. Particles further differ depending on the APOEε genotype.

Methods:
To test our hypothesis, we are differentiating astrocytes, pericytes, and microglia from human induced pluripotent stem cells (iPSC). We will investigate the protein and lipid composition of the apoE particles secreted by each cell type using liquid chromatography–mass spectrometry (LC-MS). We will compare the proteome and lipidome of cell-type-specific apoE to the composition of apoE secreted by mature human primary astrocytes, pericytes, and microglia, as well as the apoE present in commercially available human cerebrospinal fluid (CSF). We will further investigate the AD-related functions of cell-type-specific apoE particles, namely the effect on vascular inflammation, astrocyte and microglia inflammation, Aβ accumulation within the vasculature, Aβ and phosphorylated tau levels in neurons. We will test the apoE functions in vitro, using 2D cell culture and a 3D model of the human blood-brain barrier. To investigate the composition of apoE particles in a genotype-dependent manner, we will differentiate astrocytes, pericytes, and microglia from isogenic iPSC with different APOEε genotypes. We will investigate the composition and functions of apoE secreted by these cells as described above.

Results:
We have differentiated human brain pericytes and neural progenitor cells (which will be further differentiated to astrocytes) from iPSC. We have confirmed that iPSC-derived cells express cell-type-specific markers. In addition, iPSC-derived pericytes secrete apoE, which can be harvested from conditioned media. Human iPSCs also secrete apoE, although they do not express ATP-binding cassette transporter (ABCA1) mRNA. Due to the lack of ABCA1, which is involved in the lipidation of apoE particles, we hypothesize that iPSC-secreted apoE will have distinct lipidation patterns compared to mature human cells.

Conclusion:
In summary, our project delves into the relationship between cell-type-specific apoE particle composition and its functions, particularly in Alzheimer's disease. At the end of the project, we aim to answer how the compositions of apoE particles are linked to the cell type of origin and APOEε genotype, and how these particles affect cerebrovascular health in the context of AD.

682

C. Haslinger[2, 3], R. Brun[2], N. Ochsenbein-Kölble[2, 3], W. Korte[1]

Prospective, repeated observation of peripartum coagulation components in 1309 parturient women identifies coagulation factor XIII as a promising therapy approach in postpartum hemorrhage

Center for Laboratory Medicine, Hemostasis and Hemophilia Center, St. Gallen[1], Department of Obstetrics, University Hospital Zurich[2], University of Zurich[3]

Introduction:

Methods:

Results:

Conclusion:

683

PW. Schreiber[5], LD. Hoessly[1], K. Boggian[3], D. Neofytos[6], C. van Delden[6], A. Egli[7], M. Dickenmann[1], C. Hirzel[2], O. Manuel[4], M. Koller[1], S. Rossi[1], V. Banz[2], B. Schmied[3], L. Guerke[1], M. Matter[4], O. de Rougemont[5], M. Bonani[5], D. Golshayan[4], A. Schnyder[3], D. Sidler[2], F. Haidar[6], S. Kuster[5], S. Stampf[1], N. Müller[5], S. Swiss Transplant Cohort Study[1]

Surgical site infections after kidney transplantation are independently associated with graft loss

Basel University Hospital[1], Bern University Hospital[2], Cantonal Hospital St. Gallen[3], University Hospital (CHUV) of Lausanne[4], University Hospital Zurich[5], University Hospitals Geneva[6], University of Zurich[7]

Introduction:
Surgical site infections (SSIs) are common healthcare-associated infections. SSIs after kidney transplantation (K-Tx) can endanger patient and allograft survival. Multicenter studies on this early posttransplant complication are scarce.

Methods:
We analyzed consecutive adult K-Tx recipients enrolled in the Swiss Transplant Cohort Study (STCS) that received a K-tx between May 2008 and September 2020. All data were prospectively collected with the exception of the categorization of SSI that was performed retrospectively according to the Centers for Disease Control and Prevention criteria.

Results:
A total of 58 out of 3059 (1.9%) K-Tx recipients were affected by SSIs. Deep incisional (15, 25.9%) and organ/space infections (34, 58.6%) predominated. In the majority of SSIs (52, 89.6%) bacteria were detected, most frequently *Escherichia coli* (15, 28.9%), *Enterococcus* spp. (14, 26.9%), and coagulase-negative staphylococci (13, 25.0%). A BMI ≥25kg/m^2 (multivariable OR 2.16, 95% CI 1.07-4.34, P=0.023) and delayed graft function (multivariable OR 2.88, 95% CI 1.56-5.34, P=0.001) were independent risk factors for SSI. In Cox proportional hazard models, SSI was independently associated with graft loss (multivariable HR 3.75, 95% CI 1.35-10.38, P=0.011).

Conclusion:
In conclusion, SSI was a rare complication after K-Tx. BMI ≥25kg/m^2 and delayed graft function were independent risk factors. SSI were independently associated with graft loss.

684

P. Wallimann[3], B. Pouymayou[2, 3], M. Mayinger[3], S. Nowakowska[1], A. Boss[1], M. Guckenberger[3], S. Tanadini-Lang[3], N. Andratschke[3]

A new method to quantify signal intensity changes in glioblastoma during radiotherapy on an MR-Linac

Department of diagnostic and interventional Radiology, University Hospital Zurich and University of Zurich, Zurich, Switzerland[1], Department of Neuroradiology, Clinical Neuroscience Center, University Hospital Zurich and University of Zurich, Zurich, Switzerland[2], Department of Radiation Oncology, University Hospital Zurich and University of Zurich, Zurich, Switzerland[3]

Introduction:
Magnetic Resonance Linear Accelerators (MR-Linacs) have enabled longitudinal patient imaging with enhanced soft-tissue contrast during radiotherapy. This presents an opportunity for performing quantitative analyses of the acquired images, facilitating a comprehensive assessment of the evolving characteristics within both normal tissue and tumors during radiotherapy. In this study we present a novel approach for quantifying changes in daily positioning images of glioblastoma patients undergoing fractionated radiotherapy on an MR-Linac.

Methods:
The proposed method aims to identify significant longitudinal changes in MR images. It is based on a quantitative comparison of brain MR images, so we first preprocessed them (figure 1(a)). We affinely registered all daily images of a patient to the baseline image using a TRSAA approach. We performed an N4 intensity uniformity correction on the images and a custom intensity normalization method that normalizes the intensity of white matter to 0 and that of CSF to 100. After registration and normalization, a voxel wise comparison between the images was possible.

A threshold of significance for these voxel wise comparisons was determined as follows (figure 1(b)). We chose a significance level of 0.05 and corrected it for multiple testing by dividing it with the number of voxels in the brain. We then calculated the number of standard deviations that correspond to this two-sided significance level for a unit normal distribution. This value was finally multiplied with the magnitude of random intensity variation between images, defined as the standard deviation of voxel wise daily intensity changes observed in the healthy brain across all fractions.

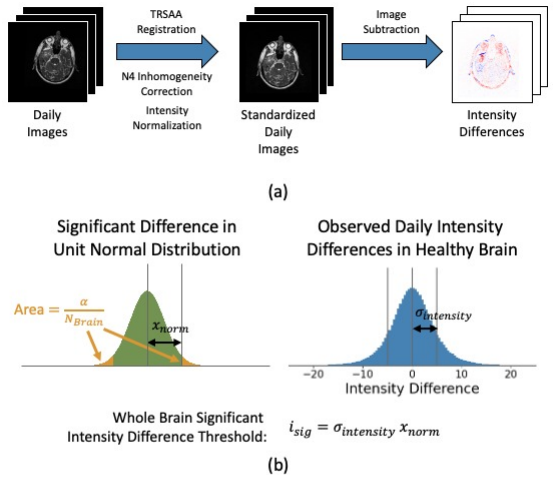

Figure 1. (a) Processing steps to obtain standardized intensity differences between images. (b) Approach for calculation of significant intensity difference threshold. N_{Brain} refers to the number of voxels in the brain contour, $\alpha = 0.05$ to the chosen significance level, x_{norm} to the threshold for siginificance in the unit normal distribution, $\sigma_{intensity}$ to the standard deviation of differences observed in healthy brain voxels of subsequent fraction images and i_{sig} to the threshold of significance for intensity changes that was used.

The proposed method was tested for feasibility using daily positioning TrueFISP scans of 6 glioblastoma patients treated on a 0.35T MR-Linac (ViewRay, Denver, CO, USA). Informed consent or general consent was given by all patients. Subjects 1 to 3 were treated with 15x2.67Gy and subjects 4 to 6 with

30x2Gy. Patients were imaged at the treatment simulation, which served as the baseline, and then at each fraction. All patients had been resected, however for patient 6 the largest lesion was not resected. Brain, GTV and CTV were delineated on the simulation images.

For each patient and each time point, we calculated the proportion of voxels showing a significant intensity change compared to the image at fraction 1 for the GTV, the CTV excluding the GTV and the brain excluding the CTV.

Results:
Figure 2(a) shows for each region of interest the proportion of voxel with significant change to the first fraction for each patient and each fraction. For patients 1, 4 and 5, the proportion of changing voxels was low throughout the treatment. For patients 2 and 3, a large number of voxels showed a change between the simulation and the first fraction. For patient 2, further changes occurred early during treatment while the images of patient 3 were more stable, except for an outlier at fraction 10 likely caused by inconsistent image quality. Patient 6 only started showing large intensity changes late during treatment.

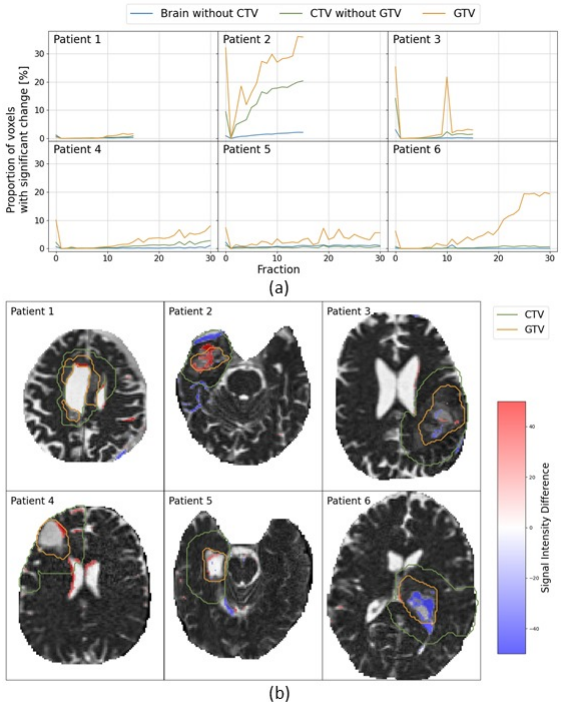

Figure 2. (a) Proportions of voxels showing significant changes over the course of radiotherapy. Fraction 0 refers to the simulation. (b) Slice of first fraction image. Significant intensity changes to last fraction image shown as colored overlay.

Figure 2(b) shows a slice of the first fraction image of each patient with the significant intensity changes to the last fraction shown as a colored overlay. For patients 1, 4 and 5, the changes are mostly limited to deformations in resection cavities and CSF structures. For patients 2 and 6, large changes occur inside the GTV, but for the former the intensity increases while for the latter it decreases.

Conclusion:
We developed a novel method for identifying significant intensity changes in longitudinal MR images acquired routinely at an MR-Linac. Feasibility was tested in daily TrueFISP images of glioblastoma patients at an MR-Linac, which showed heterogeneous longitudinal intensity changes for different patients. The ability to detect these changes on a patient level may enable a more individualized selection of the target volume.

685

A. Majcher[2], P. Bjorklund[5], A. Holfeld[3], A. Othman[1], G. Lauria[4], J. Hardfeldt[5], B. Angelin[5], T. Hornemann[2]

The increased Alanine to Serine ratio in T2D relates to diabetic neuropathy by driving the formation of neurotoxic 1-deoxysphingolipids in skin

Functional Genomics Center Zurich, Zurich, Switzerland[1], Institute of Clinical Chemistry, University Hospital Zurich[2], Institute of Molecular Systems Biology, Department of Biology, ETH Zurich, Zurich, Switzerland[3], IRCCS 'Carlo Besta' Neurological Institute, Milan, Italy[4], Karolinska Universitetssjukhuset Huddinge, Stockholm, Sweden[5]

Introduction:
Type 2 diabetes (T2D) is a global health issue, associated with complications such as diabetic peripheral neuropathy (DPN) and wound healing defects. T2D disrupts several metabolic pathways, notably carbohydrate, amino acid, and lipid metabolism. This forms an atypical class of 1-deoxysphingolipids (1-deoxySL) which are generated as side products during canonical sphingolipids (SL) de-novo synthesis. 1-DeoxySL are neurotoxic, causing HSAN1, a monogenic sensory neuropathy. They are also elevated in T2D but their connection to DPN remains unclear.

Methods:
We performed a lipidomics and proteomics analysis of plasma and skin from T2D (N=38) patients and matched controls (N=39). We used cellular models and stable isotope metabolic labeling approaches to understand the connection between changes in the serine and alanine metabolism and 1-deoxySL formation in T2D. The data were finally confirmed in diabetic animal models.

Results:
Our data showed, that 1-deoxySL formation is directly related to the plasma L-Alanine to L-Serine ratio. In T2D this ratio is increased, leading to elevated 1-deoxySL in skin and plasma while canonical sphingolipids are reduced. T2D patients with DPN showed a significantly higher 1-deoxySL to SL ratio compared to those without. A Proteomics analysis revealed deviations in amino acid metabolism and increased protein turnover in T2D skin.

Conclusion:
Our findings suggests that T2D leads to an imbalance in L-Alanine and L-Serine, causing an increased 1-deoxySL formation, which results in a toxic insult on sensory skin fibers. This offers new possibilities for diagnosing and treating DPN, including a therapeutic supplementation with L-Serine.

686

J. Bergada Pijuan[1], J. Baum[1], C. Chang[1], A. Gómez-Mejia[1], S. Mairpady Shambat[1], T. Fuhrer[2], M. Zampieri[2], R. Kouyos[1], A. Zinkernagel[1], S. Brugger[1]

Commensal Bacteria as Probiotic Candidates: Unraveling the Molecular Interplay between Nasal Commensals

Department of Infectious Diseases and Hospital Epidemiology, University Hospital Zurich, University of Zurich, Zurich, Switzerland[1], Institute of Molecular Systems Biology, ETH Zurich, Zurich, Switzerland[2]

Introduction:
The human microbiome comprises several microorganisms, such as bacteria, fungi, viruses, archaea and eukaryotes, that inhabit various body sites and form complex interconnected networks among themselves, the host and the environment. The upper respiratory tract (URT) microbiome significantly influences respiratory health, with a balanced composition providing protection against pathogens and enhancing immune responses. However, disruption of the URT microbiome can lead to overgrowth of pathobionts like *Staphylococcus aureus* and *Strptococcus pneumoniae*, which cause a wide range of respiratory infections. Recent advances in sequencing technologies have enabled detailed exploration of the nasal microbiome, revealing certain commensal bacteria like *Dolosigranulum pigrum* and *Corynebacterium spp*. to be associated with microbiome stability and reduced respiratory infections. These bacteria may serve as probiotics, offering protection against pathobionts. Studies also indicate a symbiotic relationship between *C. psudodiphtheriticum* and *D. pigrum*, although the metabolic interactions and molecular mechanisms facilitating their coexistence require further investigation.

Methods:
By means of a multi-omics approach, including transcriptomics and metabolomics analyses of different bacterial combinations, we investigated the synergy between *D. pigrum* and *C. pseudodiphtheriticum* at the molecular level. RNAseq data was used to identify genes and pathways that become differentially expressed as a result of the commensal-commensal interactions, for which we performed over-representation analyses and gene set enrichment analyses. Later, we compared the results with the metabolomics data, aiming to find links between the different approaches and to identify whether the transcriptomics observations translate into final metabolites.

Results:
Transcriptomics results showed differentially expressed genes and pathways in both species when they were grown together as compared to monocultures. Remarkably, *D. pigrum* upregulated several carbohydrate metabolism genes (especially fermentation genes) and downregulated genes implicated in the synthesis of amino acids, while *C. pseudodiphtheriticum* upregulated genes involved in iron acquisition, denitrification pathways, and the production of nucleosides and nucleotides. Metabolomics analyses revealed similar outcomes, with amino acids, amino sugars, heme and several secondary metabolic compounds being exhausted when *C. pseudodiphtheriticum* grew in the presence of *D. pigrum*. Overall, these results align with the hypothesis of a potential change in the metabolism of *C. pseudodiphtheriticum* in the presence of *D. pigrum*. Our data also indicated that *D. pigrum* may benefit from amino acids and other molecules synthetized by *C. pseudodiphtheriticum* to enhance its growth.

Conclusion:
Our results mark a crucial advance in understanding the metabolic exchange between two major beneficial microorganisms of the human nasal microbiota, *D. pigrum* and *C. pseudodiphtheriticum*, and paves the way to better illustrate their role in the fight against human nasal pathogens. To our knowledge, this is one of the first experimental studies to elucidate the molecular mechanisms of commensal bacterial interspecies interactions in the human nasal passages.

687

A. Joachimbauer[1, 2], N. Cadosch[2], C. Gil-Cruz[1, 2], C. Perez-Shibayama[2], K. Frischmann[2], F. Tanner[1], F. Ruschitzka[1], B. Ludewig[1, 2], D. Schmidt[1]

Echocardiographic strain predicts the progression of acute autoimmune myocarditis to inflammatory cardiomyopathy

Department of Cardiology, University Hospital Zurich, Switzerland[1], Institute of Immunobiology, Kantonsspital St. Gallen, Switzerland[2]

Introduction:
Myocarditis is an inflammatory heart disease that leads to myocardial remodeling and progression to inflammatory cardiomyopathy. Monitoring of myocardial function is crucial for diagnosis, treatment and prognosis of patients. However, the diagnosis of myocardial inflammation based on imaging modalities is challenging. Echocardiographic strain analysis bears the potential for accurate diagnosis and outcome prediction in various cardiomyopathies. Currently, it is still unclear to what extent strain analysis can be used for the diagnosis of acute myocardial inflammation and whether predictive parameters for the progression to inflammatory cardiomyopathy can be defined.

Methods:
Here, we have used a mouse model of CD4+ T-cell-driven acute autoimmune myocarditis that precipitates inflammatory cardiomyopathy and heart failure in approximately 50% of the animals. Monitoring of structural and functional changes was performed using high-resolution ultrasound. Detailed mechanical analysis was performed using speckle-tracking-based global strain. Flow cytometry was used for quantification and characterization of myocardial immune cell infiltration and histopathologic analysis including quantification of collagen deposition was used to quantify the degree of myocardial inflammation and fibrotic remodeling.

Results:
We found that highly activated CD4+ T cells caused changes in cardiac morphology and function during the acute phase of myocardial inflammation. Both morphological and functional alterations correlated with the degree of immune cell infiltration in the myocardium. Longitudinal assessment of morphological and functional impairment during progressive myocardial inflammation identified longitudinal and circumferential myocardial deformation as robust parameters to predict progression of acute myocarditis to inflammatory cardiomyopathy.

Conclusion:
This study indicates that the degree of early immune cell infiltration determines the severity of morphological and functional changes during the acute phase of myocardial inflammatory disease. Impairment of longitudinal and circumferential myocardial deformation represent robust parameters that predict the progression of acute myocarditis to inflammatory cardiomyopathy

688

M. Roncador[1, 2, 3], F. Bayer[1, 3], J. Kuipers[1, 3], M. Manz[2], N. Beerenwinkel[1, 3], S. Böttcher[2], S. Balabanov[2]

Dissecting the complexity of the MDS-AML continuum in 7480 patients with Bayesian covariate-aware clustering.

Department of Biosystems Science and Engineering, ETH Zurich, Mattenstrasse 26, 4058, Basel, Switzerland[1], Department of Haematology and Clinical Oncology, Zurich University Hospital, Rämistrasse 100, 8091, Zurich, Switzerland[2], SIB Swiss Institute of Bioinformatics, Mattenstrasse 26, 4058, Basel, Switzerland[3]

Introduction:
The WHO 2022 definition of myelodysplastic neoplasia (MDS) and acute myeloid leukemia (AML) further emphasizes the pathogenetic role of genetic drivers and the morphology-based classification has been widely replaced by a granular molecular definition of AML and MDS. Along this line, the body of evidence questioning the dichotomy between the two disease groups is increasing, leading to a new vision that considers them as evolving entities within a disease-continuum.

Methods:
We collected a large cohort of 7480 patients from three publicly available genomic studies encompassing the majority of MDS- and AML-subtypes. For every subject the blood parameters (hemoglobin level, white blood cell count, thrombocytes and bone marrow blasts), the mutational status for at least 32 genes (*ASXL1, BCOR, CBL, CUX1, DNMT3A, ETV6, EZH2, GATA2, GNAS, IDH1, JAK2, KIT, KRAS, MPL, NF1, NPM1, PHF6, PTPN11, RAD21, RUNX1, SF3B1, SRSF2, STAG2, TET2, TP53, U2AF1, WT1, ZRSR2, IDH2, NRAS, CEBPA, FLT3*) as well as minimal cytogenetic information (trisomy 8, loss of chromosome 17, del(5q) or monosomy 5, del(7q) or monosomy 7) was available. After a binarization step, we performed an unsupervised data analysis using a new covariate-aware clustering method (CANClust). We validated the clustering on an independent cohort of 1035 MDS and AML patients.

Results:
We obtained a novel stratification based on 9 distinct disease-groups. The clusters contained a mixture of AML and MDS sharing similar molecular features and were named according to the aggressiveness of outcome. A ultra-high risk (UHR) cluster included *TP53* mutated and complex karyotype diseases, high-risk groups (HR1, HR2, HR3) reported mainly myelodysplasia-associated mutations and cytogenetic alterations. Low-risk patients (LR1, LR2) were mainly MDS with known good prognostic markers such as *SF3B1* mutation or del(5q). AML with specific genetic drivers such as *NPM1* showed a distinct behavior and were clustered separately. These newly identified groups model the disease evolution and patients` prognosis better than current 2022 European LeukemiaNet genetic risk stratification (ELN2022) and the molecular international prognostic scoring system (IPSS-M). Our validation cohort showed similarly consistent results.

Conclusion:
In this study, we demonstrate that the mutational landscape can be combined with essential clinical parameters to re-group MDS and AML patients into novel risk groups, which predict better the actual clinical course by transcending from their initial MDS-AML separation. Our new model is particularly effective in predicting the outcomes of high-risk patients and patients within the novel International Consensus Classification (ICC) MDS/AML subclass and may serve as a guide for addressing unmet clinical needs. The definition of disease type based on blast percentage is here additionally questioned, as many of clusters included patients with blasts count both above and below the diagnostic cutoff of 10-20%.

689

MM. Müller[3, 4], NJ. Wegmann[3], DM. Heuberger[3, 4], G. Kadler[3], B. Seeliger[2], RA. Schüpbach[3, 4], S. David[1, 3]

Low plasma levels of the endothelial soluble Tie-2 receptor predict mortality in patients with sepsis and ARDS

Department of Nephrology, Hannover Medical School, Hannover, Germany[1], Department of Respiratory Medicine, Hannover Medical School, Hannover, Germany[2], Institute of Intensive Care Medicine, University Hospital Zurich, Zurich, Switzerland[3], University of Zurich, Zurich, Switzerland[4]

Introduction:
The Tie2 receptor, a key regulator of endothelial homeostasis, activates signaling cascades governing cell survival, inflammation and cell integrity. Activation by its circulating canonical ligand, angiopoietin-1 (Angpt-1), has beneficial effects on these processes. However, binding of Angpt-2, a partial antagonist, can intensify inflammatory responses and disrupt endothelial junctions, potentially causing capillary leakage and edema in conditions like Acute Respiratory Distress Syndrome (ARDS) and sepsis. In addition, shedding of Tie2 from the endothelial surface has been observed in sepsis-related animal models, further compromising cell integrity. Despite extensive research on Angpt-1 and Angpt-2, the potential utility of the shedded form of Tie2, i.e. the soluble Tie2 (sTie2), in identifying individuals at risk of an adverse outcome has remained largely unexplored. This study investigates sTie2 levels in ARDS and sepsis patients, aiming to discern their relationship with organ failure and mortality.

Methods:
This is a retrospective evaluation of a prospective single-center biobank study that investigated patients admitted to the ICU at the Medical School Hannover in Germany between 2018 and 2023, who were diagnosed with sepsis or ARDS and had a blood sample available on the day of admission. Patient characteristics and outcome parameters were retrieved from electronic patient records, while Angpt-1, Angpt-2 and sTie2 levels were measured in plasma samples from the day of admission using Multiplex Luminex Assay (R&D Systems, USA). Data were presented as medians and interquartile ranges. Group comparisons were performed using the Wilcoxon and Kruskal-Wallis tests, as appropriate. Binomial general linear models and receiver operating characteristic (ROC) curves were utilized to assess sTie2 as a predictor of 28-day mortality.

Results:
Plasma samples of 217 patients (98 had ARDS, 31 sepsis and 88 ARDS + sepsis) were analyzed. Seventy % (154) were male 30% (63) female. While plasma concentrations of sTie2 and Angpt-1 did not differ among groups (p=ns), Angpt-2 levels were remarkable elevated in patients with sepsis (ARDS vs. sepsis: 9438 [5677 – 15848] vs. 45824 [17242 – 63002] pg/mL, $p < 0.001$). sTie2 correlated negatively with the severity of organ failure, i.e. the SOFA-score ($R = -0.2$, $p = 0.003$) and plasma levels were decreased in patients requiring hemodialysis (dialysis vs. no dialysis: 17400 [12245 - 22479] vs. 21354 [14914 – 29077] pg/mL, $p = 0.002$) and in 28 days non-survivors (non-survivors vs. survivors: 14353 [10956-20467] vs. 21066 [15022 – 28107] pg/ml, $p <0.001$). Multivariate logistic regression model identified age, SOFA-score and sTie2, but not Angpt-2 to be associated with 28-day mortality. Area under the ROC curve (AUC) was 0.677 [95%CI 0.597 – 0.776] and 0.682 [95%CI 0.606– 0.759] in models including only sTie2 or SOFA-score, respectively. Integration of sTie2 with SOFA-score and age increased the AUC to 0.759 [0.688 – 0.83].

Conclusion:
We observed an inverse relationship between sTie2 and the severity of the disease in patients with ARDS and sepsis. Further investigations are warranted to discern whether this observation is attributed to elevated Tie2 shedding in patients with less severe illness or if sTie2 itself possesses protective properties. This finding holds the promise of potentially identifying a novel therapeutic target for the management of critically ill patients afflicted with ARDS and sepsis.

690

E. Payne[1, 2], A. Joachimbauer[1, 2], N. Cadosch[2], C. Gil-Cruz[1, 2], C. Perez-Shibayama[2], K. Frischmann[1, 2], F. Tanner[1], F. Ruschitzka[1], B. Ludewig[1, 2], D. Schmidt[1]

Acute and chronic myocardial inflammatory disease - the explorative prospective ImmpathCarditis study

Department of Cardiology, University Hospital Zurich[1], Institute of Immunobiology, Kantonsspital St. Gallen[2]

Introduction:
Myocarditis is an inflammatory heart disease that leads to loss of cardiomyocytes and frequently precipitates fibrotic remodeling of the myocardium culminating in heart failure. Myocarditis is caused mainly by the activation of CD4+ T cells against MHC class II-binding peptides derived from the contractile protein myosin heavy chain 6 (MYH6). Heart-specific CD4+ T cells are activated by various mechanisms, including Bacteroides species-derived peptide mimics. The goal of the ImmpathCarditis study is to elucidate the pathogenesis of myocardial inflammation using longitudinal high-dimensional analysis from prospective patient cohorts.

Methods:
The ImmpathCarditis study is a prospective exploratory study, which currently recruits patients with acute myocarditis and patients with chronic inflammatory cardiomyopathy including cardiac sarcoidosis. Integrative data analysis of clinical parameters (e.g., cardiac imaging, standard laboratory values, microbiome) will be hierarchically structured to perform longitudinal patient monitoring and multiparametric phenotyping. We will use established ELISA methods to determine IgG serum antibody reactivity against B. thetaiotaomicron and against cardiac MYH6 and troponin proteins. To broaden the longitudinal proteomic profiling of inflammatory markers in sera, we will analyze cytokines, inflammatory chemokines, growth factors such as the bone morphogenic proteins. Flow cytometry will be used to provide high-dimensional analyses of the immune cell landscape in the peripheral blood. In addition, HLA allele sequencing from PBMC samples and metagenomic sequencing of bacterial DNA from stool samples will be performed.

Results:
This study has been approved by the ethics commission (BASEC 2021-01917) of the Swiss Canton of Zurich. Patient recruitment and longitudinal data acquisition are in progress. Serum antibody profiling of patient samples will commence soon.

Conclusion:
The main hypothesis underlying this research project is that phenotypical and functional changes of serologic immune parameters, as well as heart-specific T cells critically determine the disease course during myocardial inflammatory disease.

691

L. Zurfluh[1, 3], S. Santos[1, 2], M. Mennet[4], O. Potterat[2], U. von Mandach[1], M. Hamburger[2], N. Ochsenbein-Kölble[1, 3], AP. Simões-Wüst[1, 3]

Bryophyllum pinnatum Attenuates Oxytocin-Induced Pro-inflammatory Signalling Pathways in Human Myometrial Cells

Department Obstetrics, University Hospital Zurich, Zurich[1], Division of Pharmaceutical Biology, University Basel, Basel[2], University of Zurich, Zurich[3], Weleda AG, Arlesheim[4]

Introduction:
Preterm birth is one of the leading causes of neonatal morbidity and mortality. Preterm myometrial contractions are a common cause of preterm labour and are treated with tocolytic agents. Over the past few years, the potential of anti-inflammatory substances in the treatment of preterm labour has become apparent. *Bryophyllum pinnatum* - a traditional medicinal plant with, among others, anti-inflammatory properties - has been used in the treatment of preterm labour, first in anthroposophic hospitals and, recently, in conventional settings. The main advantage of *B. pinnatum* compared to synthetic tocolytic agents is the rare occurrence of side effects. Furthermore, *in vitro* work with human myometrial cells has shown that *B. pinnatum* leaf press juice (BPJ) inhibits intracellular calcium signalling induced by oxytocin, a hormone known to play a major role in labour. The aim of this work was therefore to characterise the effect of *B. pinnatum* on the pro-inflammatory MAPK cascade of the oxytocin-signalling pathway.

Methods:
Experiments were performed with an immortalised human myometrial cell line (hTERT-C3). Cells were treated with either BPJ, corresponding fractions, single compounds or just medium and stimulated with oxytocin (for 5 min in phosphorylation experiments and 6 h for enzyme expression experiments). As a positive control, the tocolytic agent atosiban was used. Activation of the MAPK proteins p38, SAPK/JNK and ERK1/2 by phosphorylation was analysed by immunoblotting. The effect of BPJ-compounds on COX-2 expression was analysed with ELISA.

Results:
BPJ and a bufadienolide-enriched fraction inhibited the oxytocin-driven activation of the MAPKs SAPK/JNK and ERK1/2, but not of p38. Some BPJ-compounds inhibited the oxytocin-induced expression of COX-2. The effects on the MAPK signalling cascade were comparable to those of the oxytocin-receptor antagonist and tocolytic agent atosiban.

Conclusion:
BPJ, the bufadienolide-enriched fraction and some single compounds attenuate inflammatory processes triggered by oxytocin. In a next step, the effect of *B. pinnatum* on further downstream processes in the MAPK cascades (e.g. prostaglandin production) needs to be investigated. Our findings further substantiate the use of *B. pinnatum* as a well-tolerated treatment for preterm labour.

693

M. Meerang[1], M. Kirschner[1], F. Schläpfer[1], M. Ronner[1], E. Felley-Bosco[1], I. Opitz[1]

Molecular Characterization and Validation of Live Cell Biobank for Pleural Mesothelioma

Department of Thoracic Surgery, University Hospital Zürich[1]

Introduction:
The use of primary cells cultivated from fresh patient material for research approaches, especially for in vitro drug testing, can overcome the drawbacks of long-term cultures of cell lines. Here we aim to fully characterize 196 pleural mesothelioma (PM) low passage primary cell lines generated over the past 16 years at our hospital.

Methods:
For the identification of tumor cells, we performed a stepwise characterization. To exclude fibroblasts, we evaluated epithelial cell origin by immunohistochemical staining (IHC) of pan-Cytokeratin (pan-CK) in FFPE cellblocks. Pan-CK staining intensity was scored as weak (1), moderate (2) and strong (3). Finally, histo (H)-score (sum of intensity multiplied with % positive cells, range 0-300) was calculated. We performed cell growth characterization using colorimetric assay for cell metabolic activity (MTT assay).

Results:
We have taken all the frozen stock cell lines to grow in culture using our established workflow. 117 cell lines (60%) grew after thawing and we could generate more frozen aliquots. Median pan-CK H-score analyzed from 67 cell lines was 49 and ranged from 0-300 (figure 1a). Among them, 23 cell lines have an H-score over 100. The doubling time, analyzed from 14 cell lines so far, ranged from 37-292 hours (median 83.6 hours).

Conclusion:
We have successfully re-cultured a large number of primary cell stocks, and shown that the doubling time of those of epithelial origin is within a good range for future experiments. Only pan-CK high expressing cell lines (H-score >100) will be selected for further staining with additional PM tumor markers by IHC compared to the original tumor tissues. The cell lines with concordant marker expression compared to the original will be further selected for assessment of copy number variation assay for the final validation. These primary cells represent an invaluable tool for the future use as translational research model for PM.

694

S. Changkhong[1], F. Schläpfer[1], M. Ronner[1], E. Felley-Bosco[1], M. Kirschner[1], I. Opitz[1], M. Meerang[1]

Characterization of cancer associated fibroblast cell cultures from the mesothelioma cell bank

Department of Thoracic Surgery, University Hospital Zürich, Zürich, Switzerland[1]

Introduction:
Heterogeneity of cancer-associated fibroblasts (CAFs) in cancers has been increasingly demonstrated, particularly from single cell omics approaches. CAFs is identified by the lack of epithelial marker expression and can be classified into various subtypes, such as immune, desmoplastic, contractile, and aggressive subtype. The immune and desmoplastic subpopulations typically exhibit tumor-inhibitory properties, whereas the contractile and aggressive subtypes tend to support tumor growth. We aim to employ CAFs cultivated from mesothelioma primary tumor for research approaches, particularly to understand their characteristics and functions. Here we showed the preliminary characterization of 43 mesothelioma cultures enriched with primary CAFs.

Methods:
To confirm non-epithelial origin of the cells, we evaluated immunohistochemical staining (IHC) of pan-Cytokeratin (pan-CK) in Formalin-Fixed Paraffin-Embedded (FFPE) cellblocks. Pan-CK staining intensity was manually scored as weak (1), moderate (2) and strong (3). Finally, histo (H)-score (sum of intensity multiplied with % positive cells, range 0-300) was calculated. Cell growth characterization was performed using colorimetric assay for cell metabolic activity (MTT assay). We further performed IHC markers associated with CAF subpopulations including α-Smooth muscle actin (α-SMA), Vimentin (VIM) and Podoplanin (PDPN), on those with pan-CK H-score of <150. α-SMA, protein involved in the contraction of actin stress fibers, can be used to identify, the 'contractile' and 'aggressive' subpopulations. The 'aggressive' subtype can be further distinguished by VIM expression, the marker of epithelial-mesenchymal transition (EMT). The 'immune' subpopulation is associated with PDPN expression.

Results:
We have identified 43 mesothelioma cultures enriched with fibroblasts (pan-CK score <150) from our mesothelioma biobank so far. The doubling time analyzed from the 43 cell lines, ranged from 56.4-601.8 hours. 30 cell lines (69.77%) shown to be fast growing cells with median 85.9 hours, ranged from 56.4-128.2 and they will be employed for further analyses. Median pan-CK H-score was 15.5, ranged from 0 to 134. So far, we have analyzed the CAF marker expression in 9 cell lines. PDPN and α-SMA appeared to be quite heterogeneous. Median α-SMA H-score was 7 (range 0 to 300) while PDPN H-score was 124 (range 0 to 204). VIM was highly expressed in all cultures, with a median H-score of 300, ranging from 290 to 300. We also investigated the expression of these makers in three tumor specimens. From the preliminary observation, we observed similar marker expression in CAF detected within the tumor specimen, compared to our cultures. α-SMA and PDPN were positive in some CAFs whereas VIM was highly expressed in all CAFs.

Conclusion:
We have successfully cultured a large number of fast growing cultures enriched with CAFs from primary tumor for future experiments. The preliminary analyses suggested that the CAF cultures from different tumors may derive from different CAF subpopulations. We will evaluate expression of the markers using immunofluorescent staining and co-stain with pan-CK. Finally, we will investigate the association between CAF subtypes and clinical outcomes.

696

R. Werner[2], M. Eisenberg[1], S. Ries[1], T. Papasotiropoulos[2], N. Steinmann[2], M. Antonoff[1], I. Opitz[2]

Perioperative outcomes following lung resection in metastatic non-small cell-lung cancer: Results of a large multicenter database

Department of Thoracic and Cardiovascular Surgery, University of Texas MD Anderson Cancer Center, Houston, Texas, USA[1], Department of Thoracic Surgery, University Hospital Zurich, Zurich, Switzerland[2]

Introduction:
Surgical decision-making in non-small-cell lung cancer (NSCLC) relies on balancing operative risks with oncologic benefits. Recent data have emerged demonstrating survival advantages following pulmonary resection as local consolidative therapy in stage IV NSCLC, yet operative risks for these potentially more challenging surgical procedures are not well-described. We sought to characterize perioperative outcomes within a multicenter cohort of patients with resected stage IV NSCLC.

Methods:
We retrospectively reviewed patients with metastatic NSCLC who underwent resection of primary lung tumors from 1996-2023 from 2 large academic institutions. Clinicopathologic, operative, and perioperative details were obtained from patient records. Predictors of pulmonary, cardiac, renal, and wound complications were assessed and multivariable regression model performed.

Results:
179 patients were included, at median age of 59.0 (51.8-66.5) years. Neoadjuvant therapy was received by 116 (64.8%), including chemotherapy 73 (40.8%), immunotherapy in 4 (2.2%), and targeted therapy in 48 (26.8%). Most patients underwent thoracotomy (141, 78.8%). Operations included 130 (72.6%) lobectomies, 24 (13.4%) wedges, 7 (3.9%) segmentectomies, 12 (6.7%) bilobectomies, and 6 (3.4%) pneumonectomies. Median blood loss was 150 (62.5-300) mL, and median operative duration was 236 (183-286) minutes. Typical length of stay was 5.0 (3.0-8.0) days. Postoperative complications occurred in 46 (25.7%), including 18 (10.1%) pulmonary, 19 (10.6%) cardiac, 5 (2.8%) renal, and 4 (2.2%) wound-related. MVA did not identify intrathoracic stage, extent of resection, nor neoadjuvant treatment as independent predictors of postoperative complication. All patients survived 30 days, and 2 deaths (1.1%) occurred within 90 days. Complications did not impact 90-day survival (p=0.36).

Conclusion:
Surgery for stage IV NSCLC is well-tolerated, regardless of receipt of neoadjuvant therapy, intrathoracic stage, or extent of lung resection. Most complications are cardiopulmonary, without downstream impact on survival. These findings inform multidisciplinary and informed consent discussions, setting a baseline for future assessments of outcomes in this patient population.

697

F. Costa[1, 2], G. Indiveri[2], J. Sarnthein[1]

Real-time HFO analysis for intraoperative ECoG

University Hospital of Zurich, Department of Neurosurgey, Zurich, Switzerland[1], University of Zurich, Institute of Neuroinformatics, Zurich, Switzerland[2]

Introduction:
High Frequency Oscillations (HFO) in intraoperative electrocorticography (ECoG) may guide the surgeon by delineating the epileptogenic zone. The current state of the art approach for intraoperative HFO analysis involves visual annotation by experts either during or after surgery or offline application of automated software algorithms. A Brain-computer interface (BCI) employed during epilepsy surgery can facilitate the processing of ECoG signals in real-time, in a closed-loop interaction between the surgeon and the epileptic brain. Here we present a real-time framework that comprises a neuromorphic device and that can be used during epilepsy surgery for HFO analysis.

Methods:
We use the BCI2000 framework to stream the ECoG in real-time and to realize a signal encoding that drastically compresses the data. We then use a spiking neural network (SNN) realized in a low-power neuromorphic hardware to detect HFO.

Results:
We develop our approach on pre-recorded ECoG from our institution from 22 patients. The HFO rates obtained with our setup are concordant with a previously validated offline algorithm (Spearman's ρ=0.75, p = 1e-4), obtaining the same prediction accuracy for postsurgical seizure freedom.

Conclusion:
Intraoperative access to HFO analysis may improve the patient's chances for postsurgical seizure freedom. Our methodology makes HFO analysis widely accessible to epilepsy surgery centers. With the BCI2000 open-source framework and the high signal compression, this pipeline can easily be implemented in multiple hospitals, allowing performing a remote HFO analysis 'as a service'.

698

M. Ponzo[5, 6], L. Drufuca[1, 7], C. Buracchi[5, 6], S. Nucera[5, 6], C. Bugarin[6], G. Rossetti[7], R. Bonnal[7], B. Rambaldi[3], A. Biondi[4, 6], G. Gaipa[6], M. Pagani[1, 7], C.F. Magnani[2, 6]

Acquisition of an Immunesuppressive Microenvironment after CD19 CAR T Cell treatment in B-Cell Precursor Acute Lymphoblastic Leukemia

Department of Medical Biotechnology and Translational Medicine, Università degli Studi, Milan[1], Department of Medical Oncology and Hematology, University Hospital Zurich and University of Zurich,Zurich, Switzerland[2], Department of Oncology-Hematology, Azienda Socio Sanitaria Territoriale Papa Giovanni XXIII, Bergamo, Italy[3], Pediatrics, Fondazione IRCCS San Gerardo dei Tintori, Monza, Italy[4], School of Medicine and Surgery, University of Milano-Bicocca, Italy[5], Tettamanti Center, Fondazione IRCCS San Gerardo dei Tintori, Monza, Italy[6], The AIRC Institute of Molecular Oncology (IFOM), Milan,Italy[7]

Introduction:
As a therapy based on immune cells, CAR T cells treatment elicits an acute response involving both innate and adaptive immunity which is followed by a process of resolution. A major interest is to identify, within the tumor microenvironment (TME), factors that influence the activity and potency of anti-CD19 CAR T cells. However, studies on the interaction between the bone marrow (BM) TME and CAR T cells are still limited. We hypothesized that the immunological niche of the BM reacts to CAR T-cell-mediated inflammation by modulating the immune response through the activation of inhibitory pathways and molecules.

Methods:
We conducted an academic phase I/II study (NCT03389035) with donor-derived anti-CD19 CAR T cells generated with Sleeping Beauty transposon (CARCIK-CD19) in B-ALL patients relapsed after alloHSCT. Hematology laboratory data, CAR T,and CD3+ cell kinetics were analyzed in 43 pediatric and adult B-ALL patients who underwent commercial and investigational anti-CD19 CAR T cell treatment. The scRNA-seq libraries of BM samples were generated using Chromium Single Cell 5′ Reagent Kit of the 10x Genomics (v3.1). Validation was performed in 20 pre-/post- CAR-T matched BM samples by a 30-color flow cytometry panel.

Results:
Following the peak of expansion, CAR T-cell counts decreased in the third and four-week post-infusion. A similar dynamic of expansion and contraction was observed in CD3+ T cells, total white blood cells (WBC), and monocytes, indicating that a widespread resolution of CAR T-driven inflammation occurs during the first month after infusion. To elucidate the mediators involved in the resolution of CAR T-cell-mediated inflammation, the single-cell transcriptome of patients' BM cells at early time points post-CAR T-cell infusion was compared to pre-treatment samples at the moment of disease relapse and the infusion products. The more representative clusters were classified into infusion product, CD4 and CD8 endogenous population, B cells, myeloid cells, pDC, NK, and NK-T cells. We observed profound changes in the composition of BM after CAR T cells infusion compared to pre-treatment samples. CAR T-cell treatment generated a remodeling of the BM microenvironment, with an increase in the myeloid cells, NK, NK-T, and exhausted CD8+ T cell populations. After CAR T-cell infusion, myeloid cells displayed a higher resemblance to myeloid-derived suppressor cells (MDSCs). GeneSet Enrichment Analysis (GSEA) showed significant enrichment in pathways associated with immunosuppression both in the myeloid compartment and in endogenous T cells and in CAR Tcells. Of note, the genes involved are also strictly correlated to the generation of terminally exhausted T cells and the emergence of MDSCs. Spectral flow cytometry-based experiments validated our observation of an increase of monocytes, MDSC-like cells, NK, NK-T, and CD8 terminal cells. Modeling intercellular communication using NicheNet suggested the induction of immunosuppressive genes in myeloid cells by both CAR T cells and endogenous T cells and viceversa.

Conclusion:
Through sc-RNAseq and spectral flow cytometry, we have characterized changes in the BM TME after CAR T cell therapy. Specifically, CAR T cells-mediated myeloid activation is associated with pathways of immune dysregulation that may dampen CAR Tcell expansion and antagonize the effects of the therapy. Transcriptomic interrogation can infer pathways relevant to the communication between CAR T cells and the TME.

699

R. Werner[1], K. Chiffi[1], D. Schneiter[1], S. Hillinger[1], O. Lauk[1], I. Opitz[1]

Surgical complexity of anatomical lung resections after induction immunotherapy for locally advanced or metastatic non-small cell lung cancer

Department of Thoracic Surgery, University Hospital Zurich, Zurich, Switzerland[1]

Introduction:
Neoadjuvant immunotherapy has become an integral part of the multimodal treatment in advanced NSCLC. However, an increasing procedural complexity after neoadjuvant immunotherapy is described by many surgeons. We therefore aim to score the surgical complexity of anatomical resections after induction immunotherapy.

Methods:
We performed a single-institutional retrospective review of patients with clinical stage IIIA-IVB NSCLC who underwent anatomical lung resection and mediastinal lymphadenectomy after neoadjuvant immunotherapy. Surgical complexity and hilar fibrosis were scored according to the proposed scoring system by Rusch et al. (https://doi.org/10.1016/j.jtcvs.2022.10.007).

Results:
25 patients met the inclusion criteria, among which 4 (16%) were treated with neoadjuvant immunotherapy alone, 18 (72%) with neoadjuvant immunochemotherapy and 3 (12%) with neoadjuvant immunotherapy and chemoradiotherapy. Clinical UICC-stages were IIIA in 8 (32%), IIIB in 2 (8%), IVA in 9 (36%) and IVB in 6 patients (24%). Surgical access was primarily open in 13 (52%), RATS in 5 (20%) and VATS in 7 patients (28%). Resections included 15 lobectomies, 4 bilobectomies, 5 pneumonectomies and 1 segmentectomy. Conversion from minimally invasive to open approach was required in 5 patients (2 VATS and 3 RATS cases), all due to extensive hilar fibrosis. A hilar fibrosis score of 2 was present in 15 cases and a score of 0 was only seen in 4 patients. The presence of a high fibrosis score was not associated with an increased risk for perioperative complications (p=0.66), but patients with a fibrosis score of 2 showed a longer median length of hospital stay (9.4±3.9 versus 6.7±1.8 days), although not statistically significant (p=0.056).

Conclusion:
Surgical complexity after neoadjuvant immunotherapy for advanced NSCLC can be objectified by a hilar fibrosis score. The prognostic relevance of the hilar fibrosis score for early outcomes such as perioperative complications and length of stay needs to be assessed in larger prospective cohorts.

700

S M. Pickering[1], G. Pontarollo[1], A E. Kremer[1]

Seladelpar treatment reduces Interleukin-31 and Pruritus in patients with Primary Biliary Cholangitis

University of Zurich, University Hospital Zurich[1]

Introduction:
Primary Biliary Cholangitis (PBC) is a rare progressive female-predominant liver disease characterized by impaired bile flow and immune-mediated destruction of intrahepatic bile ducts. PBC is often associated with itchy skin. This type of itch is known as Cholestatic Pruritus (CP). This chronic burden can dramatically compromise the quality of life of affected patients, leading to impaired sleep, general uneasiness and severe psychological distress such as depression and, in some cases, even to the extreme point of suicidal tendencies. Current available and licensed therapies for PBC such as ursodeoxycholic acid (UDCA) or obeticholic acid (OCA) failed to reduce CP, in contrast to the off-label therapy bezafibrate which is a pan-peroxisome proliferator activated receptor (PPAR) agonist. Currently, there are further PPAR agonists being investigated in phase III clinical trials such as seladelpar. The underlying pathophysiology of CP and the anti-pruritic mode of action of PPARs remain largely elusive. Bile acids (BA), bilirubin, lysophosphatidic acid (LPA), autotaxin (ATX) and endogenous opioids have been hypothesized as potential pruritogens, despite the fact that the correlation of levels in serum and itch intensity are widely disputed. The cytokine interleukin 31 (IL-31) is another known factor which has been reported to be upregulated in pruritic patients with dermatological disorders such as atopic dermatitis.

Methods:
IL-31 levels were quantified using the ultrasensitive immunoassay kit produced by SimoaTM in serum samples coming from two seladelpar PBC studies, in which PBC patients received either daily oral doses of placebo (n=55), seladelpar at 5mg (n=53) or at 10mg (n=53) for a total number of three months. The PBC samples were then compared to healthy volunteers (n=55) recruited by matching age, sex and BMI. Itch intensity was quantified on a numerical rating scale (NRS, 0-10) and 5D-Itch score. Patients with moderate to severe itch (NRS>4) were equally distributed over the subgroups. Correlations were performed using multivariate analysis. Levels of other cytokines such as IL-4, IL-13 and IL-33 as well as pruritogens such as autotaxin were also quantified by ELISA.

Results:
Baseline IL-31 levels were found to be strongly correlated with pruritus NRS ($r=0.54$, $p<0.0001$), and total ($r=0.54$, $p<0.0001$) and conjugated BAs (up to $r=0.64$, $p<0.0001$). The decrease in IL-31 was dose-dependent for treatment with 5mg (-30%, $p=0.0003$) and 10mg (-52%, $p<0.0001$) seladelpar compared to placebo (+31%). Patients with clinically significant improvement in pruritus (NRS≥2) exhibited greater dose-dependent reductions in IL-31 when compared to those not experiencing itch improvement (NRS<2 decrease). Strong correlation was observed between IL-31 levels and total ($r=0.63$, $p<0.0001$) and conjugated bile acids in 10 mg seladelpar treatment. Moreover, seladelpar treatment had no effect on serum autotaxin levels and did not result in changes in other type 2 cytokines, IL-4, IL-13 and IL-33, known to be involved in production of IL-31 in other diseases such as atopic dermatitis.

Conclusion:
Treatment with seladelpar downregulated serum IL-31 levels, particularly in patients experiencing pruritus, while, other known pruritogens such as cytokines and ATX levels were completely unaffected by this treatment. These data support a novel mode of action on the anti-pruritic properties of PPAR agonists and paves the avenue for future causal therapeutic approaches of this agonizing symptom.

701

E. Sarti[1], R. Wolfensberger[1], C. Dolle[1], S. Sander[2], R. Speck[1], J. Nemeth[1]

M. tuberculosis promotes intracellular survival manipulating the c-MYC pathway to redirect macrophages maturation

University Hospital of Zürich[1], University of Zürich[2]

Introduction:
Counterintuitively, asymptomatic infection with Mycobacterium tuberculosis (MTB), the causative agent of tuberculosis (TB), provides protection against re-infection. This phenomenon is called “concomitant immunity” and requires the pathogen to persists in a host with an otherwise protective immune response. Here, we hypothesize that naive macrophages prior to infection protect the pathogen from the immune response by maintaining a specific niche.We Investigated the role of the sequence of activation and infection in determining outcomes of macrophage infections with Mycobacterium tuberculosis to identify possible routes used by the bacteria to survive phagocytosis and proliferate in the macrophages and recognized c-Myc as a crucial factor exploited to promote survival and growth in infected cells

Methods:
We explored major biological phenotypes (mycobacterial viability, host cell viability, host cell activation) in mouse bone marrow-derived macrophages (BMDM) infected *in vitro* with either H37Rv or the MTB Live/Dead H37Rv reporter strain. Macrophages were stimulated with IFN-γ for 24h either prior or after infection. We analyzed the resulting phenotypes with flow cytometry, plating of bacteria and RNAseq. We inhibited c-MYC signaling was inhibited with a chemical inhibitor (10058-F4) and by transducing the cells with an inducible construct to express a c-MYC inhibitor peptide (omo-MYC)**.**

Results:
Activation of macrophages with IFN-γ for 24h prior to infection significantly increased anti-mycobacterial activity of macrophages and decreased the number of live and transcriptionally active bacteria by 45 % (+/- 12 %). In contrast, macrophages activated with IFN-γ for 24 h directly after infection displayed resistance to IFN-γ and allowed bacterial growth similar to naïve macrophages. After phagocytosis of heat killed MTB, macrophages displayed resistance to activation with IFN-γ similar to infected/activated macrophages with live H37Rv. The transcriptional response comparing infected/activated versus activated/infected macrophages showed substantial differences in proinflammatory pathways and transcriptional self-renewal programs including c-MYC regulated transcriptional programs. Inhibition of c-MYC signaling with a chemical inhibitor and omo-MYC expression led to a gain of function comparable to anti-bactericidal function in macrophages comparable to activation with IFN-γ.

Conclusion:
The activation state of the macrophage prior to MTB infection is the key determinant of infection outcomes *in vitro*. Phagocytosis of MTB without pre-activation of macrophages induces c-MYC controlled self-renewal transcriptional programs inhibiting anti-bacterial activity. This effect is also detectable with heat-killed MTB, suggesting that MTB highjacks a cell intrinsic tissue repair program to allow persistence in the host. The role of c-MYC mediated persistence will be further investigated with *in vivo* experiments in a mouse model

702

Y. Kalbas[1], F. Klingebiel[1], S. Halvachizadeh[1], M. Teuben[1], A. Hülsmeier[2], T. Hornemann[2], R. Pfeifer[1], P. Cinelli[1], HC. Pape[1]

Systemic lipidomic profile changes align with injury severity and predict outcomes in polytraumatized patients.

UZH, USZ, Depatment of Traumatology[1], UZH, USZ, Institute for Clinical Chemistry[2]

Introduction:
Recent advances in analytic technology allow for characterization of lipid profile dynamics on a molecular level. Experimental models suggest individual lipid profiles based on injury severity. The aim of this study was to characterize the lipidomic response in a cohort of polytrauma patients using a prospectively established polytrauma biobank.

Methods:
Lipidomic analysis was performed on samples from our inhouse polytrauma biobank which is established since 2018. Patients were included upon arrival at the trauma bay and venous sampling was performed at 6 timepoints (Arrival, 8h, 24h, 48h, 5d and 10d). Inclusion criteria were an ISS > 25, survival > 24h and an age > 18 years. Plasma samples were analyzed using liquid chromatography mass spectrometry (LC-MS). Lipid profiles were characterized using bioinformatic approaches and dimensionality reduction. Linear mixed models were programmed to analyze lipid class dynamics over time. Demographics, injury characteristics, outcomes (e.g. LOS, mortality, complications) and laboratory markers were exported from our clinical information system. Lipid profile dynamics were collated with clinical data.

Results:
85 subjects with a total of 440 samples were analyzed to account for the optimal batch size for LC-MS. Mean ISS was 31.7 and mean NISS 38.4. Overall, 633 individual lipids were identified. Principle component analysis (PCA) revealed clustering of lipids with similar molecular characteristics, thus lipids were organized into 19 functional subgroups (classes). K-means clustering based on lipid profile revealed 2 specific patient groups, which differed in injury pattern and - severity. In more severely injured patients, we detected a significant decrease of the majority of lipid classes over the early timepoints (0-48h). Restoration of lipid levels at 24h was indicative of clinical outcome: Levels of “AcCa”, “LPC” and “HEX” were highly predictive of major complications.

Conclusion:
The early lipid profile in polytraumatized patients aligns with injury pattern and severity while the dynamic over time can predict complications. AcCa as a marker of mitochondrial damage seems to be a promising clinical marker for point of care resuscitation. Our results match nicely with previous results from animals models. This study emphasizes the importance of prospectively collected biobanks enabling researchers to perform new analytical methods on already available samples.

703

Y. Kalbas[1], F. Klingebiel[1], S. Halvachizadeh[1], M. Teuben[1], M. Weisskopf[3], A. Hülsmeier[2], T. Hornemann[2], R. Pfeifer[1], P. Cinelli[1], HC. Pape[1]

Lipidomic analysis reveals relevant lipid profile changes in a porcine model with hemorrhagic shock and multiple injuries.

UZH, USZ, Depatment of Traumatology[1], UZH, USZ, Institute for Clinical Chemistry[2], UZH, ZFC[3]

Introduction:
The role of lipid mediators in the posttraumatic response has been hypothesized but not yet proven. With vast advances in analytic technology, lipid profile changes can be characterized on a molecular level. The aim of this study was to characterize the lipididomic response to trauma in a translational large animal model.

Methods:
54 male pigs (50 ± 5kg) were randomized for three conditions: “Sham”, “Monotrauma”, and “Polytrauma”. All animals were anesthetized for 6 hours. Monotrauma group received a femoral shaft fracture only and polytrauma received additional blunt chest trauma liver laceration and a pressure controlled hemorrhagic shock for 60 min. Resuscitation was performed with crystalloid fluids and fractures were stabilized by intramedullary nailing. Venous samples were collected at 6 timepoints (baseline, trauma, resuscitation, 2h, 4h and 6h). Lipidomic analysis was performed via liquid chromatography mass spectrometry (LC-MS). Lipid profiles were characterized using bioinformatic approaches and dimensionality reduction. Linear mixed models were programmed to analyze profile changes over time.

Results:
Overall, 304 individual lipids were identified. Principle component analysis (PCA) revealed clustering of lipids with similar molecular characteristics and lipids were organized into 17 functional subgroups. Polytrauma showed a significantly different lipid profile compared to Sham and Monotrauma. These differences were most pronounced after resuscitation and at 6h post-injury. PCA confirmed strong variation between Polytrauma and the other groups at these timepoints. Lipid subgroups involved in energy metabolism showed significant ($p < 0.05$) decrease over time in polytrauma. In contrast, Acylcarnitines (AcCas) showed a highly significant ($p<0.001$) twofold increase after resuscitation in polytrauma only.

Conclusion:
Our data suggests that lipidomic profile changes align with injury severity. Causal inferences can be drawn based on the lipids’ functional characteristics: While the strong decrease of “energy lipids” points to a hypercatabolic response to polytrauma, Acylcarnitines (a lipid specific to the mitochondrial membrane) show high potential as a marker for oxidative stress.

704

E. Ranieri[2, 3], R. Brun[2, 3], N. Ochsenbein-Kölble[2, 3], W. Korte[1], C. Haslinger[2, 3]

D-dimer levels during pregnancy and postpartum: non-applicability of regularly used cut-offs for diagnosis of suspected pulmonary embolism

Center for Laboratory Medicine, Hemostasis and Hemophilia Center, St. Gallen, Switzerland[1], Department of Obstetrics, University Hospital Zurich, Switzerland[2], University of Zurich, Zurich, Switzerland[3]

Introduction:
Pregnancy represents a prothrombotic state with consequently increased risk of thromboembolic complications. In clinical practice outside pregnancy, D-dimer measurement plays an important role in the diagnostic workup of thromboembolic complications; however, due to the physiological increase of D-dimers in pregnancy, there are no established cut-off values for parturient women. Nonetheless, the Artemis study recently included D-dimer levels in the evaluation of a pregnancy-adapted YEARS algorithm for the diagnosis of suspected pulmonary embolism.
We analyzed pre- and postpartum D-dimer values of 1309 parturient women, stratified per gestational age at delivery, with a particular interest on the amount of women with apparently no thromboembolic complication but D-dimer values above cut-offs currently in use in diagnostic algorithms (0.5 or 1.0 mg/L).

Methods:
This secondary analysis of a prospective cohort study ("PPH 1300 study") was conducted at a tertiary hospital between October 2015 and November 2016 including 1309 pregnant women from 25 to 42 weeks of gestation. Women were stratified for gestational age at delivery: group A (25+0 – 29+6 weeks of pregnancy, n=10), group B (30+0 – 34+6, n=17), group C (35+0 – 36+6, n=49) and group D (37+0 – 42+0, n=1233). Blood samples for D-dimer measurement were drawn in the 36 hours before onset of delivery and 24 to 48 hours after delivery.

Results:
Overall, measured D-dimer values were 1.56 (1.20-2.12) mg/L prepartum and 1.78 (1.25-2.84) mg/L postpartum, data depicted as median (interquartile range). Referring to the above mentioned cut-offs, 1300 women (99.3%) had prepartum D-dimers ≥0.5mg/L and 1163 women (88.8%) ≥1.0mg/L; in the postpartum period 1293 women (98.8%) and 1153 women (88.1%) were above the cut-off of 0.5mg/L and 1.0mg/L, respectively. When stratifying for gestational age, prepartum D-dimers values showed a rising trend with increasing gestational age, while postpartum values did not differ significantly between groups. The percentage of prepartum women with D-dimers >0.5mg/L / >1.0mg/L in groups A, B, C, and D was 80% / 60%, 100% / 76.5%, 100% / 95.9%, and 99.4% / 89%, respectively, and 100% / 90%, 100% / 88.2%, 98% / 87.8%, and 98.8% / 88.1% in the postpartum setting, stratified per group.

Conclusion:
Our results suggest that the integration of D-dimer cut-off values in the diagnostic workup of suspected pulmonary embolism, as proposed in the Artemis study using a pregnancy-adapted YEARS algorithm, is not applicable. In our population, 99% of women had D-dimer values above 0.5mg/L and 88% of women values above 1.0 mg/L, both in the pre- and postpartum setting. Hence, it is questionable to base the decision whether to perform a computed tomography or not on certain cut-offs for D-dimer values.

705

D. Kundert[1]

Reduction in surgical site infections thanks to microbial reduction of the nasal cavity with antimicrobial photodynamic therapy

Department of Cranio-Maxillo-Facial and Oral Surgery, University Hospital Zurich and University of Zurich, Zurich, Switzerland[1]

Introduction:
Antimicrobial Photodynamic Therapy (aPDT) emerges as a promising strategy for preoperative microbial reduction, offering minimal risks, high efficacy, and a lack of known resistance development. Its proven antimicrobial activity against various infectious agents positions aPDT as a compelling alternative to existing decontamination protocols. Surgical site infections remain a prevalent concern in healthcare settings, prompting exploration into innovative methods to enhance preoperative disinfection. Current protocols involve diverse disinfecting solutions or no treatment at all to the nasal cavity, yet challenges persist in effectively applying the optimum to the nasal cavity due to anatomical constraints. The utilization of methylene blue and light presents a method that addresses these challenges, offering enhanced control and ease of standardization by our new project.

Methods:
Approval for this novel approach was obtained under BASEC-Nr. 2023-D0062 from the Cantonal Ethics Committee of the Canton Zurich, marking a significant milestone for the initiation of this project. The proposed method involves the application of the photoactive combination of methylene blue and chlorhexidine gluconate within the nasal cavity, followed by exposure to light at a standardized wavelength of 663 nm and a power of 150 mW/cm^2. This value has been shown to have an antimicrobial effect in various nostril sizes. This approach aims to overcome the limitations associated with traditional disinfection solutions, providing a more controlled and efficient means of preoperative microbial reduction. The study is poised to contribute valuable insights into the feasibility and effectiveness of aPDT in reducing microbial load in the nasal cavity.

Results:
Anticipation surrounds the potential reduction in surgical site infections at the Department of Cranio-Maxillo-Facial and Oral Surgery through the implementation of aPDT. The innovative approach is expected to yield results that surpass current decontamination protocols, showcasing the efficacy of methylene blue and light in preoperative microbial reduction. Comprehensive data analysis will be conducted to evaluate the impact of aPDT on surgical site infection rates, providing a basis for future advancements in preoperative disinfection strategies.

Conclusion:
The application of aPDT using methylene blue and light presents a novel avenue for preoperative microbial reduction in the nasal cavity. With the secured approval, this project is positioned to contribute significantly to the field of preoperative disinfection. The anticipated reduction in surgical site infections at the Department of Cranio-Maxillo-Facial and Oral Surgery underscores the potential of aPDT as an innovative and effective strategy, offering improved control and standardization compared to traditional disinfection solutions and without resistance development.

706

F. Bourquin[2], P. Verloo[1], T. Hornemann[2]

Newly identified Mutation in Serine Palmitoyl-Transferase is linked to neuropathy and crystalline retinopathy

Ghent University Hospital, Ghent, Belgium[1], Institute of Clinical Chemistry (IKC), University Hospital Zurich (USZ) & University of Zurich, Schlieren, Switzerland[2]

Introduction:
The ER located protein serine palmitoyl-transferase (SPT) plays a central role in the onset of neurological disorders such as amyotrophic lateral sclerosis (ALS) or hereditary sensory and autonomic neuropathy type 1 (HSAN 1). SPT catalyzes the first reaction of the sphingolipid metabolism, which is the condensation of the amino acid serine with a fatty acyl-CoA of various chain lengths. Human SPT is active as a complex comprised of the subunit SPTLC1 and either SPTLC2 or 3, the regulatory subunits ORMDL1, 2, or 3, and the small subunits a or b (ssSPTa/b). So far, mutations in subunit 1 and 2 have been reported in both conditions. Here, we investigate a novel mutation G79R located in the transmembrane domain of SPTLC2, close to the ORMDL and ssSPT binding site.

Methods:
The patient is a 16 years-old girl displaying slowly progressive spasticity of the lower limbs, a low amplitude tremor in hands, lingual fasciculation and crystalline retinopathy, a symptom previously not reported to be linked to a SPT mutation. The sphingolipid profile in plasma and patient-derived fibroblasts was analyzed using liquid chromatography linked to tandem mass spectrometry (LC-MS). In parallel, we performed a complementation assay and subsequent isotope labeling to assess the de novo synthesis of sphingolipids in this new variant. For that, we expressed the G79R mutation in an SPTLC2 knockout HEK293 cell line. Cells were supplemented for 24h with stable isotope-labeled serine and incorporation into de novo formed sphingolipids analyzed by LC-MS.

Results:
We observed unique changes in the sphingolipid profile in patient plasma compared to the brother and unrelated healthy controls. Certain sphingolipid species seem to be under-represented in the patient plasma. This points to a putatively altered specificity of the G79R variant for its acyl-CoA substrate.

Conclusion:
However, additional experiments are required to obtain a better understanding on the impact of the SPTLC2-G79R mutant on the sphingolipids signature and its possible link to the reported pathology.

707

C. Dorfer[1], M. Kubli[1], S. Balabanov[1]

Towards Automated Interpretations of Blood Laboratory Results

University Hospital Zurich[1]

Introduction:
Our project aims to build a clinical decision support system (CDSS). This CDSS may predict the most likely diagnoses using blood laboratory results, age, sex and symptoms. While no CDSS can replace a doctor, the aim of such systems is to ease the burden on the decision takers and reduce the rate of diagnostic errors. However, the jump from a functioning model to a practical CDSS is difficult, not least because of regulatory and organizational obstacles. Moreover, it is crucial to avoid biases in the development that leads to a loss of generalisability [1,2]. While there are difficulties, the validity of the approach and the potential benefit remains [3].

[1] Frederike H. Petzschner, Practical challenges for precision medicine. Science 383, 149-150 (2024)

[2] Adam M. Chekroud et al., Illusory generalizability of clinical prediction models. Science 383, 164-167 (2024).

[3] Eric J. Topol, Toward the eradication of medical diagnostic errors. Science 383, 9602 (2024).

Methods:
We are using data and machine learning to learn and generalize from past cases. Our dataset consists of over 122’000 unique patient records (with several admissions) over 14 years, recorded at USZ. By relating the laboratory values prior to treatment with the final diagnosis, we build a model that may have enough predictive power to serve as a clinical decision support system for use in internal medicine.

Results:
The data is well structured and large enough for the task but nonetheless needs a lot of processing. In particular selecting the appropriate time frame for indicative blood laboratory results is challenging because of the context of the admission and other factors. With that resolved, the error rate could be halved for some disease classes. Currently, we predict 30 disease classes with a top-5 accuracy of over 90% and a larger set of 60 disease classes with about 70%.

Conclusion:
We have built a model that outperforms published results [4] in terms of disease coverage and accuracy. We are currently trying to extend the number of disease classes further. To do so we both need medical input as well as additional training data.

[4] Gunčar, G. et al. An application of machine learning to haematological diagnosis. Sci Rep 8, 411 (2018).

708

S. Kakava[1, 2], E. Schlumpf[1], A. von Eckardstein[1, 2], J. Robert[1]

The low-density lipoprotein receptor defines the trafficking of high-density lipoprotein by brain endothelial cells

Institut für Klinische Chemie, Unispital Zurich[1], University of Zurich[2]

Introduction:
Alzheimer's disease (AD) is the leading cause of senile dementia. In addition to beta-amyloid (Aβ) plaques and neurofibrillary tangles, epidemiological evidence shows that cerebrovascular damage precede cognitive decline in AD patients. High-density lipoprotein (HDL), a blood lipid transporter possesses several vasoprotective functions and both clinical and preclinical lines of evidence indicate a beneficial role of HDL in promoting cerebrovascular health in the context of AD. Of note, reconstituted HDL (rHDL) injected into the tail vein of the AD mouse model APP/PS1 acutely reduced Aβ deposition within the brain. In a 3D in vitro model of the human cerebrovasculature HDL reduced Aβ deposition in the cerebrovascular wall by promoting its transport through the vasculature, delayed Aβ fibrillization, decreased cerebrovascular inflammation and promoted nitric oxide (NO) secretion. Even though blood-circulating HDL must first interact with brain endothelial cells to display its anti-AD properties, it is still unknown if HDL is transported through the brain endothelium and how this process might be regulated.

Methods:
HDL was isolated from plasma of healthy donors by gradient ultracentrifugation before being further fractionated into HDLE+ and HDLE- using apoE immunoaffinity chromatography. Fluorescent or ^{125}I-radio labeled HDL were used to measure binding (4°C), association, internalization or transport (37°C) through primary human brain EC or the cell line hCMEC/D3. siRNA was used to understand the role of different receptors in the trafficking of HDL by the brain endothelial cells. Using size exclusion chromatography we determined changes in the size of the HDL particles after being transported through the brain endothelial cells.

Results:
Our in vitro data show that HDL binds to, enters in and is transported through brain endothelial cells as an intact particle. We identified the low-density lipoprotein receptor (LDLR) as a protein limiting HDL transport through brain endothelial cells. Moreover, we found that LDLR limits a sub-population of HDL that contains apolipoprotein E (apoE, HDLE+). On the other hand, the trafficking of HDL particles lacking apoE (HDLE-) is mediated by endothelial lipase (LIPG) and scavenger receptor class B type I (SR-BI). Of note, HDLE+ particles only partially co-localized with HDLE- suggesting independent trafficking pathways. Finally we showed more interaction (binding, association and transport) of HDLE+ particles with the endothelial cells compared to HDLE-.

Conclusion:
Together our results suggest a new role of LDLR in defining the trafficking of HDL and especially HDL containing ApoE by brain endothelial cells. Moreover, with APOE being the major genetic risk factor of AD with APOE2/2 being protective, APOE3/3 being neutral and APOE4/4 being detrimental we aim to shed a new light on the role of peripheral apoE in dementia and help the development of HDL based therapeutics.

709

C. Almiñana[2], S. Makieva[2], M. Saenz-de-Juano[1], S. Bauersachs[4], S. Bernal-Ulloa[1], M. Xie[2], A. Velasco[2], N. Cervantes[2], M. Sachs[2], T. Cavazza[3], S. Ulbrich[1], B. Leeners[2]

Treatment of oocytes with follicular fluid-derived extracellular vesicles during in vitro maturation induces changes in the proteomic profile and organelle distribution

Animal Physiology, Institute of Agricultural Sciences, ETH Zurich, Zurich, Switzerland[1], Department of Reproductive Endocrinology, University Hospital Zurich, Zurich, Switzerland[2], Department of Reproductive Endocrinology, University of Zurich, Zurich, Switzerland[3], Institute of Veterinary Anatomy, Vetsuisse Faculty Zurich, University of Zurich, 8315 Lindau, ZH, Switzerland[4]

Introduction:
Extracellular vesicles (EVs), nanovesicles with diverse molecular cargo (e.g. RNAs, proteins, lipids) are present in most body fluids and have emerged as a new way of cell-to-cell communication. They have raised significant interest as potential biomarkers and therapeutic agents. Particularly, EVs derived from reproductive fluids, such as uterine, oviductal, and follicular fluids, have demonstrated to enhance oocyte nuclear maturation and sperm function, and support embryo development while inducing embryonic transcriptomic changes. However, little is known about the role of follicular fluid-derived EVs (ffEVs) in oocyte maturation in humans and their potential to improve in vitro maturation (IVM) in human assisted reproductive technologies (ARTs).

Methods:
In vitro matured oocytes cultured in the presence (treated, n=5) or absence (control, n=5) of ffEVs for 48h were obtained from a parallel study and subjected to single oocyte proteomic analysis. To assess if proteomic changes were accompanied by changes in organelle ultrastructure, oocytes (treated and control, n=6/group) were also evaluated by transmission electron microscopy. Both ffEVs and oocytes were obtained from women undergoing transvaginal oocyte retrieval after controlled ovarian stimulation (COS) at the University Hospital Zurich, who donated follicular fluid (FF) and/or immature oocytes (BASEC-Nr. 2018-00797). EVs from FF samples containing mature oocytes were isolated by ultracentrifugation and used as supplements during IVM procedure. Mass spectrometry data was analyzed by DEP, a BioConductor R-tool for proteomics analysis. Total identified proteins were filtered to select proteins present in at least 4 out of 5 samples in at least one group. Missing value imputation and statistical analysis were also performed with DEP.

Results:
Mass Spectrometry analysis identified a total of 4593 proteins across oocytes samples. After filtering, 3919 proteins present in 4 out 5 samples/group were obtained and used for further analysis. Statistical analysis revealed 59 differentially abundant proteins (DAPs) between treated versus control oocytes (44 higher and 15 lower in treated oocytes; false discovery rate <0.1) Among these 44 DAPs, 37 proteins showed a fold change >2. Hyaluronan synthase 1 (HAS1), the protein showing the most significant increase has been associated to oocyte maturation. Comparison between proteins identified in oocytes in this study and the ones in ffEVs cargo (1340 proteins) from a parallel study revealed an overlap of 550 proteins. Ten of these common proteins have been found among the 44 DAPs increased in treated oocytes vs. control. TEM observations revealed different organelle distribution in treated vs. control oocytes, particularly regarding endoplasmic reticulum (ER) aggregates, and ER-mitochondria complexes.

Conclusion:
Treatment of oocytes with ffEVs during IVM induces changes in the proteomic profile accompanied by organelle redistribution and appearance, which might support the enhanced maturation rates observed in treated vs. control oocytes. A deeper understanding of the specific mechanism of ffEVs or their cargo that driven oocyte changes may facilitate the developments of novel IVM strategies. This study was supported by EMDO-Stiftung and FAN grant University of Zurich.

710

A. Paunoiu[1], R. Dal Bello[1], P. Wallimann[1], M. Guckenberger[1], S. Tanadini-Lang[1]

Longitudinal radiomics for liver cancer patients treated with magnetic resonance-guided radiotherapy

Department of Radiation Oncology, University Hospital Zürich and University of Zürich, Zürich, Switzerland[1]

Introduction:
Radiomics describes the extraction of a large number of quantitative features from medical images which are imperceptible by the human eye. These features can be classified into a number of families, related to tumor shape, intensity or texture. For the purpose of this study, magnetic resonance (MR) scans of liver cancer patients treated with magnetic resonance-guided radiotherapy (MRgRT) at our department were retrospectively analysed. The aim of this work is to correlate each of the radiomic features extracted from the gross tumor volume (GTV) to the number of fractions. In addition, we also investigated the correlation between the radiomic features and the accumulated dose to the GTV.

Methods:
Data of 88 liver tumor treatments were provided, all of which included three to six fractions. Most patients were irradiated with a prescribed dose of 45 Gy. The treatment plans were normalized so that the prescribed dose covers 65% of the planning target volume (PTV). MR images and contours of the regions of interest (ROI) were exported and processed for comparability using bias field correction and Z-score normalization. Images were resized and radiomic features were extracted from the GTV using an in-house developed software, Z-rad. For all patients, the Spearman correlation factor between each feature and the fraction number was calculated. This analysis was also conducted to assess the correlation between the radiomic features and the accumulated dose to the GTV, with calculations performed individually for each patient. A correlation factor larger than 0.5 indicated a positive correlation, while a factor smaller than 0.5 indicated a negative correlation. All values in between were considered non-correlating behaviours. The percentage of positive and negative values was calculated for both approaches.

Results:
165 radiomic features were extracted from the GTV. When investigating the correlation between the radiomic features and the number of fractions, Grey Level Co-occurrence Matrix (GLCM)-, as well as Grey Level Run Length Matrix (GLRLM)-based features showed a larger number of positively correlated treatments compared to negatively correlated ones: *mGLCM_sum_entropy* (13.7% vs. 5.8%), *mGLCM_InformationMeasuresCorrelation1* (19.6% vs. 7.8%) and *GLRLM_LongRunVariance* (19.6% vs. 15.6%). Other features, intensity-based, showed a smaller number of positive correlations compared to negative correlations: *MaxIntensityTumorVolume30%* (9.8% vs. 15.6%), *entropy* (17.6% vs. 25.4%) and *kurtosis* (13.7% vs. 21.5%). When investigating the correlation between the radiomic features and the accumulated dose to the GTV, for two patients out of a subset of three, there was a larger number of radiomic features which were positively correlated to the accumulated dose to the GTV compared to negatively correlated ones: 17.5% vs. 1.2% for the first patient and 23.0% vs. 7.8% for the second patient.

Conclusion:
The study investigated the correlation between the radiomic features and both the number of fractions and accumulated dose to the GTV. GLCM- and GLRLM-based features showed more positive correlations to the number of fractions, while intensity-based features displayed more negative correlations. In terms of the correlation between the radiomic features and the accumulated dose to the GTV, the initial results were promising. Future work will aim to include additional patients and focus the analysis on accumulated dose instead of fraction number. The analysis of the early reaction of the healthy liver tissue and the correlation to treatment outcome is ongoing.

711

I. Martinez Lopez[2], T. Papasotiropoulos[2], F. Schläpfer[2], S. Ulrich[1], I. Opitz[2], M. Kirschner[2]

MicroRNA Expression Correlates with Clinical Presentation of Chronic Thromboembolic Pulmonary Hypertension

Department of Pulmonology, University Hospital Zurich[1], Department of Thoracic Surgery, University Hospital Zurich[2]

Introduction:
Chronic Thromboembolic Pulmonary Hypertension (CTEPH) is a rare, debilitating disease characterized by pathological changes that obstruct both sides of the pulmonary arteries (PA). To understand a possible contribution of microRNA expression to the thus far poorly understood pathophysiology underlying CTEPH development, we here analysed the expression of four candidate miRNAs in pulmonary endarterectomy (PEA) specimens and plasma samples.

Methods:
MiRNA specific RT-qPCR for miR-939, miR-942, let-7b and let-7d was done on RNA extracted from: a) PEA specimens of 50 CTEPH patients and from PAs resected from explant lungs of 49 transplant recipients (27 due to COPD, and including 22 with PH), and b) pre-operative plasma from 47 CTEPH patients and 21 lung transplant patients (12 due to COPD, and including 3 with PH). Associations between miRNA expression and clinical presentation (not all factors available for every patient) were assessed by Spearman correlation and Kruskal Wallis test. MiRNA expression between CTEPH and reference PAs was compared by Mann Whitney test.

Results:
Expression levels in PEA-derived tissues correlated negatively for two right-sided miRNAs: let-7b and mPAP (n = 43, R = -0.34, p=0.02), miR-942 and 6-minute walk distance (6MWD) (n = 46, R = -0.34, p=0.02), as well as for two left-sided ones: let-7d and CRP (n = 49, R = -0.296, p=0.04), miR-939 and oxygen saturation (SpO2) at peak 6MWD (n = 47, R = -0.4, p=0.005). Positive correlation was found with SpO2 before 6MWD for let-7b (n = 41, R = 0.318, p = 0.043). Jamieson left showed association with mean expression levels of let-7b (n = 43, H = 8.25, P = 0.04) and left-sided let-7d (n = 43, H = 9.19, P = 0.03). **Plasma analysis** showed positive correlations with SpO2 after 6MWD and miR-939 (n = 40, R = 0.35, p = 0.026) and for let-7b with CRP (n = 44, R = 0.299, p = 0.048), and NYHA (n = 45, H = 16.56, P = 0.0009). Relative to the comparator groups, **significance was reached in PAs** for expression of let-7b regardless of side (n = 49 CTEPH vs n = 49 Comparator, p <0.0001), **and in plasma** for miR-939 (n = 49 CTEPH vs n= 19 Comparator, p <0.0001).

Conclusion:
Correlations and associations with clinical parameters suggest that miRNA expression is associated with the severity of the disease. The analysis in plasma samples highlights the potential of these miRNAs as circulating biomarkers. Furthermore, the significant elevation compared to comparator PA tissue and plasma suggest that miRNA dysregulation might be involved in CTEPH pathophysiological mechanisms.

712

M. Mastall[1], G. Dunkel[2], D. Villars[1], M. Silginer[1], N. Okada[3], C. Rössig[4], T. Weiss[1], B. Weigelin[2], M. Weller[1], P. Roth[1]

VEGFR2-specific CAR T cells with anti-glioma and anti-angiogenic activity against glioblastoma

Department of Neurology and Clinical Neuroscience Center, University Hospital and University of Zurich, Zurich, Switzerland, Zurich, Switzerland[1], Department of Preclinical Imaging and Radiopharmacy, Eberhard Karls University of Tuebingen, Tuebingen, Germany, Tuebingen, Germany[2], Laboratory of Vaccine and Immune Regulation (BIKEN), Graduate School of Pharmaceutical Sciences, Osaka University, Osaka, Japan, Osaka, Japan[3], University Children's Hospital Muenster, Muenster, Germany[4]

Introduction:
Chimeric antigen receptor (CAR-) T cell therapy has emerged as a potent immunotherapy against hematological malignancies. In glioblastoma, however, limited infiltration of the tumor by CAR-T cells, tumor heterogeneity, antigen escape and an immunosuppressive tumor microenvironment remain significant obstacles. Vessel-targeting CAR-T cells have been shown to infiltrate solid tumors more efficiently and have the additional benefit of co-targeting the tumor vasculature. Therefore, vascular endothelial growth factor receptor 2 (VEGFR2)-CAR T cells may represent a promising strategy by targeting the tumor vasculature as well as VEGFR2-expressing tumor cells. Here, we explored the efficacy of VEGFR2-specific CAR T cells against experimental gliomas, the contribution of anti-tumor and anti-vasculature-dependent effects of this strategy as well as the infiltration capacity upon systemic administration.

Methods:
Tissue microarrays of glioblastoma patients (n = 109) were stained for VEGFR2 expression. Human CAR-T cells (hCAR) were generated by lentiviral transduction to express a second generation CAR construct against either mouse or human VEGFR2 (mVEGFR2 or hVEGFR2). Their activity was assessed in co-culture assays *in vitro* against murine endothelial and human glioma cells, respectively. Several orthotopic xenograft mouse glioma models were used to test the *in vivo* activity of the newly generated hCAR-T cells. Additionally, murine CAR-T cells (mCAR) were generated by retroviral transduction to express a second generation CAR construct targeting mVEGFR2. Syngeneic orthotopic mouse glioma models were used to explore the infiltration of intravenously administered mCAR-T cells by *in vivo* fluorescence molecular tomography (FMT), *ex vivo* flow cytometry as well as *ex vivo* 3D light-sheet fluorescence microscopy.

Results:
We confirmed high VEGFR2 expression on endothelial cells in glioblastoma tissue of stained tissue microarrays as well as in a subset of tissue sections (21.1%) also on tumor cells. In co-culture assays, hVEGFR2-hCAR T cells were exclusively active against human glioma cells and mVEGFR2-hCAR-T cells against mouse endothelial cells, respectively. In all three *in vivo* xenograft glioma models, intratumoral treatment of hVEGFR2-hCAR-T cells significantly prolonged the survival of glioma-bearing mice and cured a substantial fraction of these animals in one model. Additionally, we found that survival was prolonged after mVEGFR2-hCAR-T cell treatment in one glioma model, which correlated with high vascularization of these tumors. Finally, intravenous treatment with fluorescently labeled mVEGFR2mCAR-T or mock-transduced T cells of syngeneic tumor-bearing mice resulted in a higher FMT signal at the tumor site. This was confirmed by *ex vivo* flow cytometry, wherein mVEGFR2mCAR-T cells represented a larger fraction of all T cells within the tumor (26.5% CAR versus 5.4% Mock, p=0.0013). Similarly, significantly more mVEGFR2-mCAR-T cells were detected at the tumor site compared to tumor-targeting (but not vessel-targeting) control CAR-T cells.

Conclusion:
Our dataset demonstrates that VEGFR2-CAR-T cells prolong the survival of glioma-bearing mice through anti-glioma and anti-glioma-vasculature activity. The results suggest that the magnitude of the vasculature-targeting activity depends on vessel-density within the tumor. Ultimately, VEGFR2-CAR-T cells show improved glioma infiltration in syngeneic mouse models. In conclusion, VEGFR2 might be a relevant target that could be exploited for a novel CAR-T cell-based immunotherapeutic approach against glioblastoma.

713

R. Odabasi[2], K. Gegenschatz-Schmid[2], L. Moser[2], L. Krattiger[2], P. Briquez[1, 3], N. Ochsenbein-Kölble[2, 4], M. Ehrbar[2]

Bioengineering Smart Regenerative Biomaterials for the Healing of Fetal Membrane Defects

Department of General and Visceral Surgery, Medical Center – University of Freiburg, Faculty of Medicine[1], Department of Obstetrics, University and University Hospital of Zurich, Zurich, Switzerland[2], Pritzker School of Molecular Engineering, University of Chicago, Chicago, USA[3], The Zurich Center for Fetal Diagnosis and Therapy, Zurich, Switzerland[4]

Introduction:
Minimally invasive surgeries in the utero have brought numerous advantages to fetal health. However, the surgeries come with a high risk of iatrogenic preterm prelabor rupture (iPPROM). The impact of preterm birth can be severe on the newborn's quality of life. Associated effects range, among others, from respiratory distress syndrome, blindness to cerebral palsy. Despite numerous efforts, there is currently no clinical measure for the prevention of iPPROM, as there is no available method to seal or heal the injured fetal membranes (FMs). A recent study by our group showed that transglutaminase crosslinked polyethylene glycol (TG-PEG) loaded with PDGF-BB was able to promote FN healing in vitro and in vivo. However, the model relied on diffusion of the growth factor, rather than active binding and releasing to and from the TG-PEG hydrogel. We hypothesize by having a controlled growth factor release, healing of FM defects will be improved. Therefore, this project will present a modular TG-PEG matrix where recombinant PDGF-BB will be bound and presented actively. The optimized material will allow for a controlled growth factor release, which will be beneficial for healing of the FM in vitro and in vivo.

Methods:
Sequences encoding for PDGF-BB/Linker will be transfected to and expressed in mammalian Hek293-cells. Binding activity of the recombinant growth factor to the hydrogel will be assessed via ELISA. The growth factor release will be assessed using ELISA. Growth factor activity will be evaluated via migration assays of human amniotic mesenchymal stromal cells (AMSCs).

Results:
-

Conclusion:
With this smart TG-PEG hydrogel, we will have a viable strategy to prevent iPPROM-related morbidities.

714

V. Dimakopoulos[1], J. Sarnthein[1]

Multicenter comparison of interictal high frequency oscillations as a predictor of seizure freedom

Klinik für Neurochirurgie, Universitätsspital Zürich[1]

Introduction:
In drug-resistant focal epilepsy, the intracranial EEG channels that contain interictal high frequency oscillations (HFO) are hypothesized to delineate the epileptogenic zone; their resection should lead to postsurgical seizure freedom. We here extend our previous pilot studies with a larger patient cohort to improve statistical power. The main objective of this study is to test whether our prospective definition of clinically relevant HFO is in agreement with postsurgical seizure outcome. The aim is to assess the reliability of our automated HFO detector and analysis approach.

Methods:
We use a prospective definition of clinically relevant HFO. We combine retrospectively collected datasets from nine independent epilepsy centers. The data analysis is blinded to clinical outcome. For each patient we detect HFO during non-rapid-eye-movement sleep and delineate the HFO area. The study center then enters the patient's clinical information via a REDcap survey. The survey documents whether the HFO area was resected and whether seizure freedom was achieved at ≥2 y follow-up

Results:
So far, we have received 200 datasets from eight study centers.

Conclusion:
Applying a previously validated algorithm to a large cohort from several independent epilepsy centers may advance the generalizability and clinical relevance of the HFO.

715

K. Arnke[1]

Fibroblast produced ECM for improved osteogenesis

Traumatology[1], University Hospital of Zurich

Introduction:
Regeneration of large bone defects remains challenging in orthopedic surgery and is often associated with poor outcomes and complications. The current “gold standard treatment” to reconstruct bone in case of critical-size bone defects is autologous bone grafting. This treatment has optimal osseointegration and does not show rejection of the body as the patient's own tissue is used. In many cases, the autologous bone marrow aspirate obtained is not sufficient and must be filled with allogenic splinters of cancellous bone. However, these methods require additional surgery for harvesting the graft material, often leading to donor site pain and morbidity. Bone tissue engineering represents an appealing alternative. A major issue with bioengineered constructs is achieving a continuous interface between host bone and graft to enhance biological processes and mechanical stability. Since many years, several studies suggest that bioengineered cell-derived extracellular matrices (CD-ECMs) are a promising alternative for regenerative medicine. CD-ECMs almost perfectly imitate their natural counterparts in their structural and component-specific complexity. In bone regeneration, mesenchymal stromal cells (MSCs) and osteoblasts are commonly used to generate the ECM. However, their clinical application faces various challenges. Obtaining these cells from the patient also requires an additional invasive procedure and their in vitro expansion requires time. The use of allogenic pre-produced CD-ECMs carries the risk of rejection.

Methods:
In this project, we used fresh isolated dermal fibroblasts to generate the ECM instead of the usually used MSC-derived (MD-) or osteoblast-derived (OD-) ECM. Fibroblasts were incubated either in normal proliferation medium or supplemented with 1 µg/mL or 10 µg/mL of dextran-sulfate for 4 days to produce the ECM. After decellularization of the fibroblasts, skeletal stem cells (SSCs) were seeded on the fibroblast-derived ECM (FD-ECM) and differentiated into osteoblasts. We compared our FD-ECM with MD- and OD-ECM because they are commonly used for ECM production. Osteogenic differentiation was determined macroscopically by AlizarinRed staining and by expression of osteogenic markers.

Results:
The SSCs differentiated into osteoblasts much faster on the FD-ECM than on the plate alone. When 10 µg/mL dextran sulfate was added as a “booster”, the first calcium deposits could be observed after just 4 – 7 days, while, as with the control, it usually takes up to 14 – 21 days. MD and OD-ECM also improved osteogenesis of SSCs compared to control. Nevertheless, although the MSCs and osteoblasts produced ECM for seven days and not just four days like the fibroblasts, both ECMs did not support osteogenic differentiation as well as the FD-ECM. In addition to macroscopic analysis, expression of osteogenic markers confirms the improved and faster osteogenesis of SSCs on FD-ECM compared to SSCs on ECM derived from other cell types or compared to SSCs alone.

Conclusion:
Overall, our preliminary results show that the use of patient’s own fibroblasts to generate ECM represents a promising alternative as a biomaterial for improved bone healing. Dermal fibroblasts can be easily isolated from skin biopsies without the need for additional invasive procedure, as is the case with autologous bone grafts or isolation of MSCs from adipose or bone tissue to generate MD or OD ECM. However, what is most notable is the positive effect of FD-ECM on osteogenic differentiation and, in particular, that its supporting effect is even higher than the effect of ECM of osteoblasts and MSCs.

716

G. Panteloglou[7], A. Othman[6], P. Zanoni[7], E. Schlumpf[7], M. Yalcinkaya[7], S. Kakava[7], S. Radosavljevic[7], R. Meier[8], M. Futema[1], S. Humphries[2], R. Geha[5], A. Shum[3], W. März[9], B. van de Sluis[4], J. Kuivenhoven[4], J. Robert[7], L. Rohrer[7], a. von Eckardstein[7]

The COPI coatomer regulates lipoprotein metabolism

Cardiology Research Centre, Molecular and Clinical Sciences Research Institute, St George's, University of London, London, UK[1], Cardiovascular Genetics, Institute of Cardiovascular Science, University College London, WC1E 6JJ London, UK[2], Department of Medicine, Division of Pulmonary and Critical Care, University of California San Francisco, San Francisco, CA, USA[3], Department of Pediatrics, Section Molecular Genetics, University of Groningen, University Medical Center Groningen, the Netherlands[4], Division of Immunology, Boston Children's Hospital, Boston, Massachusetts, USA[5], Functional Genomics Center Zurich, ETH Zurich, 8057, Zurich, Switzerland[6], Institute of Clinical Chemistry, University & University Hospital of Zurich, Switzerland[7], Scientific center for optical and electron microscopy (ScopeM), ETH Zurich, 8093, Zurich, Switzerland[8], Vth Department of Medicine (Nephrology, Hypertensiology, Endocrinology, Diabetology, Rheumatology), Medical Faculty of Mannheim, University of Heidelberg, Mannheim, Germany[9]

Introduction:
Plasma levels of both Low and High Density Lipoprotein-Cholesterol (LDL-C and HDL-C, respectively) are mainly determined by the catabolism of these lipoproteins. While the limiting effect of the LDL receptor (LDLR) for the hepatic removal of LDL is well understood and exploited for hypolipidemic and anti-atherogenic drug therapy, the catabolism of HDL is only partially resolved. Scavenger Receptor Class B Type I (SR-BI) mediates the selective uptake of lipids but the HDL holoparticle receptor is unknown.

Methods:
To identify novel regulators of hepatic LDL and HDL uptake, we performed a genome wide siRNA screen in Huh-7 hepatocarcinoma cells. We validated the candidate genes by in vitro experiments and exploring associations of their genetic variants with plasma lipoprotein levels in humans and genetically modified mice.

Results:
The genome-wide siRNA screen identified six and three COPI genes that limit the uptake of HDL and LDL uptake, respectively, into Huh-7 cells. In targeted replication experiments, silencing of the six indispensable components of the COPI coatomer but not the three dispensable or paralogous COPI genes resulted in decreased uptake of labeled LDL as well as both lipid- and protein-labeled HDL and decreased cell surface expression of both LDLR and SR-BI due to aberrant glycosylation and subcellular trafficking. In the 1.65 million individuals of the Global Lipid Gene Consortium, single nucleotide polymorphisms of ARCN1 were associated with higher levels of both LDL-C and HDL-C. Rare missense mutations of COPA and COPG1 were found at increased prevalences in patients with hypercholesterolemia. Patients with inherited interferonopathy or combined immunodeficiency due to missense mutations in COPA and COPG1, respectively, had low plasma levels of HDL-C. Genetic mouse models with these mutations also had lower levels of HDL-C and triglycerides but higher levels of LDL-C and apoB than control mice. Liver specific knock-out of Copg1 led to lower plasma levels of HDL-C and triglycerides as well as higher plasma levels of nonHDL-C and apoB.

Conclusion:
Taken together, our data indicate that the COPI coatomer regulates the activity of several pivotal proteins in lipoprotein metabolism and thereby influences plasma levels of lipoproteins. The elevated levels of apoB containing lipoproteins in humans and mice with COPI mutants corroborate the limiting effect of the COPI coatomer on LDLR activity. The finding of low HDL-C despite reduced SR-BI activity and HDL holoparticle uptake indicates more complex effects of the COPI coatomer on multiple proteins regulating HDL metabolism.

717

I. Iskender[1], S. Hillinger[1], D. Schneiter[1], O. Lauk[1], G. Lang[1], I. Opitz[1], C. Caviezel[1]

Is it Safe to Remove Chest Drains Without a Priori Chest X-ray Following Anatomical Lung Resections in Patients With Non-Small Cell Lung Cancer

University Hospital Zurich[1]

Introduction:
After anatomical lung resections, routine postoperative chest X-rays are common. Advances in chest drain monitoring and enhanced recovery programs in thoracic surgery (ERAS) raise questions about the necessity of these routine X-rays. We hypothesize that, for non-small cell lung cancer (NSCLC) patients, chest drains connected to a digital system can be safely removed without consulting prior X-ray findings following anatomical lung resections.

Methods:
Patients undergoing anatomical lung resections for NSCLC, excluding wedge resection or pneumonectomy, have been retrospectively analyzed between June 2020 and June 2023. Unless there was a clinical concern, such as prolonged air leak>7days, ICU admission, abnormal pleural effusion, and hypoxia or the decision of consultants, routine post-operative chest X-rays prior to drain removal were intentionally no longer performed.

Results:
The cohort consisted of 270 consecutive patients undergoing anatomical lung resections for NSCLC. Twenty-eight patients were excluded, most patients left the theatre with 2 drains (n=24). The remaining 242 patients underwent lung resections via minimal invasive approaches, VATS/RATS (94%). Patients were grouped into three categories. Group 1: No pre-pull X-ray (n=125), Group 2: Pre-pull X-ray routine check (n=71), and Group 3: Pre-pull X-ray due to clinical concern (n=46). Central venous catheter insertion (n=42) and postoperative follow-up (n=29) were the two main indications for pre-pull X-ray in Group 2. The incidence of reoperation, including re-tube and re-VATS was comparable between the groups (Group 1: n=6 (4.8%), Group 2: n=4 (5.6%), Group 3: n=7 (15.2%); p=0.053. The mean duration of chest tube and hospital stay were markedly lower in Group 1 (2+2.7 vs 4.9+4.7 days; p<0.001) than Group 2 (3.1+3.4 vs 5.8+3.8 days; p=0.011), respectively.

Conclusion:
Chest drains can be removed safely without pre-pull X-ray after uneventful anatomical lung resections. Together with other ERAS measures, this practice change helped us to reduce the length of hospital stay significantly.

718

K. Arnke[1]

Influence of Dextran Derivatives on trilineage Differentiation

Traumatology[1], University Hospital of Zurich

Introduction:
A faithful reconstruction of the native cellular microenvironment is instrumental for tissue engineering, especially for bone and cartilage regeneration. Cells are mostly embedded in a niche specific extracellular matrix (ECM). Thus, it is useful to mimic the components of their ECM to facilitate the deposition of cell-own ECM compartments and to improve tissue regeneration. Dextran-sulfate (Dx-S) is a polymeric dextran derivative with negatively charged sulfated groups. Dx-S mimics negatively charged components of the ECM like glycosaminoglycans. It is known to enhance the production and deposition of ECM proteins like collagen I and fibronectin and improves osteogenesis. Compounds, which are similar to the positively charged components of the ECM like collagen, are known to improve osteogenesis through charge-induced adhesion of ECM proteins. DEAE-dextran (Dx-N) is a polymeric dextran derivative with a positively charged tertiary amine and usually used as a transfection reagent. In this study we combine both derivatives with different charged side chains to improve the *in vitro* osteogenesis and chondrogenesis of human mesenchymal stromal cells.

Methods:
In a first round, we treated human MSCs with Dx-N in different concentrations (0, 6, 8 and 10 µg/mL) for 20 h. Afterwards we initiated the trilineage differentiation into adipocytes, chondrocytes and osteocytes or incubated them in proliferation medium. We measured also specific differentiation markers after 1, 3, 7 and 17 days. In a second round, we added Dx-S (1 µg/mL, 10 µg/mL or 15 µg/mL) to the proliferation medium and to the differentiation media, either with a previous Dx-N (8 µg/mL) treatment for 20 h or without and repeated the trilineage differentiation. The specific differentiation markers were also determined at the same time points as in the first round. Cells without any dextran-derivatives served as controls.

Results:
Cells treated with Dx-N showed increased capacity for osteogenic differentiation, while adipogenesis and chondrogenesis were decreased with increasing Dx-N concentration. Most interestingly, cells treated with Dx-N but incubated in proliferation medium, also differentiated into osteocytes in a concentration dependent manner. The two high concentrations reached even similar differentiation levels as the control. When Dx-S was added to the differentiation media it showed a positive effect for osteogenesis in a dose dependent manner and chondrogenesis with a peak at 1 µg/mL, but the adipogenic differentiation was inhibit. Same was true for the differentiation marker expression. Dx-S alone was able to induce chondrogenesis in a dose-dependent manner even without differentiation medium and the highest chondrogenic differentiation was observed at 15 µg/mL Dx-S added to proliferation medium. The combination of both dextran derivatives resulted in an improved osteogenic differentiation independent if the cells were incubated in proliferation or differentiation medium.

Conclusion:
Our results show that the two sugar derivatives DEAE-dextran and dextran sulfate in the right concentrations have a great influence on the trilineage differentiation potential of MSCs. The combination of both showed great ability to induce osteogenesis without any growth factors or specific induction medium. Dx-S alone appeared to be able to induce chondrogenesis without specific differentiation media. Since both sugars are harmless to humans and Dx-S is already used in other clinical approaches, our study provides evidence that these dextran derivatives hold promise for further studies on bone and cartilage regeneration and provide alternatives to expensive and specialized growth factors and chemicals.

719

L. Linzmeier[2], E. Goljat[1], V. Matus[2], M. Determann[2], M. Wilmink[2], M. Schwarzfischer[2], R. Sanchez Alvarez[2], D. Pöhlmann[2], N. Joller[1], M. Scharl[2], M. Spalinger[2]

The macrophage specific effect of PTPN23 KO in colonic inflammation and alveolar infection

University of Zurich, Department of Quantitative Biomedicine[1], University of Zurich, University Hospital Zurich, Departement of Gastroenterology and Hepatology[2]

Introduction:
Protein Tyrosine Phosphatase Non Receptor Type 23 (PTPN23) is a member of the PTP family. It plays a critical role in endosomal sorting and EGFR internalization and thereby negatively controls EGFR signalling. Our preliminary data demonstrate that a knockout (KO) in intestinal epithelial cells leads to spontaneous intestinal inflammation and death of the animals. Next to intestinal epithelial cells, PTPN23 is also highly expressed in intestinal macrophages. However, the mechanistic role of PTPN23 in immune cells remains elusive.

Methods:
For the chemically induced acute colitis PTPN23$^{fl/fl}$LysMCre$^{+/-}$ (KO) and PTPN23$^{fl/fl}$LysMCre$^{-/-}$ (WT) mice were treated with 2% DSS in the drinking water for 7 days. For the chronic colitis a cycle of 7 days of administrating 1,5% DSS followed by 10 days of recovery phase was repeated 4 times. The state of inflammation was determined by colonoscopy, staining of colonic tissue, flow analysis of cells isolated from colon, spleen and mesenteric lymph nodes, and further molecular biology analysis. The alveolar infection was realized by infection of the same mouse strains with *Legionella pneumophila* intranasally. Bacterial titters in the lung were determined and samples for flow cytometry analysis were collected after 3 days.

Results:
KO mice showed a less severe colitis phenotype in the DSS induced acute and chronic colitis. The DSS-induced weight loss was less pronounced, as were the colon shortenings. Additional no elevated spleen weights and lower endoscopic scores could be seen in the KO vs WT mice. Histological analysis of colon tissue showed less damaged colon tissue in KO. Further pro-inflammatory cytokines were higher in WT than KO. A higher number of tissue infiltrating pro-inflammatory monocytes could be observed in WT compared to KO.
KO and WT mice exhibited the same bacterial titres 3 days after infection with *Legionella pneumophila*. Nevertheless, in flow cytometry analysis higher numbers of inflammatory monocytes could be observed in KO compared to WT. Furthermore, expression of TNF-α in T-cells and inflammatory monocytes was significantly higher in KO mice.

Conclusion:
PTPN23 appears to play a different role in macrophages in colonic vs lung tissue, as the protection of PTPN23 KO against chemically induced colitis could not be seen to the same extend in alveolar inflammation.

720

R. Erlebach[4], A. Buhlmann[4], R. Andermatt[4], B. Seeliger[3], K. Stahl[2], C. Bode[1], R. Schüpbach[4], P. Wendel-Garcia[4], S. David[4]

Carboxyhemoglobin Predicts Oxygenator Performance and Imminent Oxygenator Change in Extracorporeal Membrane Oxygenation

Department of Anesthesiology and Intensive Care Medicine, University Hospital Bonn, Bonn, Germany[1], Department of Gastroenterology, Hepatology, Infectious Diseases and Endocrinology, Hannover Medical School, Hannover, Germany[2], Department of Respiratory Medicine, Hannover Medical School, Hannover, Germany[3], Institute of Intensive Care Medicine, University Hospital Zurich, Zurich, Switzerland[4]

Introduction:
Hemolysis during extracorporeal membrane oxygenation (ECMO) is a common complication often caused by increasing resistance to flow due to progressive thrombosis and excessive mechanical stress, especially high negative pressures. Carbon monoxide - formed through degradation of heme by heme-oxygenase binds with high affinity to hemoglobin producing Carboxyhemoglobin (COHb). High COHb levels caused by excessive hemolysis and reduced elimination due to impaired gas exchange through the oxygenator might therefore be a novel pointof-care marker of oxygenator dysfunction.

Methods:
Retrospective single-center analysis of all patients requiring ECMO support having experienced at least one oxygenator exchange between 2018 and 2021 at our Institute of Intensive Care Medicine. Multivariable, generalized mixed-effects models and time-varying proportional hazards models, adjusting for a set of predefined, causally identified confounders of hemolysis and ECMO circuit lifespan, were employed.

Results:
In total 484 ECMO patients were screened of whom 89 required one or more oxygenator exchanges and were included into the final cohort. Of these 33 (37%) patients received ECMO in v-v configuration and 56 (63%) in v-a configuration. Cumulatively, 116 oxygenator exchanges were detected over 1’833 patient days, including 20’000 COHb measurements. COHb was independently associated with oxygenator performance assessed by means of the partial pressure of oxygen in a post-oxygenator blood gas analysis sampled after the performance of an oxygen challenge (log Effect Size -7.0 [95% CI -11.5 to -2.5], p=0.032). Similarly, increasing COHb levels were independent predictors of an oxygenator exchange in the ensuing 6 hours (log Odds Ratio 0.78 [95% CI 0.18 to 1.38], p=0.0111) and rising levels were independently associated with an absolute increase in the hazard of oxygenator exchange (Hazard Ratio 1.55 [95% CI 1.11 to 2.17], p=0.0102).

Conclusion:
COHb is independently associated with reduced oxygenator performance and predicted imminent oxygenator exchange in a retrospective fashion. Its universal bedside availability, rapid turnover, and association with oxygenator performance makes COHb an interesting candidate for routine monitoring of ECMO patients.

Programm und Abstracts

Organisation und Kontakt

Universitätsspital Zürich
Direktion Forschung und Lehre
Rämistrasse 100
8091 Zürich

+41 43 253 01 10
dfl@usz.ch

Das vollständige Programm und die Abstracts finden Sie unter:
www.usz.ch/veranstaltung/docr

Anmeldung und Kosten

Es ist keine Anmeldung nötig.
Die Teilnahme ist kostenlos.

Video-Aufzeichnung

Die Veranstaltung findet vor Ort statt. Alle Beiträge werden gefilmt und im Anschluss an die Veranstaltung online aufgeschaltet.

Veranstaltungsort

Universitätsspital Zürich
Grosser Hörsaal OST
Rämistrasse 100
8091 Zürich

Anfahrt

Tramlinien 6, 9, 10 bis Haltestelle
ETH/Universitätsspital

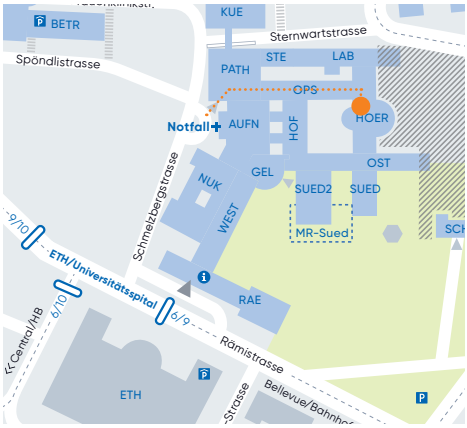

Folgen Sie dem USZ unter

04.24